C.P. No. 1263

PROCUREMENT EXECUTIVE, MINISTRY OF DEFENCE

AERONAUTICAL RESEARCH COUNCIL

CURRENT PAPERS

The Design of a Series of Warped Slender Wings for Subsonic Speeds

by

Patricia J. Davies

Aerodynamics Dept, R A E, Farnborough

LONDON: HER MAJESTY'S STATIONERY OFFICE

1974

PRICE £1 35 NET

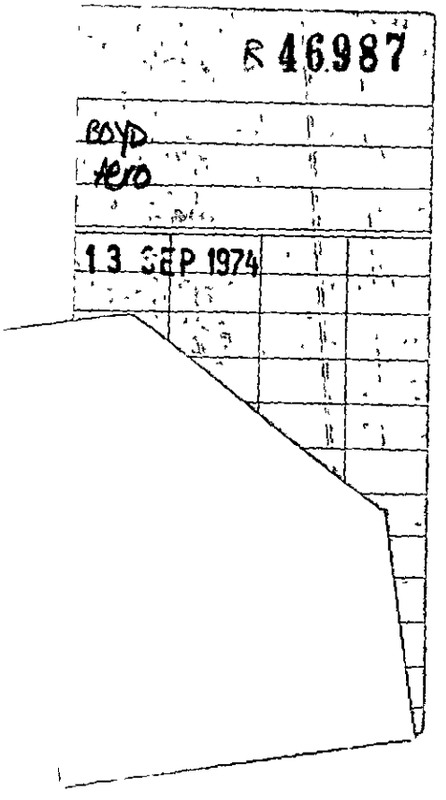
R 46987
BOYD
HERO
13 SEP 1974

UDC 533.6.043.2 : 533.693.3 : 533.6.013.12/13

* CP No.1263
August 1971

THE DESIGN OF A SERIES OF WARPED SLENDER WINGS FOR SUBSONIC SPEEDS

by

Patricia J. Davies

SUMMARY

This Report describes how warped (i.e. cambered and twisted) mean surfaces have been derived for a series of wind-tunnel models of low aspect ratio wings with pointed apexes, 'mild-gothic' planforms and sharp leading edges. The primary aim was to obtain higher ratios of lift to drag than those of the plane wing while maintaining the same orderly development of the flow. Subsidiary aims were to assess how far performance might be compromised by varying the centre of pressure of the wing and by shaping it to reduce the lateral propagation of noise from an overwing engine installation.

The mathematical basis is the linearised theory of subsonic flow. The shapes and pressure distributions of the models are shown.

* Replaces RAE Technical Report 71173 - ARC 33723

CONTENTS

1 INTRODUCTION

The design of an aircraft to carry two hundred or more passengers over short distances at high subsonic speeds has been considered in Ref.1, and a slender, all-wing type of aircraft has been proposed. The advantages envisaged for this type of aircraft are a compact layout, a large payload fraction and a degree of noise shielding. One of the main aerodynamic problems confronting the designer of such an aircraft, with its wing of low aspect ratio, is that of take-off performance, since the high thrust of the supersonic, slender-wing transport aircraft is not available. This Report is concerned with the design of warp (i.e. camber and twist) aimed at increasing the ratio of lift to drag of a slender wing of given planform and thickness at lift coefficients typical of take-off conditions.

Warp designed for a supersonic cruising condition has been applied to slender wings (see, for example, Ref.2) with a substantial measure of success, and wings designed in this way for supersonic cruise have shown improved performance at low speeds (see, for example, Ref 3). The aim of the earlier work[2] was to seek performance benefits at supersonic speeds, including reduction of trim drag through control of centre of pressure position, while maintaining the orderly type of flow development typical of a plane slender wing. The same general aims apply to the present investigation, except that the performance benefits are now required at subsonic speeds and higher lift coefficients, and so a similar approach is followed.

The flow development on a plane slender wing involves the onset of separation along the whole length of the leading edge at a very small angle of incidence, with the formation of continuously-fed, coiled vortex sheets above the wing, which maintain their smooth, tightly rolled structure until they break down at some large incidence beyond the typical range of operating conditions. These leading-edge separations dominate any other separations which may occur. Warp of a general kind will disrupt this pattern, with the formation at low incidences of vortex separations both above and below the wing from different parts of the leading edge. To avoid this, the type of warp chosen must be restricted by requiring the wing to have an attachment incidence, that is, an incidence at which the flow is attached over the whole wing and above which vortex sheets are formed only above the wing. For there to be no tendency for the flow to separate at the sharp leading edges at this attachment incidence, the pressure difference between the upper and lower

surfaces must tend to zero there in a physically appropriate fashion. Elsewhere on the wing, the pressure distribution must be compatible with the development of attached boundary layers. Since these requirements, and that of centre of pressure specification, are related directly to the distribution of lift over the wing, it is reasonable to adopt a design method in which the wing shape is determined from the lift distribution.

In the earlier work at supersonic speeds[2], the wing shape was related to the lift distribution using the linearised theory of supersonic flow. The corresponding linearised theory for subsonic flow therefore seems appropriate for the present investigation, though larger viscous effects are to be expected in subsonic flow and the disturbances are larger at the larger lift coefficients. A linearised theory has the important advantages in a design problem of permitting the superposition of solutions and allowing the separation of lifting and thickness effects. The theory provides an expression for the local slope of the mean surface of the wing as a double integral over the planform of a function related to the lift distribution. When the position of some line connecting root and tip (in the present case the trailing edge) is specified, the distribution of surface slope can be integrated to yield the shape of the mean surface of the wing. The calculation of mean surfaces from lift distributions with appropriate behaviour at the wing edges has been programmed by Carr[4]. Some indication is given (see Appendix B) that adding the wing thickness normal to the mean surface is more likely to preserve the attachment condition than adding it normal to the wing plane, as was the earlier practice, so the final wing shape is derived by adding, in the cross-flow plane, the wing thickness normal to mean surface.

Lift-dependent drag is conveniently discussed in terms of a lift-dependent drag factor:

$$K = \pi A(C_D - C_{D_0})/C_L^2$$

where A is the aspect ratio and C_{D_0} is the drag coefficient of the unwarped wing of the same planform and thickness distribution at zero incidence. Previous work has shown that, for warped wings designed for an attachment incidence, K is smaller at lift coefficients greater than that at which the flow is attached. This is due to two effects: the non-linear growth of the lift with incidence,

and the alleviation of the drag at higher incidences, obtained because the warped wings have leading edges drooped to meet the incident flow at the attachment incidence, so that the leading edge vortices generate their suction peaks on forward-facing surfaces. Consequently, the attachment lift coefficient (i.e. C_L at the attachment incidence) should be lower than the lift coefficient at which the best performance is required, which we may call the operating lift coefficient. This introduces an empirical element into the design process, since the methods available for the design of wings can only be applied in conditions of attached flow.

The problem is then how to choose a lift distribution at the attachment condition to produce desirable properties at the operating condition. So far, only an appropriate behaviour at the edges has been specified. The centres of pressure at the attachment and operating lift coefficients can be related approximately by a knowledge of the aerodynamic centre of the plane wing, so the condition on the centre of pressure can be transferred to one at the attachment condition. On the basis of previous measurements, the attachment lift coefficient should be about half the operating lift coefficient if the lowest values of lift-dependent drag are to be obtained. It seems reasonable that low drag at the operating condition will be associated with low drag at the attachment condition, so the lift distribution at attachment should be chosen to give a spanwise distribution of chord loading close to the elliptic distribution which is the optimum for inviscid attached flow. To these somewhat imprecise quantitative requirements can be added two entirely qualitative considerations. The pressure distribution resulting from the lifting and thickness contributions should involve only modest adverse pressure gradients, so that boundary layer separation is avoided at the attachment condition and the leading-edge vortices dominate any subsequent separation at higher incidences. Finally, the shape of the wing resulting from the addition of the thickness to the warp surface should be free from unnecessary waviness.

The approach described above has been followed in the design of five exploratory warped models for flow visualization and three-component balance measurements in the low speed 4ft × 3ft tunnel at RAE Farnborough. All have a common 'mild gothic' planform (see Fig.1) of aspect ratio 1.4, which has suitable performance and balance properties. The volume distribution is biconvex in cross-section, with a centre section related to the incorporation

of a pressure cabin within the wing[4] in the 9% thick version shown in Fig.2. Four of the warped wings have this thickness and one has a similar volume distribution of 4% thickness intended for combination with a fuselage. The test programme includes two unwarped wings with these volume distributions. All the warp distributions were designed for a Mach number of zero and for the same spanwise distribution of chord loading. Other factors influencing the design have been kept simple where possible.

The first warped wing was designed for an attachment lift coefficient of 0.1, which is the largest attachment lift coefficient used in previous investigations of slender wings, but still less than half the lift coefficient of 0.4 to 0.5 envisaged for the 'operating' condition of take-off[5]. Its centre of pressure was chosen to coincide with an estimated position of the aerodynamic centre of the plane wing, so that it should vary little between the attachment and operating conditions. Its trailing edge was a straight line.

The other four warped wings each differ from this specification in one particular. One has an attachment lift coefficient of 0.2, to assess more precisely the appropriate relation between the attachment and operating lift coefficients. Another has its centre of pressure at attachment 0.05 of its length further forward, to indicate whether increasing longitudinal stability introduced a performance penalty. The next is the wing of 4% centreline thickness. The last has its trailing edge modified to a gull-wing form by the incorporation of dihedral inboard and anhedral outboard (see Fig.43). The object was to discover whether a performance penalty arises from an attempt to use the wing to reduce the lateral propagation of noise from an overwing engine installation. A summary of the wings designed is given in Table 1.

Some results of the tests are already available[6], but no attempt will be made to assess them here, as the programme is not complete.

2 DETAILS OF THE DESIGN PROCEDURE

These models were designed using the linearised theory of subsonic flow past thin wings to have specified distributions of lift at the attachment incidence. In linearised theory, the effects of warp and volume can be considered separately. Thus a volume distribution chosen independently can be added to a warped mean surface without affecting its lifting properties. The pressure distributions on the upper and lower surfaces, are, in this approximation, just the sums of those produced by the warp and the volume separately.

2.1 Choice of planform and volume distribution

All the warped models have a common planform and the same form of volume distribution, though one of the models has approximately half the thickness to chord ratio of the other four.

The choice of planform and volume distribution for a slender all-wing aircraft depends mainly on layout, stability and trim considerations. Structural aspects and aerodynamic performance interact with these, so that a detailed study aimed at a specific application is needed to resolve them. For the present purpose it was decided to continue with a simple planform and volume distribution which had been chosen by Handley Page Ltd. as typical of what might emerge from a more detailed examination. A similar planform was used by Küchemann and Weber[1] in a discussion of layout and balance problems.

The planform, shown in Fig.1, is of the gothic type, but is intermediate in form between the full, parabolic gothic and the delta. In fact, its area, for given span and length, falls midway between those of the gothic and the delta. It is called a 'mild gothic'. Using a Cartesian coordinate system (x,y,z), nondimensionalised with respect to the root chord c, which has its origin at the apex, x axis along the planform centreline, y axis to starboard and z axis vertically, see Fig.1, the equation for the starboard leading edge is

$$y = s(x) = \frac{s_T}{4}(5x - x^5) \qquad (1)$$

where s_T is the semispan at the trailing edge.

This has been taken as $s_T = 0.40385$,

giving an aspect ratio $A = 1.385$,

planform parameter $p = 7/12$,

and leading-edge sweep-back angle at the apex of $63^\circ 13'$.

The distribution of volume over the wing was originally defined in relation to a broad central pressure cabin. Cross-sections of biconvex parabolic form were drawn to contain the cabin, so defining much of the centre section. This part of the centre section was continued smoothly forward to the apex and aft to the trailing edge, and the remaining cross-sections were also taken to be parabolic for simplicity. This produced the wing shown in Fig.2,

with a thickness to chord ratio of about 9% on the centreline and leading edge angles which are small enough not to interfere with vortex development. The pressure distribution, shown in Figs.3-5 involves only modest adverse pressure gradients. The upper surface ordinate of the volume distribution is of the form

$$z_v(x,y) = B(x)\left(1 - \frac{y^2}{s(x)^2}\right) \qquad (2)$$

where $B(x)$ can be represented to sufficient accuracy by the sixth order polynomial:

$$B(x) = x(1 - x)(0.29224 - 0.68199x + 1.60782x^2 - 1.72866x^3 + 0.69079x^4) \quad .(3)$$

This distribution of volume was used for four of the warped wings. The remaining warped wing was made thinner, with a view to eventual combination with a fuselage. The same planform was retained and a thickness-to-chord ratio of 4% on the centreline was chosen for consistency with an extensive series of measurements on unwarped wings[7]. The same variation of thickness was used as on the other models, the volume distribution being

$$z_v(x,y) = 0.44314\ B(x)\left(1 - \frac{y^2}{s(x)^2}\right) \quad . \qquad (4)$$

The pressure distribution due to the volume distribution was calculated using the linearised theory of subsonic flow past thin wings. In this theory, the flow due to the volume distribution is represented by a distribution of sources over the planform, where the source strength is twice the streamwise derivative of the upper surface ordinate. The disturbance velocity potential of this flow is therefore

$$\phi(x,y,z) = -\frac{U}{2\pi}\iint_S \frac{\partial z_v}{\partial x_1}(x_1,y_1)\,\frac{dx_1 dy_1}{[(x - x_1)^2 + \beta^2(y - y_1)^2 + \beta^2 z^2]^{\frac{1}{2}}}$$

where U is the free stream velocity, z_v is the upper surface ordinate of the volume distribution, S denotes the planform area, and $\beta^2 = 1 - M^2$, where M is the Mach number of the undisturbed flow.

Using the linearised theory approximation for the pressure coefficient, C_p, i.e.,

$$C_p = -\frac{2}{U}\frac{\partial \phi}{\partial x}$$

the pressure coefficient at a point (x,y) on the wing is

$$C_p(x,y) = \frac{1}{\pi}\frac{\partial}{\partial x}\iint_S \frac{\partial z_v}{\partial x_1}(x_1,y_1)\,\frac{dx_1 dy_1}{[(x-x_1)^2+\beta^2(y-y_1)^2]^{\frac{1}{2}}}$$

This integral can be integrated by parts with respect to x_1, and the differentiation with respect to x then leads to an expression for C_p which is easy to evaluate numerically for sharp-edged wings, on which the slope is everywhere finite:

$$C_p(x,y) = \frac{1}{\pi}\left[\int_{-s_T}^{s_T}\left\{\frac{\lambda(x_L,y_1)}{[(x_L-x)^2+\beta^2(y-y_1)^2]^{\frac{1}{2}}} - \frac{\lambda(x_T,y_1)}{[(x_T-x)^2+\beta^2(y-y_1)^2]^{\frac{1}{2}}}\right\} dy_1 + \iint_S \frac{\partial\lambda(x_1,y_1)}{\partial x_1}\,\frac{dx_1 dy_1}{[(x-x_1)^2+\beta^2(y-y_1)^2]^{\frac{1}{2}}}\right] \tag{5}$$

where

$$\lambda(x,y) = \frac{\partial z_v}{\partial x}(x,y) \tag{6}$$

and $x_L(y_1)$ and $x_T(y_1)$ are the values of x at the leading and trailing edges.

The integration (5) has been programmed[4] in Extended Mercury Autocode. The volume distribution can be specified by providing numerical values of derivatives of the volume distribution, λ and $\partial\lambda/\partial x$, at points of a grid over the planform. The volume derivatives at any point on the planform are then obtained by the program by interpolation. Alternatively, if the volume distribution can be specified analytically, a small section can be written into the program to evaluate the derivatives directly. The latter procedure has been used as it takes less computing time for simple shapes and is more accurate.

The pressure distributions calculated using the program for various spanwise and chordwise sections on the thicker symmetrical wing, with volume distribution (2), are shown in Figs.3 and 4, and the isobars on the wing are drawn in Fig.5. The calculated pressure distributions are not valid in the immediate neighbourhood of the edges of the planform, since the linearised theory predicts an unrealistic logarithmic singularity at an edge which is sharp but not cusped. The figures suggest that the regions affected by these singularities are small. Fig.5 shows that the pressure distribution is smooth, with a broad, low suction peak. The adverse pressure gradients over the rear are moderate and fairly uniform across the span.

2.2 Choice of load distribution and the resulting mean surface

According to the linearised theory of subsonic flow over thin wings, the local streamwise slope $\alpha(x,y)$ of the mean surface, which will give a specified load distribution over the wing, is given by a double integral over the wing planform of the product of a kernel function and a function directly related to the load distribution $\ell(x,y)$, i.e. each lifting element induces a downwash and the resulting surface slope is the sum of these contributions. Thus

$$\alpha(x,y) = -\frac{1}{8\pi}\iint_S \frac{\ell(x_1,y_1)}{(y-y_1)^2}\left[1+\frac{(x-x_1)}{\{(x-x_1)^2+\beta^2(y-y_1)^2\}^{\frac{1}{2}}}\right]dx_1dy_1 \quad (7)$$

where the integral must be interpreted as a principal value integral.

The wings considered here are designed at their attachment condition, when the load vanishes along the leading edges of the wing. For this case, the integral (7) can be expressed[4] in a form suitable for direct numerical evaluation as

$$\alpha(x,y) = \frac{1}{4\pi U}\iint_S \left[\beta^2\frac{\partial^2\Delta\phi}{\partial x_1^2}+\frac{\partial^2\Delta\phi}{\partial y_1^2}\right]\frac{dx_1dy_1}{[(x-x_1)^2+\beta^2(y-y_1)^2]^{\frac{1}{2}}}$$

$$-\frac{1}{4\pi U}\int_{-s_T}^{s_T}\frac{\partial^2\Delta\phi(x_T,y_1)}{\partial y_1^2}\log\left[x_T(y_1)-x+[(x_T(y_1)-x)^2+\beta^2(y-y_1)^2]^{\frac{1}{2}}\right]dy_1 \quad \ldots (8)$$

where $\Delta\phi(x,y)$ is the difference in the velocity potential between lower and upper surfaces. The local load, which is the difference in pressure coefficient between lower and upper surfaces of the wing, is

$$\ell(x,y) = -\frac{2}{U}\frac{\partial \Delta\phi}{\partial x} \quad . \tag{9}$$

Some method for specifying $\Delta\phi$ was required in order to program the integration (8) for α. Experience in designing slender wings for supersonic flow led to this general expression for $\Delta\phi$ being adopted

$$-\frac{\Delta\phi}{2U} = (1-\eta^2)^{3/2}\left[(1-x)^{3/2}\sum_{n=0}^{N} a_n(x)\eta^{2n} + s(x)\sum_{\ell=0}^{L} h_\ell \eta^{2\ell}\right] \tag{10}$$

where

$$a_n(x) = \sum_{m=1}^{M} b_{n,m}x^m \tag{11}$$

and

$$\eta = \frac{y}{s(x)} \quad ,$$

so that the local load is given by

$$\ell(x,y) = 4\left\{(1-\eta^2)^{\frac{1}{2}}(1-x)^{\frac{1}{2}}\sum_{n=0}^{N}\sum_{m=1}^{M} b_{n,m}\eta^{2n}x^{m-1}\left[x\frac{s'(x)}{s(x)}(1-x)\{(3+2n)\eta^2-2n\}\right.\right.$$
$$\left.\left. + (1-\eta^2)\left\{m-x\left(m+\frac{3}{2}\right)\right\}\right]$$
$$+ s'(x)(1-\eta^2)^{\frac{1}{2}}\left[(1+2\eta^2)\sum_{\ell=0}^{L} h_\ell\eta^{2\ell} - \eta(1-\eta^2)\sum_{\ell=1}^{L} 2\ell h_\ell \eta^{2\ell-1}\right]\right\} \quad .$$

The program is restricted to planforms with streamwise tips and unswept trailing edges. The leading edge is represented by a polynomial or series of polynomials

$$s(x) = \sum_{J=0}^{J_k} c_{k,J}x^J \quad \text{for} \quad x_{k-1} \leqslant x \leqslant x_k \quad . \tag{12}$$

The use of the combination $\eta = y/s(x)$ in (10) makes it possible to specify an appropriate behaviour at the leading edges. Although a similarly defined chordwise variable, such as $\xi = (x - x_L(y))/(x_T(y) - x_L(y))$, would also permit the specification of the leading edge behaviour, it would lead naturally to a consideration of streamwise sections, rather than of spanwise sections, which are more significant on a slender wing. The required behaviour, that the load vanishes at the leading edge like the square root of the distance from it, is enforced by the first factor in (10). The form (10) was chosen before the singular behaviour of the loading at the apex of the plane wing had been calculated[8]. The form given is appropriate for wings of vanishing aspect ratio and no difficulty has been found in calculating smooth distributions of surface slope from it. The restriction to terms in η^2 produces lateral symmetry and avoids the difficulties which arise when differentiating functions of $|\eta|$. The second factor on the right of (10) contains two terms. The first of these is included to provide the appropriate behaviour of the load very near the trailing edge, which is that the load tends to zero like the square root of the distance from the edge. This term also controls the variation of the load along the length of the wing. However its contribution to the chord loading (proportional to $\Delta\phi$ at $x = 1$) is zero, and the chord loading is determined entirely by the second term in the second factor on the right of (10).

We discuss the spanwise distribution of chord loading in terms of

$$D(\eta) = \frac{1}{2\bar{c}} \int_{x_L}^{x_T} \ell(x,\eta)\, dx$$

$$= \frac{2}{\bar{c}} (1 - \eta^2)^{3/2} s_T \sum_{\ell=0}^{L} h_\ell \eta^{2\ell} \qquad (13)$$

where $\bar{c}$ is the geometric mean chord, which is 7/12 for the mild gothic planform. The lift coefficient is given by

$$C_L = \int_{-1}^{1} D(\eta) d\eta$$

$$= \frac{3\pi s_T}{\bar{c}} \left[\sum_{\ell=1}^{L} h_\ell \frac{(2\ell-1)(2\ell-3)\ldots 1}{2^{\ell+1}(\ell+2)!} + \frac{h_0}{4} \right] . \qquad (14)$$

The dependence of the lift-dependent drag on $D(\eta)$ and hence on the coefficients h_ℓ in equation (10) is discussed in Appendix A.

The other features of interest in the loading involve all the coefficients $b_{n,m}$. In particular, the distance of the centre of pressure from the apex, x_{cp}, is given by

$$\iint_S (x - x_{cp})\ell(x,y)dxdy = 0$$

so that

$$\left(s_T^2(1-x_{cp}) - \int_0^1 [s(x)]^2 dx\right) \frac{C_L \bar{c}}{3\pi s_T} = \sum_{m=1}^{M} \int_0^1 s(x)(1-x)^{3/2} x^m \left[\sum_{n=1}^{N} \frac{(2n-1)\ldots 1}{2^{n+1}(n+2)!} b_{n,m} + \frac{b_{0,m}}{4}\right] dx \quad . \tag{15}$$

The design of the warp distributions for the present models starts with a choice of chord loading. As discussed in section 1, this should correspond to a low vortex drag at the attachment condition. In addition, we wish to avoid the waviness of surface and load distributions often associated with optimum solutions (e.g. Smith and Mangler[9]). Accordingly we choose the chord loading previously used in the design of slender wings for supersonic speeds[2]:

$$D(\eta) = \frac{2}{\bar{c}} (1 - \eta^2)^{3/2} s_T h_0 (1 + 0.6\eta^2 + 1.6\eta^4) \tag{16}$$

illustrated in Fig.6. According to slender wing theory, this corresponds to a smooth load distribution and yields a surface which is almost flat inboard, with leading edge droop outboard of a 'shoulder'. Its lift-dependent drag factor is calculated in Appendix A to be only 10% above the overall minimum. The lift coefficient follows from (14):

$$C_L = \frac{0.9\pi s_T h_0}{\bar{c}} \tag{17}$$

so that h_0, and hence the second part of the expression for $\Delta\phi$, are fixed when the attachment lift coefficient is specified.

To illustrate the procedure used to specify the remainder of $\Delta\phi$, the design of the warp surface for the first of the warped wings (see section 3.1)

is described below. Superposition of solutions is used to generate suitable warp surfaces from simple basic distributions.

The simplest choice for the coefficients in the first part of (10) is to make them proportional to those in the second part, i.e. if h_p is the first non-zero coefficient in the second part, we write

$$a_n(x) = \frac{h_n}{h_p} a_p(x) \qquad \text{for} \quad p \leqslant n \leqslant N = L$$

and $$a_n(x) = 0 \qquad \text{for} \quad n \leqslant p - 1 \quad .$$

A simple distribution of $\Delta\phi$ with this similarity condition and $M = 1$, $N = 2$ was considered, so that

$$-\frac{\Delta\phi}{2U} = (1 - \eta^2)^{3/2} h_0 \left[(1 - x)^{3/2} x \frac{b_{0,1}}{h_0} + s(x) \right] [1 + 0.6\eta^2 + 1.6\eta^4] \quad . \quad (18)$$

The ratio $b_{0,1}/h_0$ is fixed by x_{cp}, and is given from equations (15) and (17)·

$$\frac{b_{0,1}}{h_0} \int_0^1 s(x)(1 - x)^{3/2} x dx = s_T^2(1 - x_{cp}) - \int_0^1 [s(x)]^2 \, dx \quad . \quad (19)$$

The loading specified by the form (18) of $\Delta\phi$ for a C_L of 0.1 and x_{cp} of 0.53306 (chosen for reasons given in section 3.1) was called loading (a), and chordwise distributions of this are shown in Fig.7. Sections in the cross flow plane of the mean surface produced by loading (a) are shown in Fig.8 with the vertical scale multiplied by five for clarity. Although the chordwise sections of the mean surface are smooth, the cross-sections were regarded as being unnecessarily wavy near the centreline, especially towards the apex.

This effect was caused by the spanwise variation of the downwash, and a different variation of $\Delta\phi$ across the span was sought at lengthwise stations other than the trailing edge, where the spanwise distribution of $\Delta\phi$ had been fixed by vortex drag considerations.

From earlier work[2] it is known that if a spanwise distribution of $\Delta\phi$ of the form

$$\Delta\phi = (1 - \eta^2)^{3/2} (a + b\eta^2 + c\eta^4)$$

is considered using slender wing theory, a ratio of a:b:c = 1:0.6:1.6 will produce a camber surface with almost flat central part and a shoulder near $\eta = 0.75$, while a ratio of a:b:c = 1:0.6:0 produces one with a shoulder near $\eta = 0.5$. A distribution of $\Delta\phi$ which varied from the latter spanwise distribution at the apex to the former at the trailing edge was therefore considered.

The $\Delta\phi$ distribution can be written from equation (10), using a single polynomial of the form (12) for the leading edge, as

$$-\frac{\Delta\phi}{2U(1-\eta^2)^{3/2}} = (1-x)^{3/2} \sum_{n=0}^{N} \sum_{m=1}^{M} b_{n,m} x^m \eta^{2n} + \sum_{j=1}^{J} c_j x^j \sum_{\ell=0}^{L} h_\ell \eta^\ell \quad .(20)$$

The condition at the trailing edge becomes

$$h_0 : h_1 : h_2 = 1:0.6:1.6$$

and that at the apex

$$b_{0,1} + h_0 c_1 : b_{1,1} + h_1 c_1 : b_{2,1} + h_2 c_1 = 1:0.6:0 \quad .$$

Thus

$$\begin{aligned} h_1 &= 0.6h_0 \qquad & h_2 &= 1.6h_0 \\ b_{1,1} &= 0.6b_{0,1} \qquad & b_{2,1} &= -1.6h_0 c_1 \end{aligned} \tag{21}$$

and the remaining $b_{n,m}$ coefficients have been made zero. The form of $\Delta\phi$ corresponding to this loading, denoted by loading (b), is then

$$-\frac{\Delta\phi}{2U} = (1-\eta^2)^{3/2} h_0 \left[(1-x)^{3/2} x \left\{ \frac{b_{0,1}}{h_0} (1 + 0.6\eta^2) - 1.6c_1\eta^4 \right\} + s(x)(1 + 0.6\eta^2 + 1.6\eta^4) \right] . \tag{22}$$

The ratio $b_{0,1}/h_0$ can be found by substituting equations (21) and (17) into equation (15), and depends on x_{cp}. The coefficient $c_1 = 1.25s_T$ is 0.50481 for the planform chosen, given by equation (1).

Chordwise distributions of loading (b) for a C_L of 0.1 and x_{cp} of 0.53306 are shown in Fig.9, and cross-sections of the mean surface calculated using this loading are shown in Fig.10, with the vertical scale multiplied by

five for clarity. These are much smoother than those for loading (a), especially near the apex. Moreover, the peak loadings near the leading edge are smaller.

To obtain still smoother cross-sections, it is obviously advisable to proceed further in the same direction, so a loading (c) of twice loading (b) minus loading (a) was considered. The $\Delta\phi$ distribution specifying loading (c) is then

$$-\frac{\Delta\phi}{2U} = (1-\eta^2)^{3/2} h_0 \left[(1-x)^{3/2} x \left\{\frac{b_{0,1}}{h_0}(1+0.6\eta^2) - \frac{1.6}{1.3}\left(2.4c_1 + 1.1\frac{b_{0,1}}{h_0}\right)\eta^4\right\} + s(x)(1+0.6\eta^2+1.6\eta^4)\right] \quad (23)$$

where the dependence of the ratio $b_{0,1}/h_0$ on x_{cp} is, from equations (15), (17) and (23),

$$s_T^2(1-x_{cp}) - \int_0^1 [s(x)]^2\,dx = \frac{1}{1.3}\left(1.1\frac{b_{0,1}}{h_0} - 0.2c_1\right)\int_0^1 s(x)(1-x)^{3/2}\,x\,dx \quad .(24)$$

The chordwise distributions of loading (c) for a C_L of 0.1 and x_{cp} of 0.53306 are shown in Fig.11. They show the expected reduction in peak loadings. The very small negative loads which arise near the trailing edge are not thought to be significant and no steps were taken to remove them in this design. However, negative loads were avoided in the design of the warp surface for the model with the forward centre of pressure position, described in section 3.2. The lengthwise distribution of the cross loading

$$D^*(x) = \frac{1}{S}\int_{-s}^{s} \ell(x,y)\,dy$$

is shown in Fig.12. The cross and chordwise sections of the corresponding mean surface are shown in Figs.13 and 14, with the vertical scale multiplied by five for clarity. These are satisfactorily smooth. Fig.15 shows 'contours' of $\Delta\phi$ (i.e. curves along which $\Delta\phi$ is constant, drawn for equal intervals of $\Delta\phi$). These curves are everywhere in the direction of the bound vorticity vector and are commonly referred to as bound vortices. They provide a discrete approximation to the vorticity distribution 'bound' in the wing, i.e. the vorticity distribution which would generate the same flow field as the wing. The smoothness and even spacing of the bound vortices in Fig.15 are a further indication of the suitability of the design.

2.3 Addition of the volume distribution to the mean surface

It has been customary to define the surface of the warped thick wing such that the z-ordinate of the surface is the sum of the z-ordinates of the mean surface and the volume distribution at each point of the planform. This means, in effect, that the wing thickness z_v is added to the mean surface in a constant direction normal to the plane of the planform. It is shown in Appendix B that to preserve the attachment condition of the warp surface it would be more appropriate to add z_v at each point in the direction normal to the mean surface at this point.

In the design of the present models, the volume distribution has been added to the mean surface in a number of cross-sectional (i.e. y, z) planes, in a direction normal to the cross-section of the mean surface but in the (y, z) plane. This has been done by fitting a fifth order polynomial through those points P_i defining the mean surface outboard of the flat central section and from this calculating the normal to the section of the mean surface by the (y, z) plane at each of the points P_i. The volume ordinate can then be added in the normal direction at each point P_i, so that the upper and lower surfaces of the model in that cross-sectional plane are specified by a distribution of points. This technique produces surface ordinates at points in the same cross-sectional plane as the warp and volume were specified, but at uneven spanwise intervals. This was adequate for model manufacture using cross-sectional templates. A more elaborate numerical technique would be needed if surface ordinates at specified spanwise locations were required.

3 DETAILS OF MODELS

3.1 Basic models with C_L of 0.1 and C_L of 0.2 - wings 1 and 2

For the first warped model, the choice of design parameters was deliberately conservative. An attachment lift coefficient of 0.1 was selected, corresponding to the highest value used in previous work on slender wings at RAE, because the operating lift coefficient envisaged is substantially larger than before, as explained in section 1. In order to concentrate on lift-dependent drag, no attempt was made to affect the stability of the wing through the warp distribution, i.e. the centre of pressure at the attachment condition was chosen to lie at the aerodynamic centre of the unwarped wing.

Neither measurements nor adequate calculations of the behaviour of the unwarped wing were available, so an empirical estimate[10] of its aerodynamic centre was used, based on an extensive series of measurements[7,11] on wings of similar aspect ratios, planform shapes and thicknesses. One advantage of planforms intermediate between the delta and the parabolic gothic is that their aerodynamic centres can be almost independent of lift coefficient over a range of C_L between 0.1 and 0.6 (Ref.7, Fig.25d). The estimated position of the aerodynamic centre was 0.12 of the root chord ahead of the centre of area at $C_L = 0.5$ and the estimate of centre of pressure varied little from this for C_L between 0 and 1. The centre of pressure was chosen to be at this point, i.e. $x_{cp} = 0.53306$.

The warp surface for this model was designed as described in section 2.2, and its properties are displayed in Figs.11 to 15. The volume distribution given by equation (2) was added to the warp surface as described in section 2.3. Cross-sections of the resulting wing are shown in Fig.16 and a side view of the wing at its attachment incidence is shown in Fig.17. The attachment incidence (of the line joining the apex to the mid-point of the trailing edge) is 5.32°. The centre section, shown in Fig.17, has noticeable negative camber, in spite of the attempt to reproduce the longitudinal stability of the unwarped wing. The change of cross-sectional shape of the warp surface, with a shoulder that is further inboard near the apex, produces an effect of this kind.

The pressure distribution, obtained by adding the lifting and thickness contributions, is shown in Figs.18 and 19 in the chordwise and spanwise directions. The isobar pattern on the upper surface is shown in Fig.20. At this attachment condition, the disturbances to the flow are small, the pressure distributions are smooth and the adverse gradients are modest. It therefore seems likely that the main properties of the wing can be described by an inviscid, small-disturbance theory. Doubt about the applicability of the present linear theory may be confined to the use of the thin-wing approximation near the apex, as suggested by the example treated in Appendix B.

For the second warped model the attachment lift coefficient was increased to 0.2, which is around half the operating lift coefficient. Again no attempt was made to influence the stability of the wing. The warp design of the first wing was used with a factor of 2 on the ordinates. The resulting sections are shown in Fig.21, with a side view in Fig.22, the attachment incidence being

10.54°. The pressure distribution is shown in the same form as before in Figs.23, 24 and 25. Although the adverse pressure gradients have steepened, particularly outboard, they are still not severe.

3.2 Model with forward centre of pressure - wing 3

A model with its centre of pressure further forward than in the basic models was designed to investigate the effect of an increase of stability on the performance. The model was designed for a C_L of 0.1 and a centre of pressure of 5% of the root chord further forward (i.e. $x_{cp} = 0.48306$) at the attachment incidence, with a volume distribution given by equations (2) and (3).

It was found that a loading of type (c) produced significant negative load at the rear of the wing. However, by including higher-order terms in x in the first half of the expression (10) for $\Delta\phi$, i.e. $M > 1$, the dominant term in the load near the trailing edge can be made positive instead of negative. Thus the local load $\ell(x,y)$ and the cross-loading $D^*(x)$ can be made non-negative for all x. Proceeding only as far as quadratic terms in x, i.e. $M = 2$, led to load distributions with high loads in the apex region, but the use of cubic terms ($M = 3$) as well allowed the load at the apex ℓ_A to be reduced to a more reasonable value. This could be specified by the choice of $b_{0,1}$ since

$$\ell_A = 4(b_{0,1} + c_1 h_0) \quad . \tag{25}$$

Accordingly, load distributions with $M = 3$ were considered which gave non-negative loadings, a specified local load at the apex, a C_L of 0.1, x_{cp} of 0.48306, the form of chord loading given in equation (14), and which had, for simplicity,

$$b_{n,m} = k_m b_{n,1}$$

where k_2 and k_3 were constants. Loadings (d) and (e) were two such load distributions. Loading (d), like loading (a), had

$$b_{n,m} = \frac{h_n}{h_0} b_{0,m} \quad ,$$

and loading (e) had similarity properties like loading (b):

$$b_{1,1} = 0.6 b_{0,1} \qquad b_{2,1} = -1.6 h_0 c_1 \quad .$$

A loading (f) comprising

$$1.5 \times \text{loading (e)} - 0.5 \times \text{loading (d)}$$

gave reasonably smooth spanwise mean-surface sections and was adopted for this forward-x_{cp} model.

The details of this wing are given in Figs.26-35. Comparison with the first warped model, which has the same C_L but a further aft centre of pressure, is relevant, so the numbers of the corresponding figures for that wing are given in brackets. Fig.26 (11) shows the chordwise distributions of loading. The increase in peak values is marked, in spite of the limitation placed on ℓ_A. The reduction in loading is found near the centre section over the rear of the wing, the load on the tips being maintained in order to keep the lift-dependent drag at the same level. Fig.27 (12) shows the cross loading and suggests that the forward shift has been accomplished smoothly. The bound vortices are shown in Fig.28 (15). The cross-sections shown in Fig.29 (13), with the vertical scale multiplied by five, are rather less smooth than before, and more highly cambered near the apex. The chordwise sections in Fig.30 (14) show increased negative camber, as would be expected, and an increased attachment incidence of 7.62°. The sections of the model, Figs.31 (16) and 32 (17), show the same features. The pressure distributions, Fig.33 (18) and Fig.34 (19), show the concentration of the loading towards the apex and tips. The upper surface isobars are shown in Fig.35 (20).

3.3 The thin model - wing 4

The volume distribution of this model is of the same form as that of the other wings, but the thickness is 4% instead of about 9%. It is described by equation (4) and illustrated in Fig.36.

In principle, the reduction in thickness reduces the beneficial effect which the favourable pressure gradient due to volume over the forward part of each chord (see Fig.3) exerts on the steepest part of the adverse gradients due to lift (see Fig.11). In the present case no attempt was made to compensate for this and the warp surface of the basic design for $C_L = 0.1$, $x_{cp} = 0.53306$ was used with the smaller volume.

The resulting wing is illustrated in Figs.37 and 38. The pressure distributions are shown in Figs.39-41. These closely resemble in shape those for the basic wing with an attachment C_L of 0.2, since both the lifting and volume contributions have been approximately halved (cf. Figs.23-25).

3.4 The gull-wing model - wing 5

Considerable attention is now being paid to alleviating the noise caused by aircraft, and proposals for noise reduction include the mounting of high-bypass-ratio engines above the wings to shield their noise from the ground. This model is an example of the wing of an aircraft adapted to exploit these ideas.

To obtain maximum shielding of both fan and jet noise, the engines must be close to the centre of the wing. In addition, high-bypass-ratio engines have large diameter and must probably be mounted well clear of the wing surface. Thus for a typical airbus configuration with a rootchord of 40 metres, and semispan at the trailing edge of 16 metres, the high-bypass-ratio engines may be mounted close to the centre section at 60% of the root chord at a height such that the noise source of the engines is about 3 metres above the upper surface of the wing. At spanwise sections near the engines, around 60 or 70% of the root chord, the noise sources will thus be about 3 metres above the upper surface of a cross-section of about 10 metres semispan. In order to provide adequate sideways noise-shielding at these sections, noise propagated laterally from the engines at more than about 15^{o} below the horizontal should be cut off. Moreoever, recent work[12] suggets that the wing surface outboard of the cut-off point should have curved droop to minimise the diffracted noise field within the shadow of the aircraft. To fulfil these conditions, the wing upper surface outboard of the centreline must curve first upwards and then droop downwards, as sketched in Fig.42. In other words, in the region of the engines, the wing must have dihedral inboard and anhedral outboard.

Such a gull-wing model has been designed to discover whether incorporating these features, desirable for noise reduction, involves performance penalties. Slender gull-wings have previously been designed[13] by slender thin-wing theory and experimental investigations[14] have shown that the behaviour of slender wings in cross winds can be considerably improved by anhedral over the rear part of the wing.

The model was designed to have the same volume distribution, lift, centre of pressure position and load distribution at the same attachment incidence as the $C_L = 0.1$ model, and thus its mean surface has the same streamwise slopes. However, it differs from the $C_L = 0.1$ model in that its trailing edge, from which the mean surface slopes are integrated, is warped and not straight. A trailing edge warp was chosen that gives the required shielding

in the neighbourhood of the engines, and produces little effect on the warp of the forward sections. It has about 20° dihedral inboard and 40° anhedral outboard with a smooth transition between dihedral and anhedral so that the rear sections of the model are curved smoothly.

The trailing edge warp chosen is given by: a blending section near the centreline

$$z = \frac{0.90992}{s_T} y^2 \qquad \text{for } 0 \leqslant |y| \leqslant 0.2s_T;$$

an inboard section with dihedral

$$z = 0.36397\ y - 0.03640s_T \qquad \text{for } 0.2s_T \leqslant |y| \leqslant 0.6s_T;$$

a blending section outboard

$$z = \frac{-2.00512}{s_T} y^2 + 2.77011\ y - 0.75824s_T \qquad \text{for } 0.6s_T \leqslant |y| \leqslant 0.9s_T;$$

and an outboard section with anhedral

$$z = -0.8391\ y + 0.86591s_T \qquad \text{for } 0.9s_T \leqslant |y| \leqslant s_T.$$

The trailing-edge warp and cross-sections of the model are shown in Fig.43. The centre section and streamwise variation of the leading edge are illustrated in Fig.44a and the side view of the model in Fig.44b. The pressure distribution on the model is the same as for the C_L 0.1 model and is illustrated in Figs.18, 19 and 20.

4 CONCLUSIONS

It has been demonstrated that smoothly warped wings embodying various desirable features can be designed for subsonic flight using mean surfaces which, according to linear lifting-surface theory, sustain specified distributions of aerodynamic loading. The examples calculated all have an attachment condition at non-zero lift and are intended to have low vortex drag at and above this condition. They cover variations in the attachment lift coefficient, in the centre of pressure at the attachment condition, in thickness and in the warp of the trailing edge. They form a series of wings on which a number of wind tunnel tests are to be carried out to investigate the performance and stability benefits introduced by warp of this form.

Appendix A

THE CALCULATION OF VORTEX DRAG

The vortex drag, D_v, of a lifting surface is given[15] by

$$\frac{D_v}{\frac{1}{2}\rho U^2} = -\frac{1}{2\pi}\int_{-1}^{1}\int_{-1}^{1}\frac{d}{d\eta}\left(\frac{\Delta\phi_T(\eta)}{U}\right)\frac{d}{d\eta'}\left(\frac{\Delta\phi_T(\eta')}{U}\right)\log|\eta-\eta'|\,d\eta d\eta' \qquad (A\text{-}1)$$

where $\eta = y/s_T$ and $\Delta\phi_T$ is the jump in velocity potential at the trailing edge. We represent this by

$$\frac{\Delta\phi_T}{U} = \sum_{n=1}^{N}\frac{\alpha_n}{n}\sin n\theta \qquad (A\text{-}2)$$

where

$$\cos\theta = \eta \ . \qquad (A\text{-}3)$$

This expression satisfies the condition that $\Delta\phi_T$ is zero for $\eta = \pm 1$, i.e. when $\theta = 0$ or π. For the symmetrical case which interests us, the summation is over odd values of n only. We have then

$$\frac{d}{d\eta}\left(\frac{\Delta\phi_T(y)}{U}\right) = -\frac{1}{\sin\theta}\sum_{n=1}^{N}\alpha_n\cos n\theta \ . \qquad (A\text{-}4)$$

Substituting in equation (A-1), we obtain

$$\frac{D_v}{\frac{1}{2}\rho U^2} = -\frac{1}{2\pi}\int_0^{\pi}\int_0^{\pi}(\Sigma\alpha_m\cos m\theta)(\Sigma\alpha_n\cos n\theta')\log|\cos\theta-\cos\theta'|\,d\theta d\theta'$$

$$= -\frac{1}{2\pi}\sum_{m=1}^{M}\sum_{n=1}^{N}\alpha_m\alpha_n\int_0^{\pi}\int_0^{\pi}\cos m\theta\cos n\theta'\log|\cos\theta-\cos\theta'|\,d\theta d\theta' \ .$$

Consider the integral

$$\int_0^{\pi}\int_0^{\pi}\cos m\theta\cos n\theta'\log|\cos\theta-\cos\theta'|\,d\theta d\theta' = \int_0^{\pi}\cos n\theta' f_m(\theta')\,d\theta'$$

where

$$f_m(\theta') = \int_0^{\pi} \cos m\theta \log |\cos\theta - \cos\theta'| \, d\theta$$

$$= \left[\frac{\sin m\theta}{m} \log |\cos\theta - \cos\theta'|\right]_0^{\pi} - \int_0^{\pi} \frac{\sin m\theta}{m} \cdot \frac{-\sin\theta}{(\cos\theta - \cos\theta')} \, d\theta$$

$$= \frac{1}{2m} \int_0^{\pi} \frac{\cos(m-1)\theta - \cos(m+1)\theta}{\cos\theta - \cos\theta'} \, d\theta \quad .$$

So, by 332.21c of Ref.16,

$$f_m(\theta') = \frac{1}{2m} \frac{\pi}{\sin\theta'} (\sin(m-1)\theta' - \sin(m+1)\theta') = \frac{-\pi \cos m\theta'}{m} \quad .$$

Thus

$$\int_0^{\pi}\int_0^{\pi} \cos m\theta \cos n\theta' \log |\cos\theta - \cos\theta'| \, d\theta d\theta' = -\frac{\pi}{m} \int_0^{\pi} \cos n\theta' \cos m\theta' \, d\theta'$$

$$= \begin{cases} 0 & \text{for } m^2 \neq n^2 \\ \dfrac{-\pi^2}{2m} & \text{for } m = n, \text{ as } m \text{ and } n \text{ are } \geq 1 \end{cases} .$$

Therefore, we obtain

$$\frac{D_v}{\frac{1}{2}\rho U^2} = \frac{\pi}{4} \sum_{m=1}^{N} \frac{\alpha_m^2}{m} \quad . \tag{A-5}$$

The lift, L, of the surface is given by

$$\frac{L}{\frac{1}{2}\rho U^2} = 2 \int_{-S_T}^{S_T} \frac{\Delta\phi_T}{U} \, dy = 2s_T \int_0^{\pi} \Sigma \frac{\alpha_n}{n} \sin n\theta \sin\theta \, d\theta$$

$$= \pi s_T \alpha_1 \quad . \tag{A-6}$$

The lift-dependent drag factor K is

$$K = \pi A \frac{(C_D - C_{D_0})}{C_L^2}$$

$$= 4\pi s_T^2 \left(\frac{D_v}{\frac{1}{2}\rho U^2}\right) \Big/ \left(\frac{L}{\frac{1}{2}\rho U^2}\right)^2 \quad .$$

Substituting from equations (A-5) and (A-6), we obtain

$$K = \sum_{m=1}^{N} \frac{1}{m} \left(\frac{\alpha_m}{\alpha_1}\right)^2 \quad , \tag{A-7}$$

from which it is clear that $K \geqslant 1$, with $K = 1$ when $\alpha_m = 0$ for $m \geqslant 2$.

In the present work, the form of $\Delta\phi_T/U$ has been taken as

$$\frac{\Delta\phi_T}{U} = (1 - \eta^2)^{3/2} \times (\text{a polynomial of order M in } \eta^2) \ .$$

This can easily be rewritten as

$$\frac{\Delta\phi_T}{U} = \sin^3\theta \ (b_0 + b_1 \sin^2\theta + b_2 \sin^4\theta + \ldots\ldots + b_M \sin^{2M}\theta) \ . \tag{A-8}$$

By comparison with equation (A-2) we obtain

$$\sum_{p=0}^{M+1} \frac{\alpha_{2p+1}}{2p+1} \sin(2p+1)\theta = \sum_{m=0}^{M} b_m \sin^{2m+3}\theta \tag{A-9}$$

whence, multiplying by $\sin(2p+1)\theta$, integrating from 0 to π, and using equations 332.6b and 332.8c of Ref.16,

$$\frac{\alpha_{2p+1}}{2p+1} \frac{\pi}{2} = \sum_{m=\max(0,p-1)}^{M} b_m \frac{(-1)^p}{2^{2m+3}} \binom{2m+3}{m+1-p} \pi$$

or

$$\alpha_{2p+1} = (-1)^p(2p + 1) \sum_{m=\max(0,p-1)}^{M} \frac{b_m}{2^{2m+2}} \binom{2m + 3}{m + 1 - p} \qquad \text{for } 0 \leqslant p \leqslant M + 1 \qquad \ldots \text{(A-10)}$$

For an example consider a distribution of $\Delta\phi_T$ given by

$$\frac{\Delta\phi_T}{U} = K_0(1 - \eta^2)^{3/2}(1 + 0.6\eta^2 + 1.6\eta^4) \qquad \text{(A-11)}$$

where K_0 is a constant and M = 2. Then

$$\frac{\Delta\phi_T}{U} = K_0 \sin^3\theta\ (3.2 - 3.8 \sin^2\theta + 1.6 \sin^4\theta)$$

so $b_0 = 3.2K_0$ $b_1 = -3.8K_0$ $b_2 = 1.6K_0$

whence, by equation (A-10)

$$\alpha_1 = 0.9K_0 \quad \alpha_3 = -0.4125K_0 \quad \alpha_5 = -0.3125K_0 \quad \alpha_7 = -0.175K_0 \ .$$

Substituting in the expression for the lift-dependent drag factor, which is, from equation (A-7),

$$K = \sum_{p=0}^{M+1} \frac{1}{(2p + 1)} \left(\frac{\alpha_{2p+1}}{\alpha_1}\right)^2 \qquad \text{(A-12)}$$

we obtain $K = 1.0995$.

This can be compared with the minimum lift-dependent drag factor of unity. Another meaningful comparison is with the minimum value which can be obtained using an expression of the form given in (A-8). For this $\Delta\phi_T/\sin\theta$ tends to zero as θ tends to zero, and so

$$\sigma \equiv \sum_{p=0}^{M+1} \alpha_{2p+1} = 0 \ .$$

For K to be a minimum subject to this condition we require

$$\frac{\partial}{\partial\alpha_{2p+1}} (K - \lambda\sigma) = 0 \ ; \ \sigma = 0 \quad \text{for } M + 1 \geqslant p > 0$$

or

$$\frac{2}{(2p+1)}\frac{\alpha_{2p+1}}{\alpha_1^2} - \lambda = 0 \quad ; \quad \sigma = 0 \quad .$$

Therefore

$$\alpha_{2p+1} = \frac{\lambda\alpha_1^2}{2}(2p+1) \qquad \text{for } p = 1, \ldots, M+1$$

and

$$\alpha_1\left(1 + \frac{\lambda\alpha_1}{2}\sum_{p=1}^{M+1} 2p+1\right) = 0 \quad .$$

Therefore

$$\lambda = \frac{-2}{\alpha_1(M+1)(M+3)} \quad \text{and} \quad \frac{\alpha_{2p+1}}{\alpha_1} = \frac{-(2p+1)}{(M+1)(M+3)} \quad .$$

Hence the minimum value of K, K_{min}, is

$$K_{min} = 1 + \sum_{p=1}^{M+1}\frac{1}{(2p+1)}\left(\frac{2p+1}{(M+1)(M+3)}\right)^2$$

therefore

$$K_{min} = 1 + \frac{1}{(M+1)(M+3)} \quad .$$

Thus for a $\Delta\phi_T$ distribution with three terms in the polynomial in η^2 (i.e. $M = 2$), the minimum value of K attainable is 1.0667. The value obtained from the distribution in equation (A-11) is 1.0995, which is close to the minimum.

Appendix B

THE ATTACHMENT INCIDENCE OF A THICK WARPED WING

In the linear theory of subsonic (or supersonic) flow, the effects of thickness and warp are separable. A thick warped wing is represented by a distribution of sources (volume-producing elements) and lift-producing elements over a mean plane, on which the boundary conditions satisfied on the surface are applied in a linearised form. It is customary to construct a thick wing by adding thickness equally above and below a warp (or mean) surface in a direction normal to the mean plane, and to construct the warp surface of a thick wing by taking the average of upper and lower surface ordinates measured from the mean plane. This is geometrically simple and retains the relation between source strength and volume which is useful in supersonic linear theory.

However, it is not obvious that another relationship between the thick warped wing and its 'warp surface' might not be more appropriate, for instance, to make the attachment incidences of the thick wing and the warp surface correspond more closely. Indeed, it seems intuitively that adding thickness normal to the warp surface is less likely to change the attachment incidence than adding it in some direction unrelated to its local shape. A systematic investigation of this idea has not been attempted for the present purpose, though it could be undertaken by a surface singularity method like that of Hummel[17] for slender body theory or A. Roberts, of BAC, Weybridge, for incompressible flow. Instead, some evidence is presented from earlier work using slender body theory.

Before presenting this evidence, a little further examination of the idea is necessary. If we are designing a wing, then the warp surface is likely to be the starting point, the direction of its normal is known and the thickness can readily be added in the normal direction. On the other hand, if we are considering the direct problem of the properties of a given thick, warped wing, the construction of a warp surface which lies midway between the upper and lower surfaces, measured normal to the warp surface, presents considerable difficulty. Instead, it seems natural to start from the given upper and lower surfaces and proceed along the normals to them, to define a warp surface which is midway between them, measured normal to the upper and lower surfaces themselves. Obviously, these definitions of warp surfaces are

distinct from one another, as well as from the usual definition used in linear theory. We shall show now that the two new definitions of the warp surface agree to second order in the wing slope, but differ from the linear theory definition by a term of second order.

Consider a wing whose upper and lower surfaces, in a given cross-flow plane x = constant, are given by $z = z_u(y)$ and $z = z_\ell(y)$ (see Fig.45). We define three warp surfaces $z_i(y)$, $i = 1,2,3$ with associated thickness $\delta_i(y)$. The first is the classical definition of linear theory:

$$\left.\begin{aligned} z_1(y) &= \tfrac{1}{2}(z_u(y) + z_\ell(y)) \\ \delta_1(y) &= \tfrac{1}{2}(z_u(y) - z_\ell(y)) \end{aligned}\right\} \qquad \text{(B-1)}$$

For the other two definitions we need to introduce an angle $\psi(y)$ between the tangent to the curve $z = z(y)$ and the y axis, with subscripts u, ℓ, 1, 2 and 3 to ψ and z. Then if we start from the warp surface $z = z_2(y)$ and add thickness $\delta_2(y)$ normal to the warp surface (the design problem) we find

$$\left.\begin{aligned} z_2(y) + \delta_2(y)\cos\psi_2(y) &= z_u(y - \delta_2(y)\sin\psi_2(y)) \\ z_2(y) - \delta_2(y)\cos\psi_2(y) &= z_\ell(y + \delta_2(y)\sin\psi_2(y)) \end{aligned}\right\} \qquad \text{(B-2)}$$

The third case is a little more complicated. Normals of length $\delta_3(y)$ are drawn to the upper and lower surfaces to meet at a point $(y, z_3(y))$ on the warp surface. If the values of ψ_u and ψ_ℓ at the points from which these normals are drawn are $\bar{\psi}_u$ and $\bar{\psi}_\ell$, we have

$$\left.\begin{aligned} z_3(y) + \delta_3(y)\cos\bar{\psi}_u(y) &= z_u(y - \delta_3(y)\sin\bar{\psi}_u(y)) \\ z_3(y) - \delta_3(y)\cos\bar{\psi}_\ell(y) &= z_u(y + \delta_3(y)\sin\bar{\psi}_\ell(y)) \end{aligned}\right\} \qquad \text{(B-3)}$$

and

$$\left.\begin{aligned} \bar{\psi}_u(y) &= \psi_u(y - \delta_3(y)\sin\bar{\psi}_u(y)) \\ \bar{\psi}_\ell(y) &= \psi_\ell(y + \delta_3(y)\sin\bar{\psi}_\ell(y)) . \end{aligned}\right\} \qquad \text{(B-4)}$$

Now assume, as usual, that the warp and thickness are small, so that ψ is small compared with unity, and expand equations (B-2) and (B-3), keeping terms of second order in ψ, using Taylor's theorem for the right hand sides and noting that z' is of the order of ψ:

$$\left.\begin{aligned} z_2 + \delta_2 - \tfrac{1}{2}\delta_2\psi_2^2 &= z_u - z_u'\delta_2\psi_2 \\ z_2 - \delta_2 + \tfrac{1}{2}\delta_2\psi_2^2 &= z_\ell + z_\ell'\delta_2\psi_2 \end{aligned}\right\} \qquad \text{(B-5)}$$

$$\left.\begin{aligned} z_3 + \delta_3 - \tfrac{1}{2}\delta_3\bar{\psi}_u^2 &= z_u - z_u'\delta_3\bar{\psi}_u \\ z_3 - \delta_3 + \tfrac{1}{2}\delta_3\bar{\psi}_\ell^2 &= z_\ell + z_\ell'\delta_3\bar{\psi}_\ell \end{aligned}\right\} \qquad \text{(B-6)}$$

The arguments of all the functions are now y and have been suppressed for compactness. Now the terms involving $\bar{\psi}$ in (B-6) are of second order, so a first order approximation to $\bar{\psi}$ is adequate. From (B-4) this is clearly

$$\bar{\psi}_u(y) = \psi_u(y) \quad \text{and} \quad \bar{\psi}_\ell(y) = \psi_\ell(y)$$

provided ψ' is of the same order as ψ, as is the case for smooth wings. With the bar removed from (B-6), the terms in (B-5) and (B-6) involving ψ are all of second order, so again a first order approximation to ψ is adequate. This is

$$\psi(y) = z'(y)$$

for all suffixes. Equations (B-5) and (B-6) now become

$$\left.\begin{aligned} z_2 + \delta_2 - \tfrac{1}{2}\delta_2 z_2'^2 &= z_u - \delta_2 z_u' z_2' \\ z_2 - \delta_2 + \tfrac{1}{2}\delta_2 z_2'^2 &= z_\ell + \delta_2 z_\ell' z_2' \end{aligned}\right\} \qquad \text{(B-7)}$$

$$\left.\begin{aligned} z_3 + \delta_3 - \tfrac{1}{2}\delta_3 z_u'^2 &= z_u - \delta_3 z_u'^2 \\ z_3 - \delta_3 + \tfrac{1}{2}\delta_3 z_\ell'^2 &= z_\ell + \delta_3 z_\ell'^2 \end{aligned}\right\} \qquad \text{(B-8)}$$

Taking the sums and differences of the pairs of equations (B-7) and (B-8) and eliminating z_u and z_ℓ by (B-1), we have

$$\left.\begin{aligned} z_2 &= z_1 - \delta_2\delta_1' z_2' \\ z_3 &= z_1 - \delta_3\delta_1' z_1' \\ \delta_2 &= \delta_1 - \delta_2 z_2'(z_1' - \tfrac{1}{2}z_2') \\ \delta_3 &= \delta_1 - \tfrac{1}{2}\delta_3(z_1'^2 + \delta_1'^2) \end{aligned}\right\} \qquad \text{(B-9)}$$

The second terms on the right hand side of (B-9) are all of second order, so again first order approximations may be made in them, giving

$$z_2 = z_3 = z_1 - \delta_1\delta_1'z_1' \tag{B-10}$$

$$\delta_2 = \delta_1 - \tfrac{1}{2}\delta_1 z_1'^2 \tag{B-11}$$

$$\delta_3 = \delta_1 - \tfrac{1}{2}\delta_1 z_1'^2 - \tfrac{1}{2}\delta_1\delta_1'^2 = \delta_2 - \tfrac{1}{2}\delta_1\delta_1'^2 \quad . \tag{B-12}$$

Therefore, the three definitions of warp and thickness agree to the first order. To second order, the two modified definitions of the warp agree, but differ from the classical definition by a term which vanishes for an unwarped wing or for a wing of uniform thickness. All three definitions of thickness differ in the second order, the first pair agreeing for an unwarped wing and the second pair for a wing of uniform thickness.

Having established that the warp surfaces obtained by the design approach (z_2) and the direct approach (z_3) agree to second order, equation (B-10), we proceed to our example, which is based on the direct approach.

Consider a slender, thick warped wing in the form of one half of a circular cone. Its cross-section is a semi-circle. Consequently the warp surface obtained by the classical method of bisecting the ordinates normal to a mean plane (say the plane surface of the wing) is a conical surface whose cross-section is an ellipse with minor (vertical) axis one half of its major (horizontal) axis. On the other hand, we find that the cross-section of the warp surface obtained by constructing equal normals from the upper and lower surfaces of a cross-section of the wing is a parabola whose focus is on the plane surface and whose directrix touches the curved surface. Fig.46 shows a parabolic arc L'ML, with focus F, directrix C'DC and latus rectum L'FL. Then if P is a general point on the parabola and PN is normal to C'DC, we have PN = PF by definition of the parabola. In particular, with P at L we see FL = FD; and so a semi-circle L'DL with centre at F can be constructed. If FP produced meets this semi-circle at Q and NP produced meets L'L at R, we see that

$$PQ = FQ - PF = RN - PN = PR \quad .$$

Thus P is equidistant from L'FL and L'DL, each distance being measured normal to the appropriate surface.

The attachment incidences of thin conical wings whose sections are elliptic and parabolic arcs have been found, on the basis of slender body theory, by Ward[18]. He used an electrical resistance network developed by Redshaw[19], containing 144 × 136 square mesh intervals, with electric potential corresponding

to fluid stream function, to simulate Laplace's equation in the cross-flow plane. He was able to recover the analytical results for circular arc sections[20] and found, for the cases of present interest

$$\left(\frac{\alpha}{K}\right)_{att} = \begin{cases} 0.72 & \text{for parabolic-arc section} \\ 1.02 & \text{for elliptic-arc section} \end{cases}$$

where α is the incidence of the plane of the leading edges, K is the tangent of half the apex angle in the plane of the leading edges and each wing has a vertical extent one half of its lateral extent.

The original thick cambered wing in the form of the half-cone has properties that have been found analytically by Portnoy[21], using slender body theory. He treats a more general problem of a wing-body combination, from which the half cone emerges when (in his notation) $\varepsilon = 1$, $f = 1/\sqrt{3}$, and $S' = \pi Ka$, where a is the radius of the circular section. Substituting these values into his equation (20) for the complex potential W in a transformed complex plane ω, we have

$$W = -\frac{8a\alpha}{3\sqrt{3}}\left\{\frac{3}{4} - \frac{2}{(3\omega^2+1)}\right\} + Ka \log\left\{\frac{3^{\frac{3}{4}}a^{\frac{1}{2}}(2\omega + \sqrt{\omega^2-1})^2}{(3\omega^2+1)^{\frac{1}{2}}(\omega+\sqrt{\omega^2-1})}\right\} \qquad \text{(B-14)}$$

where we have changed the sign of the incidence, α, to correspond to a wing with its plane face down. Hence

$$\frac{dW}{d\omega} = -\frac{32a\alpha\omega}{\sqrt{3}(3\omega^2+1)^2} + 3Ka\left\{\frac{1}{(2\omega+\sqrt{\omega^2-1})} - \frac{\omega}{(3\omega^2+1)}\right\} \qquad \text{(B-15)}$$

is the conjugate of the complex velocity in the transformed plane. The transformation between the physical cross-flow plane and the ω-plane is singular at the point $\omega = 1$ corresponding to the leading edge, so the condition for α to be equal to the attachment incidence is that $dW/d\omega = 0$ for $\omega = 1$, i.e.

$$\left(\frac{\alpha}{K}\right)_{att} = \frac{3\sqrt{3}}{8} = 0.65 \quad .$$

The attachment incidence of the thick wing (B-16) is therefore closer to that of the parabolic thin wing than that of the elliptic thin wing (B-13), i.e. the approach adopted in the present work is superior to the usual one in this example. The example is admittedly extreme and the discrepancy between the attachment incidences is large even on the present definition of the warp surface, but it is qualitatively typical of the forward part of thick warped wings like those shown in Figs.21 and 31.

Table 1

SUMMARY OF THE WINGS DESIGNED

Wing number	At attachment condition		Thickness to chord ratio %	Trailing edge shape
	C_L	Centre of pressure		
1 (B of Ref.6)	0.1	aerodynamic centre	9	plane
2 (C of Ref.6)	0.2	aerodynamic centre	9	plane
3	0.1	aerodynamic centre -5% root chord	9	plane
4	0.1	aerodynamic centre	4	plane
5	0.1	aerodynamic centre	9	gull-wing

SYMBOLS

A	aspect ratio
$a_n(x)$	coefficients in expression for $\Delta\phi$, see equations (10) and (11)
$B(x)$	root chord thickness distribution
$b_{n,m}$	coefficients in expression for $\Delta\phi$, see equation (11)
C_D	drag coefficient
C_L	lift coefficient
C_p	pressure coefficient
c	root chord, taken as unit of length
$\bar{c}$	nondimensional geometric mean chord
$c_j, c_{k,j}$	coefficients in the polynomial for the leading edge, see equation (12)
$D(\eta)$	spanwise distribution of chord-loading
$D^*(x)$	lengthwise distribution of cross-loading
D_v	vortex drag
h_ℓ	coefficients in the expression for $\Delta\phi$, see equation (10)
J, J_k	orders of leading-edge polynomials, see equation (12)
K	lift-dependent drag factor
L	overall lift
	also, see equation (10)
ℓ	local load = ΔC_p
ℓ_A	local load at apex
M	Mach number,
	also, see equation (11)
N	see equation (10)
p	planform parameter, = (plan area)/(span × length)
S	planform area
$s(x)$	nondimensional local semispan
s_T	nondimensional semispan at trailing edge
U	free stream velocity
x,y,z	nondimensional Cartesian coordinates
x_{cp}	centre of pressure position
x_L, x_T	values of x at leading and trailing edges
z_v	volume-distribution ordinate
$\alpha(x,y)$	streamwise slope of mean surface
α_n	coefficients in expression (A-2)
β	$= \sqrt{1 - M^2}$

SYMBOLS (concluded)

Δ	difference operator across wing, lower-upper
η	$= y/s(x)$
θ	$= \cos^{-1} \eta$, see equation (A-3)
λ	$= \partial z_v / \partial x$, local streamwise slope of volume distribution
ϕ	disturbance velocity potential
$\Delta\phi_T$	jump in velocity potential at trailing edge

REFERENCES

No.	Author(s)	Title, etc.
1	D. Küchemann J. Weber	An analysis of some performance aspects of various types of aircraft designed to fly over different ranges at different speeds. RAE Technical Report 66188 (ARC 28369) (1966) Progress in Aeronautical Sciences, 9, 329-456 Pergamon (1968)
2	J.H.B. Smith J.A. Beasley Diana Short F. Walkden	The calculation of the warp to produce a given load and the pressures due to a given thickness on thin slender wings in supersonic flow. ARC R&M 3471 (1965)
3	P.B. Earnshaw	Low-speed wind-tunnel tests on a series of cambered ogee wings. ARC CP 775 (1963)
4	M.P. Carr	The calculation of warp to produce a given load and pressures due to a given thickness on thin slender wings in subsonic flow. Handley Page APRO Report 99 (1968)
5	D.H. Perry	An analysis of some major factors involved in normal take-off performance. ARC CP 1034 (1967)
6	P.J. Butterworth	Low-speed wind-tunnel tests on a family of cambered wings of mild gothic planform of aspect ratio 1.4. ARC CP 1163 (1970)
7	D.A. Kirby	An experimental investigation of the effect of planform shape on the subsonic longitudinal stability characteristics of slender wings. ARC R&M 3568 (1967)
8	Patricia J. Rossiter	The linearised subsonic flow over the centre-section of a lifting swept wing. ARC R&M 3630 (1969)

REFERENCES (continued)

No.	Author(s)	Title, etc.
9	J.H.B. Smith K.W. Mangler	The use of conical camber to produce flow attachment at the leading edge of a delta wing and to minimise lift-dependent drag at sonic and supersonic speeds. ARC R&M 3289 (1957)
10	D.L.I. Kirkpatrick	Private communication
11	D.A. Kirby D.L.I. Kirkpatrick	An experimental investigation of the effect of thickness on the subsonic longitudinal stability characteristics of delta wings of 70 degree sweepback. ARC R&M 3073 (1969)
12	F.G. Leppington	Curvature effects in the diffraction of short waves into a shadow. ARC CP 1193 (1970)
13	J. Weber	Design of warped slender wings with dihedral and anhedral at the rear. RAE Technical Note Aero 2719 (ARC 22736) (1960)
14	W.J.G. Trebble D.A. Kirby	Reduction of the rolling moments of slender wing models by the application of full and part span anhedral. RAE Technical Report 67300 (ARC 30084) (1967)
15	M.A. Heaslet H. Lomax	Supersonic and transonic small perturbation theory. Part D of General Theory of High Speed Aerodynamics, (ed. W.R. Sears), pp.226-229, Oxford University Press (1955)
16	W. Gröbner M. Hofreiter, *et al.*	Table of integrals, Part 2 - definite integrals. Ministry of Supply (1948)

REFERENCES (concluded)

No.	Author(s)	Title, etc.
17	D. Hummel	Berechnung der Druckverteilung an Schlanken Flugkörpern mit Beliebiger Grundriss- und Querschnittsform in Unter- und Überschall-strömung. The Sixth Congress of the International Council of the Aeronautical Sciences ICAS Paper 68-44 (1968)
18	H.S. Ward	A study of slender cambered wings by an electrical resistance network. Unpublished Report of Department of Civil Engineering; University of Birmingham (1961)
19	S.C. Redshaw	The use of an electrical analogue for the solution of a variety of torsion problems. Brit. Journ. Appl. Phys., 2, 461-468 (1960)
20	J.H.B. Smith	The properties of a thin conically cambered wing according to slender body theory. ARC R&M 3135 (1958)
21	H. Portnoy	The slender wing with a half body of revolution mounted beneath. Aeronautical Journal, 72, 803-807 (1968)

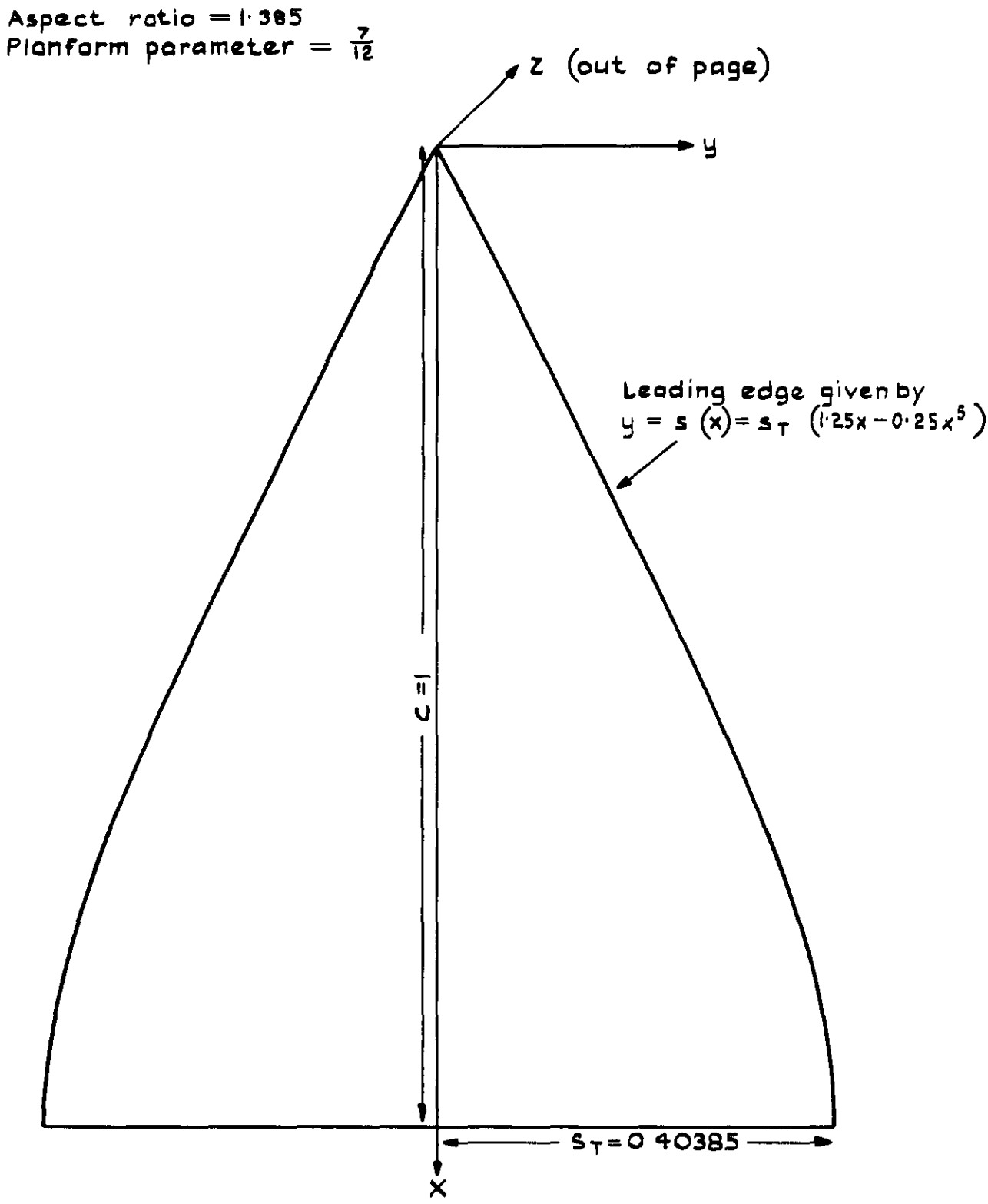

Fig. 1 Mild gothic planform

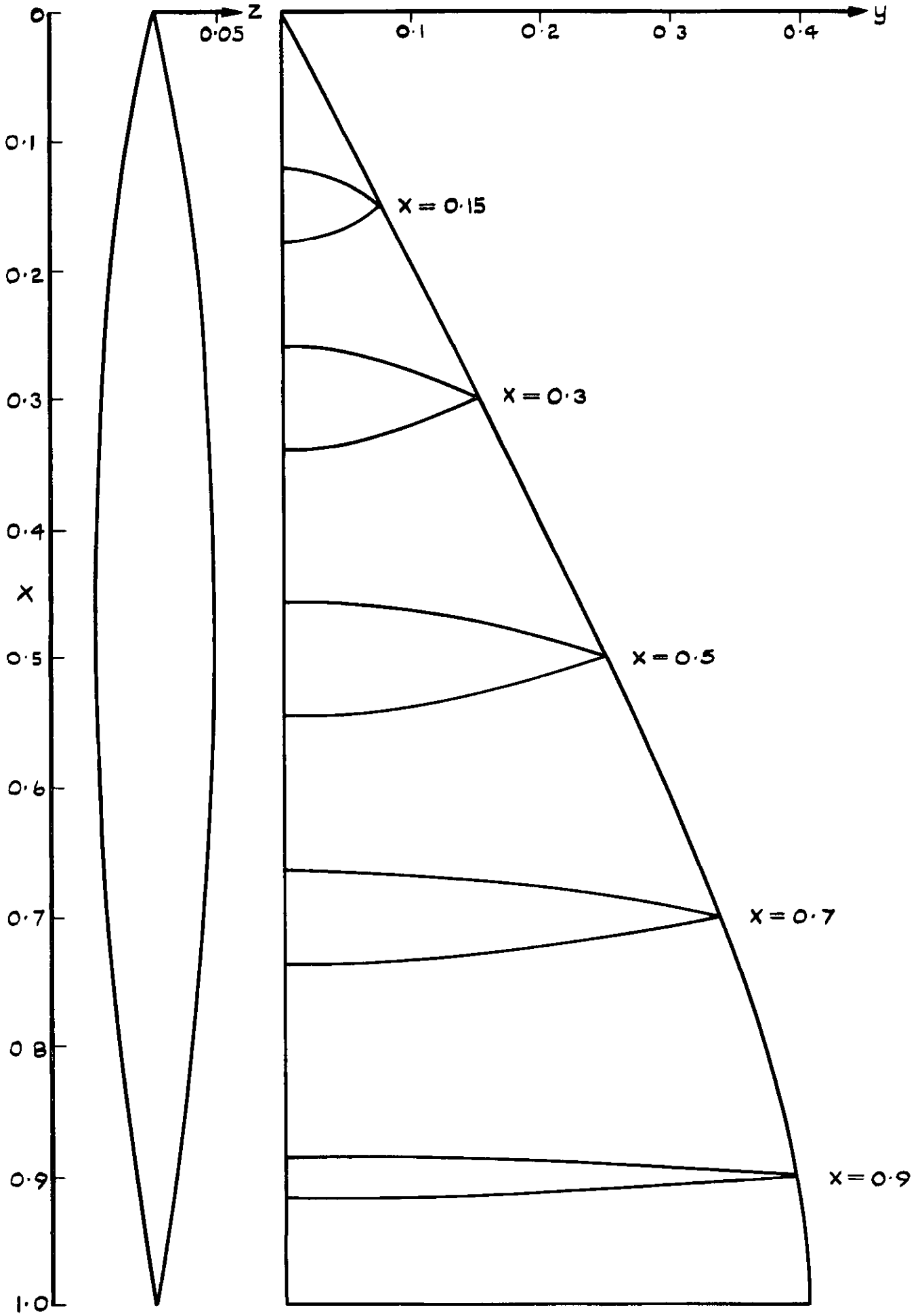

Fig. 2 Volume distribution

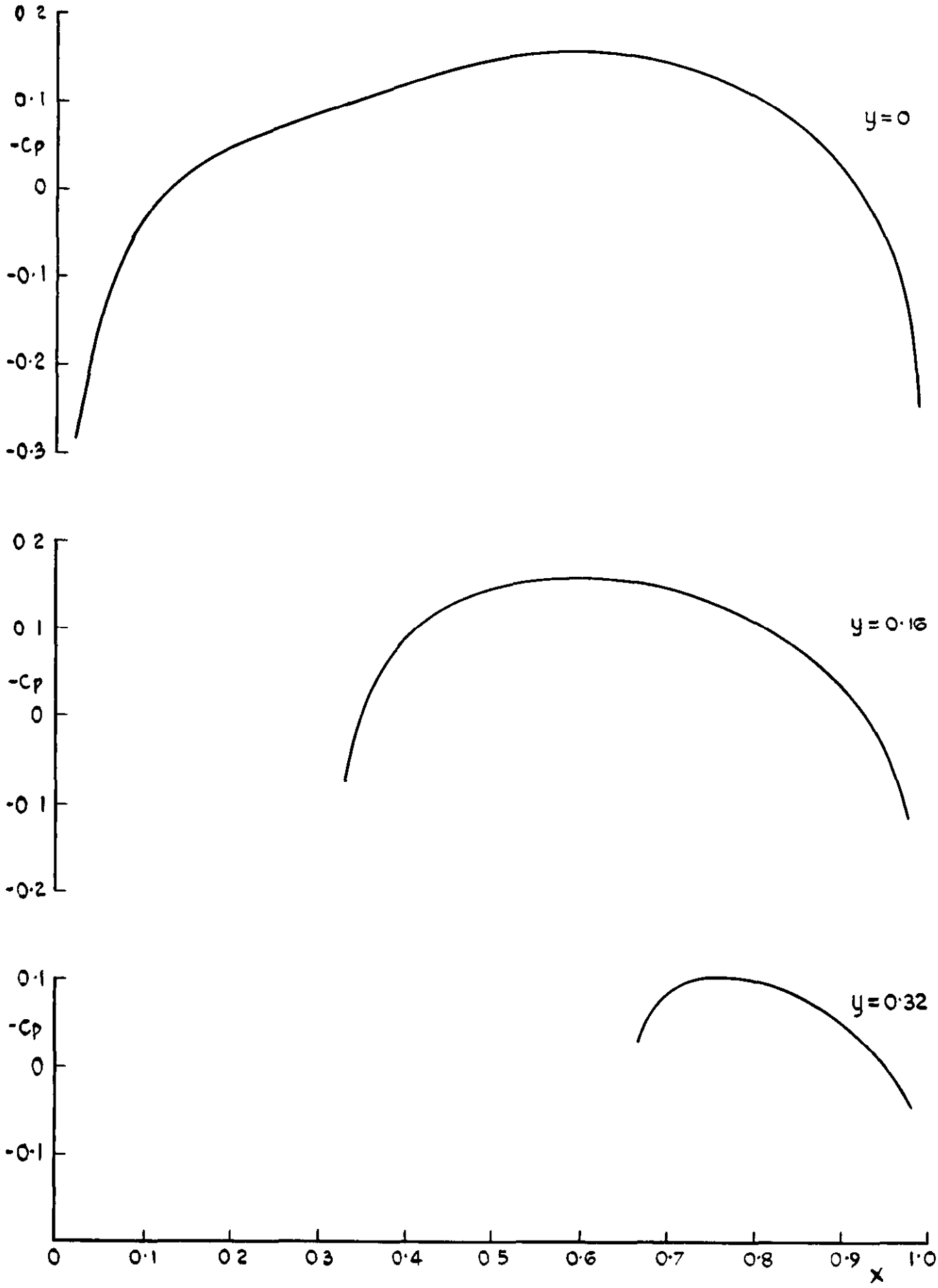

Fig.3 Pressure due to volume distribution at various chordwise sections

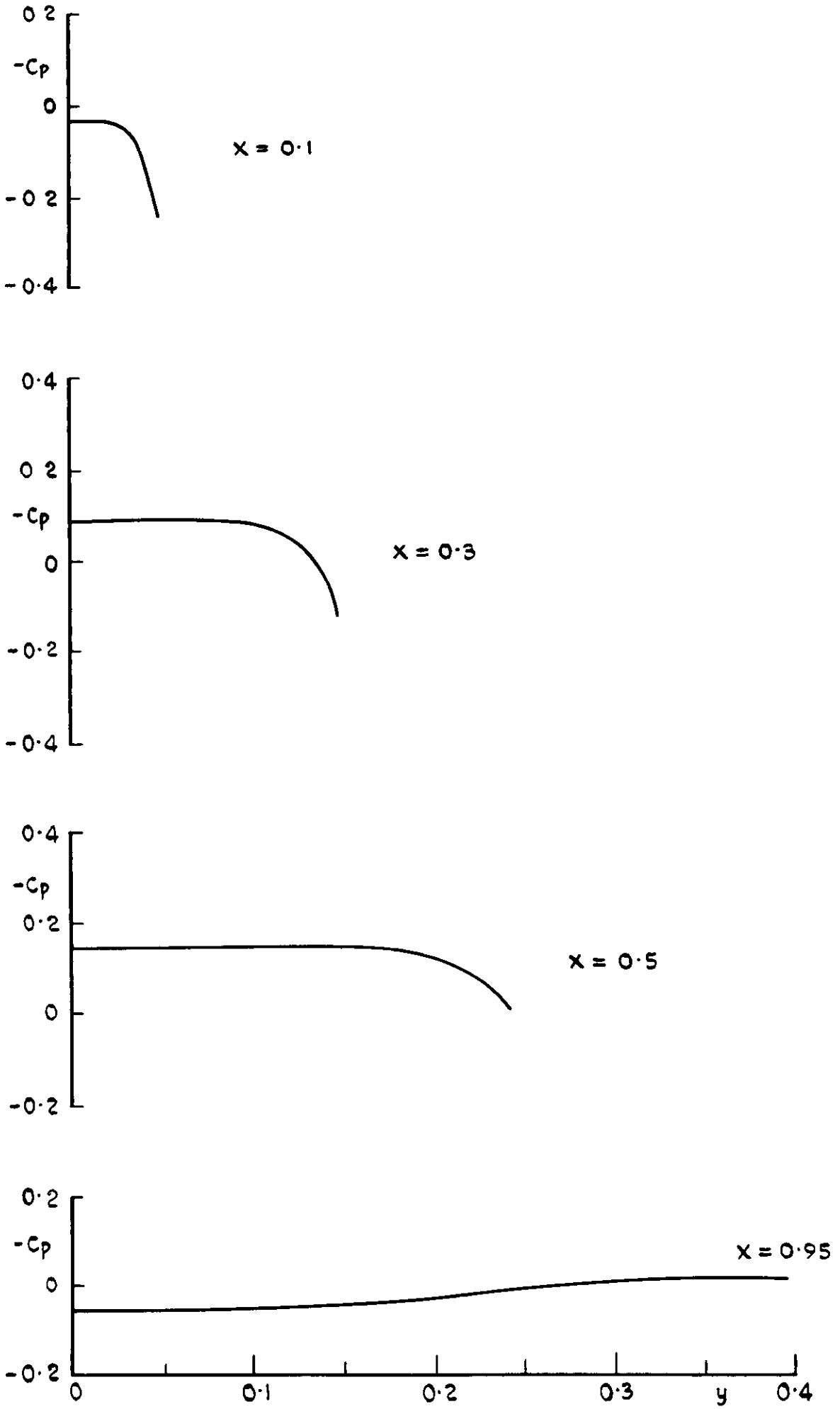

Fig.4 Pressure due to volume distribution at various spanwise sections

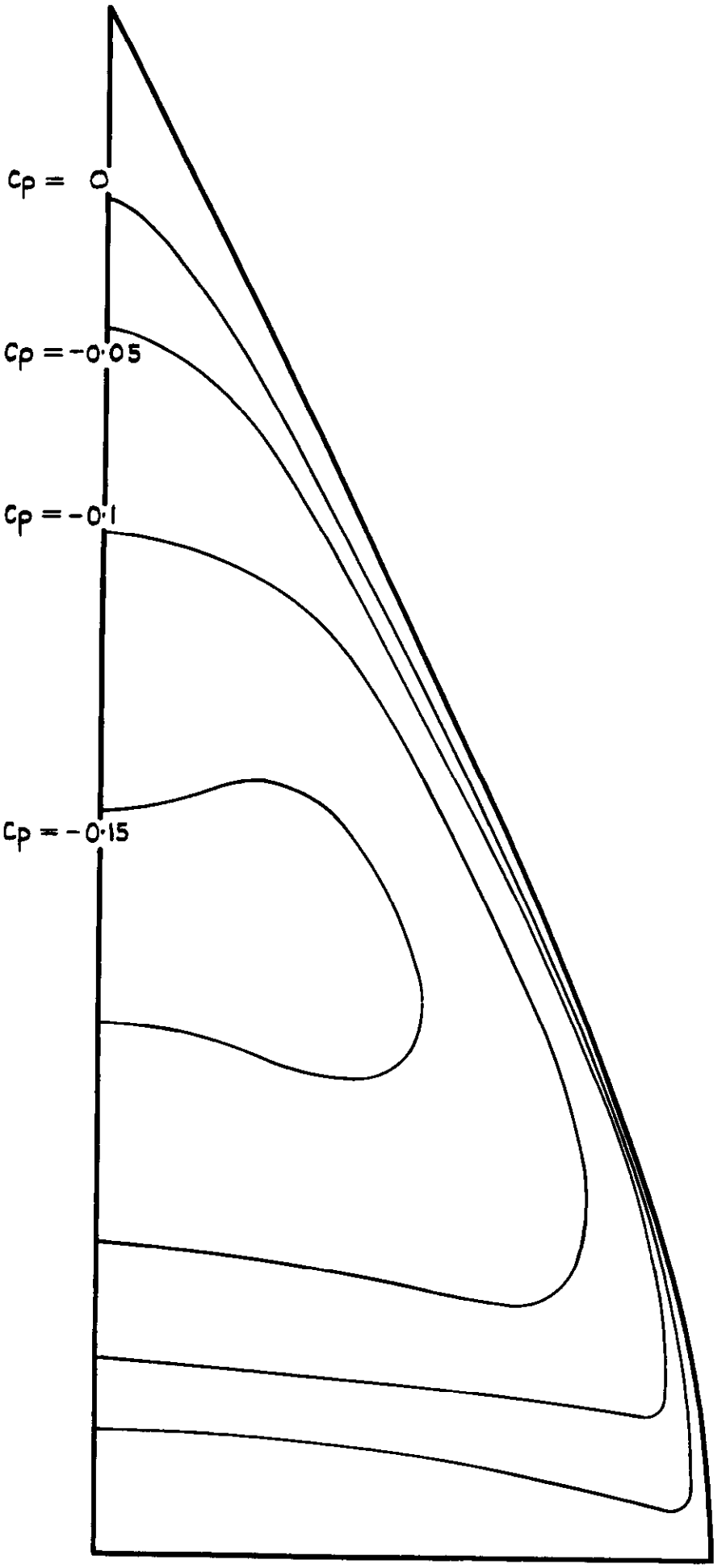

Fig.5 Isobars on symmetrical wing

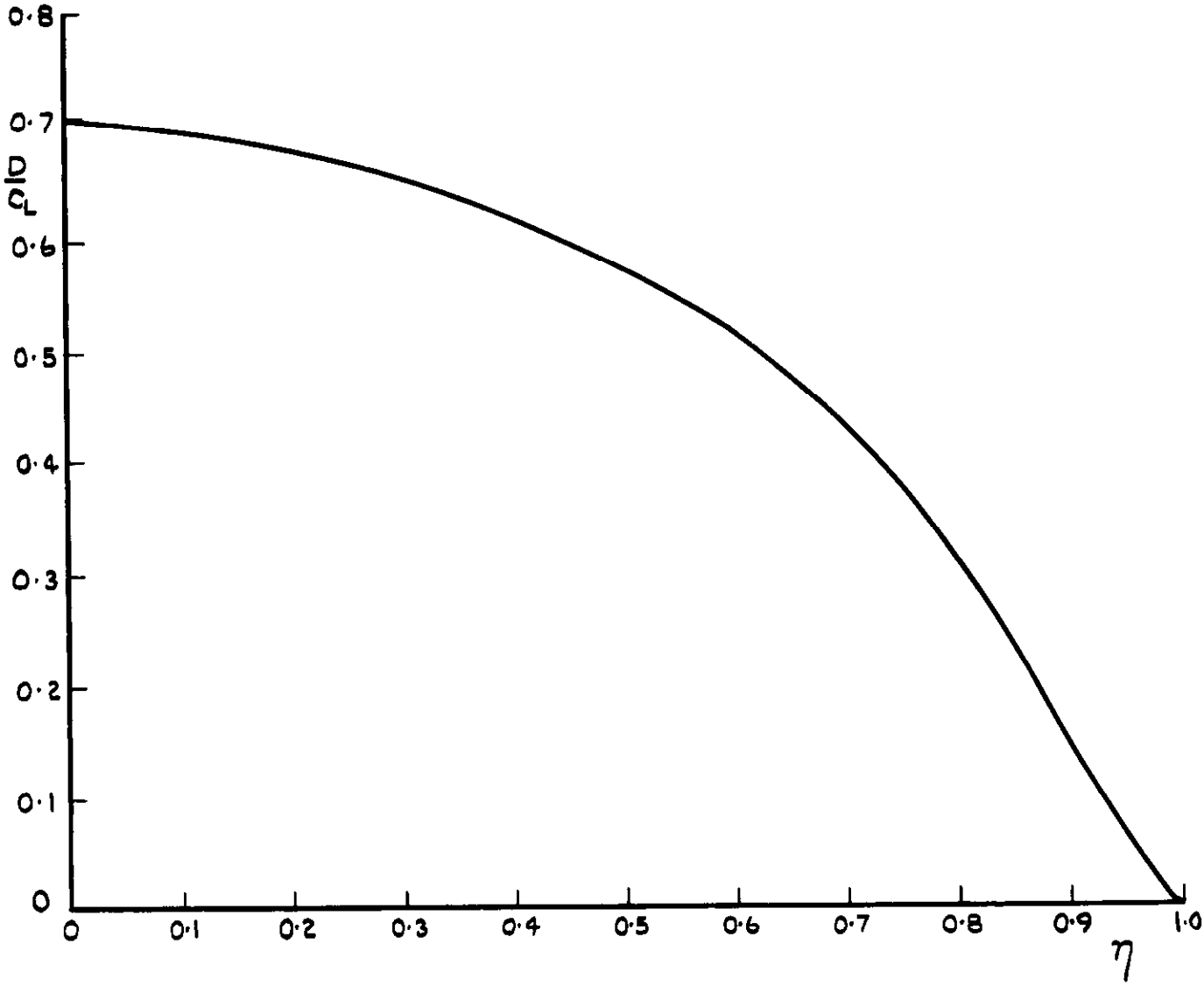

Fig. 6 Spanwise distribution of chord loading

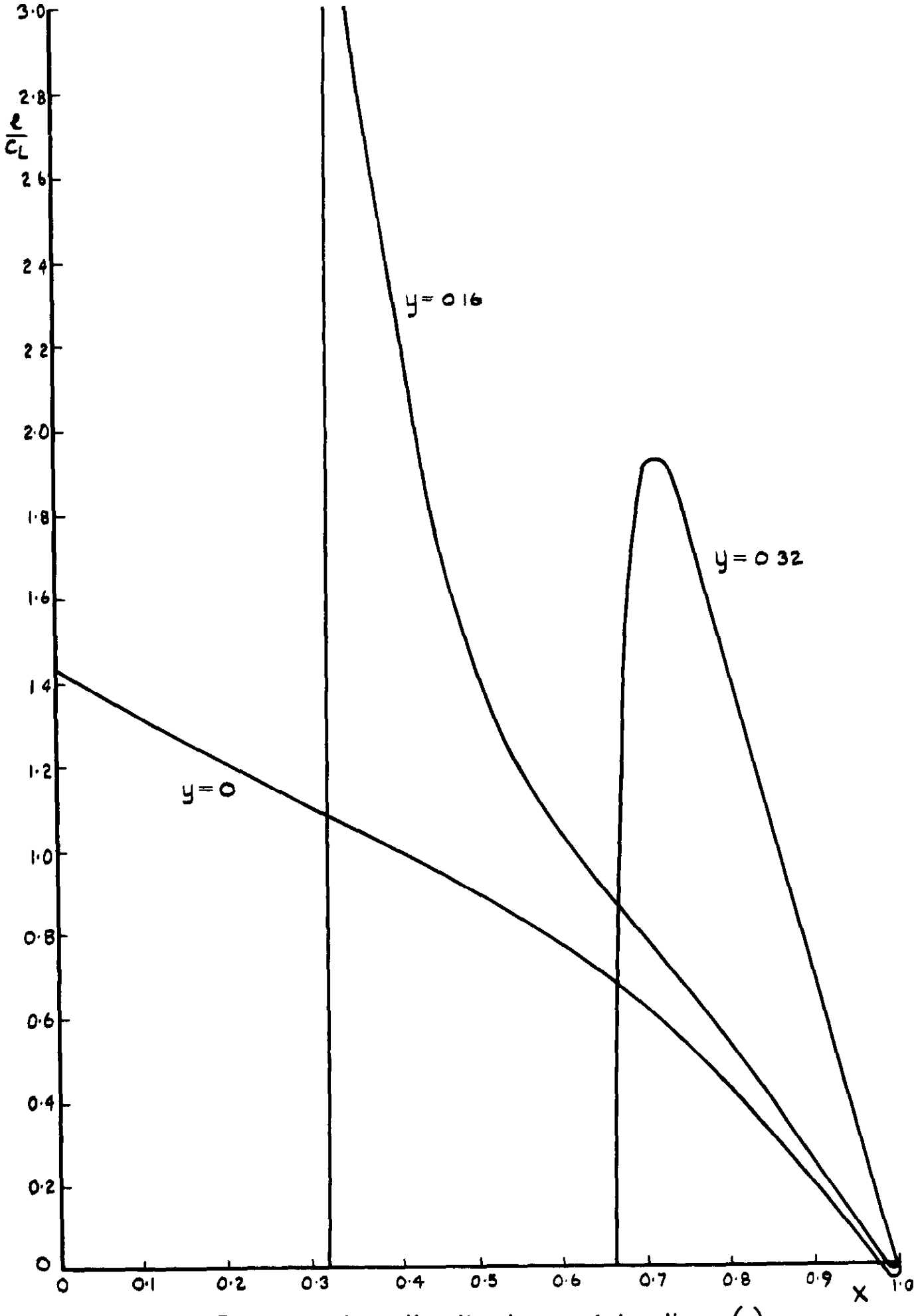

Fig. 7 Chordwise distributions of loading (a)

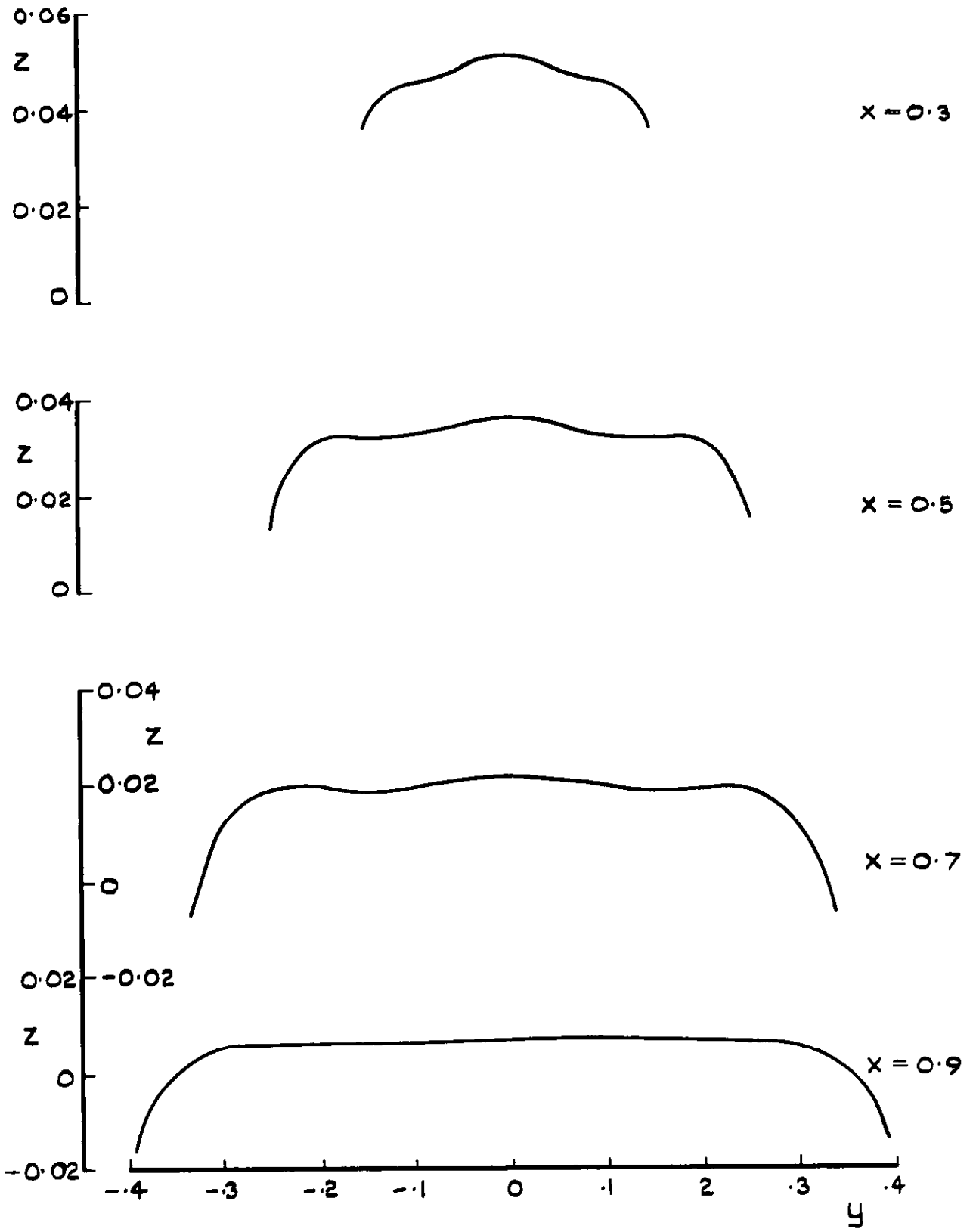

Fig. 8 Cross-sections of mean surface due to loading (a)

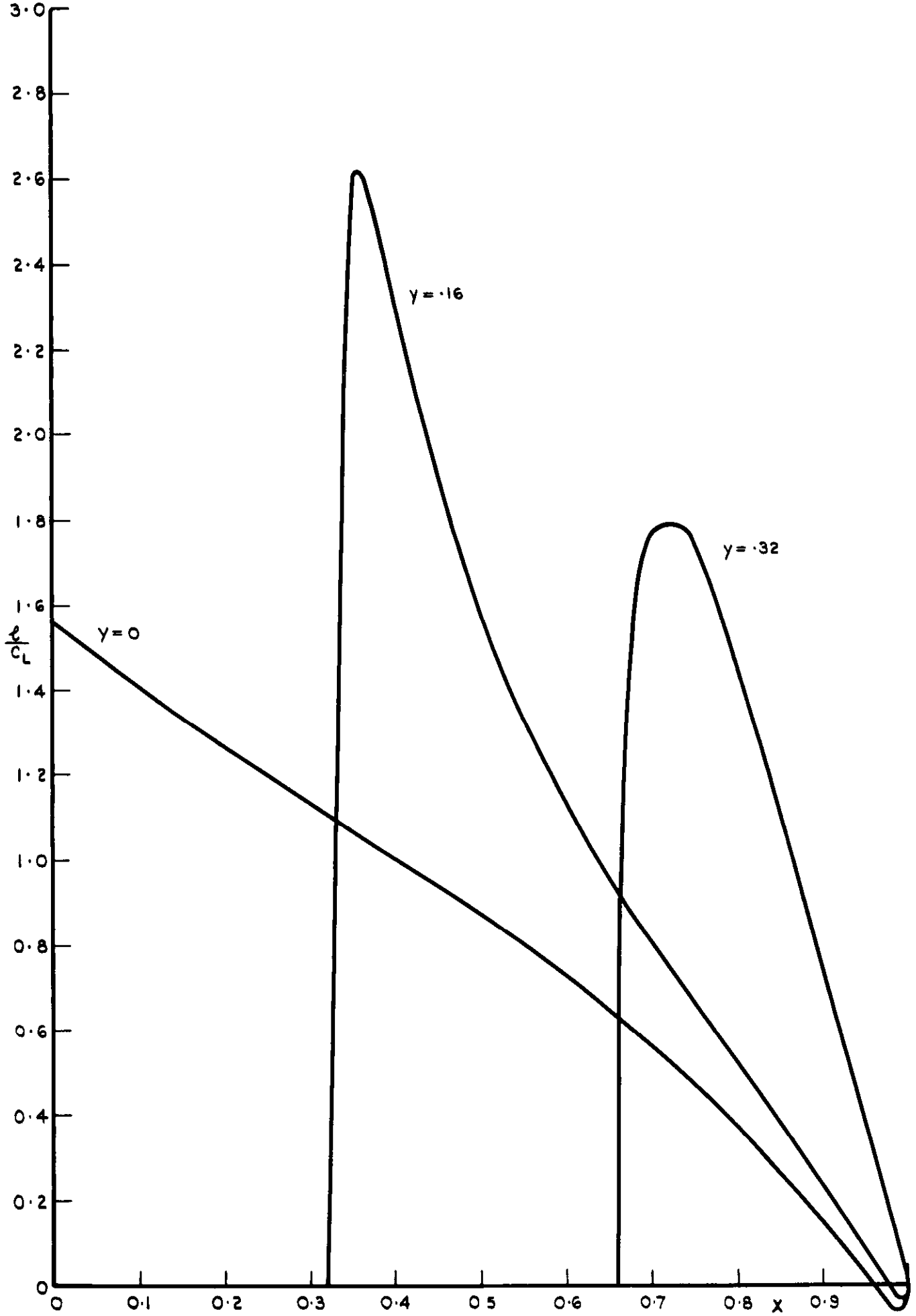

Fig.9 Chordwise distributions of loading (b)

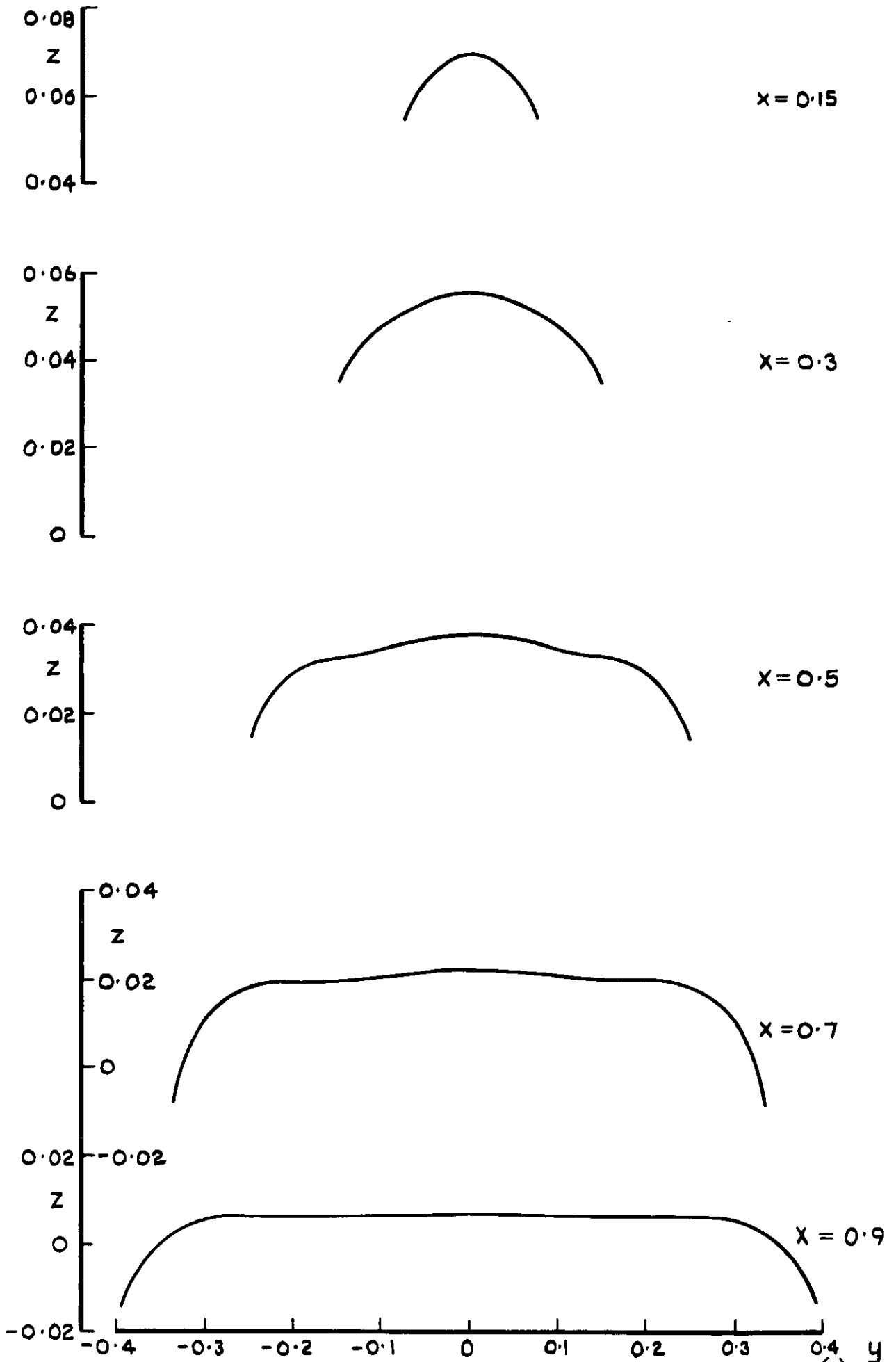

Fig 10 Cross-sections of mean surface due to loading (b)

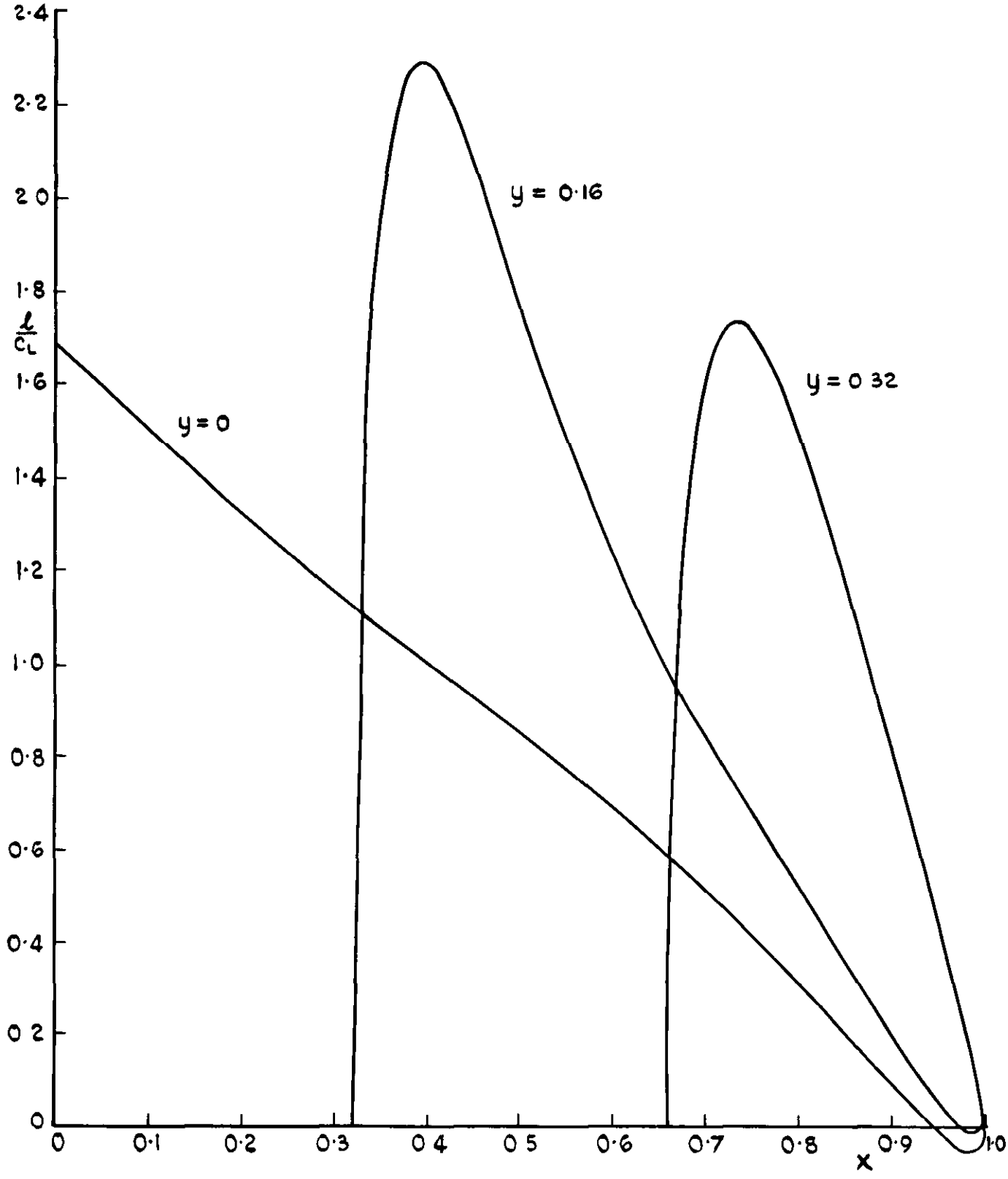

Fig.11 Chordwise distributions of loading (c)

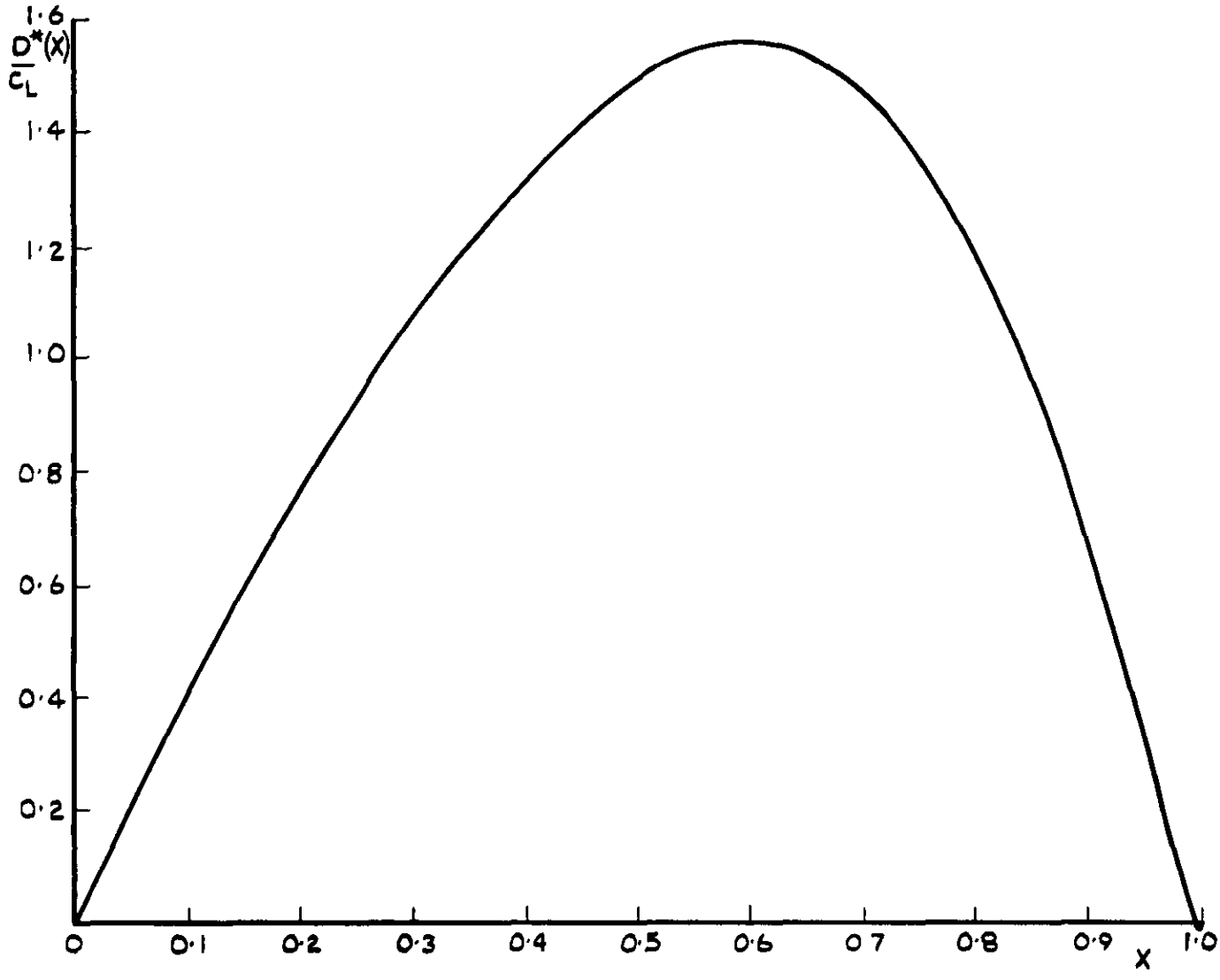

Fig 12 Lengthwise distribution of cross loading for loading (c)

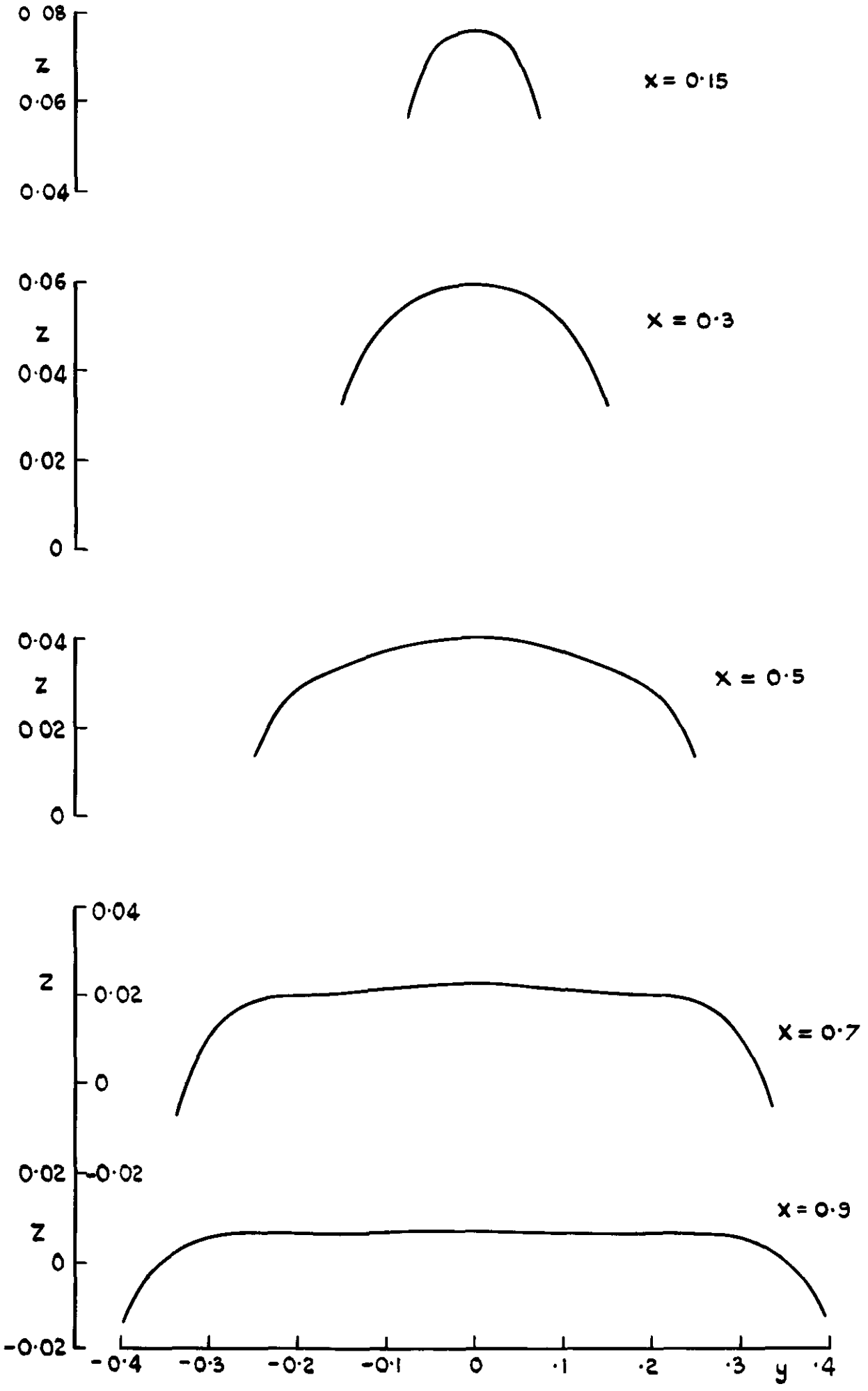

Fig.13 Cross-sections of mean surface due to loading(c)

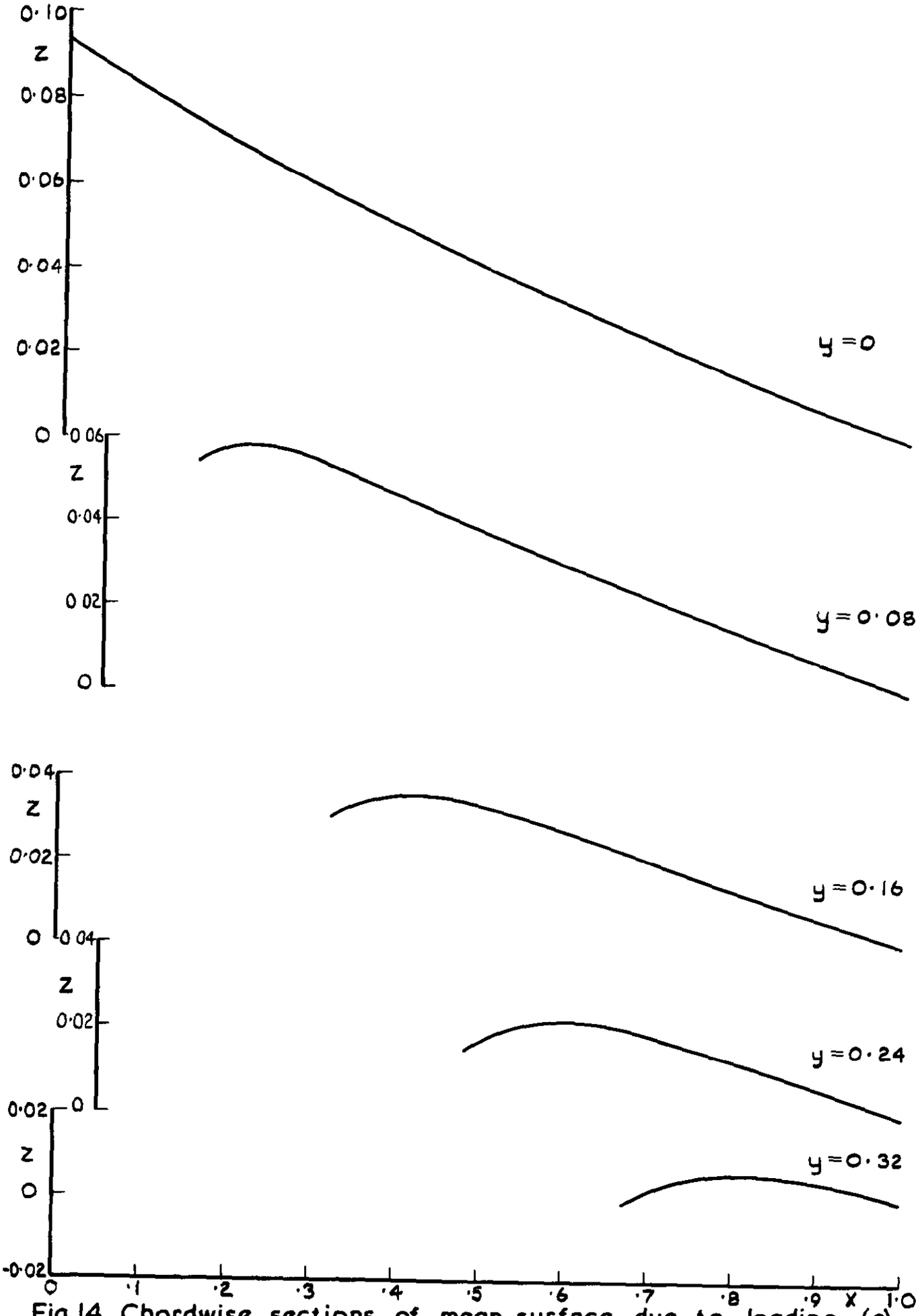

Fig. 14 Chordwise sections of mean surface due to loading (c)

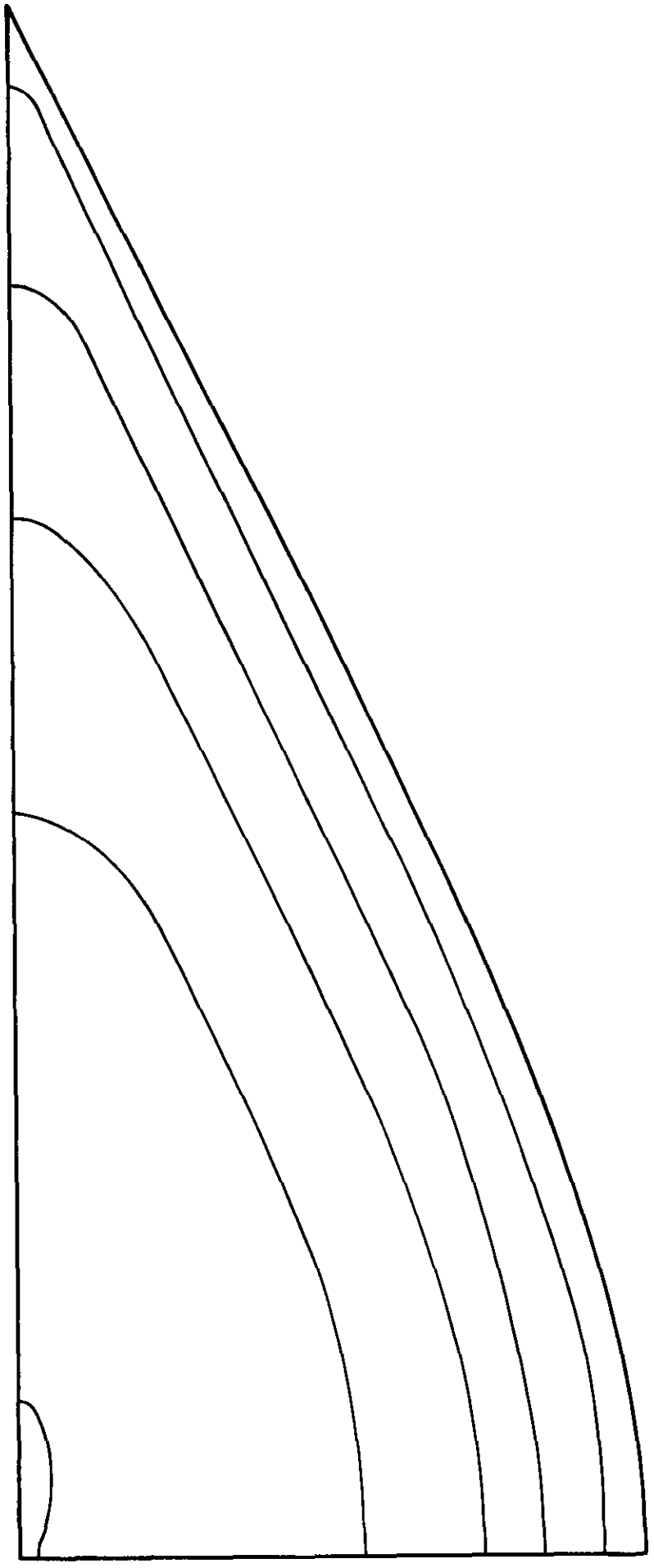

Fig.15 Bound vortices due to loading (c)

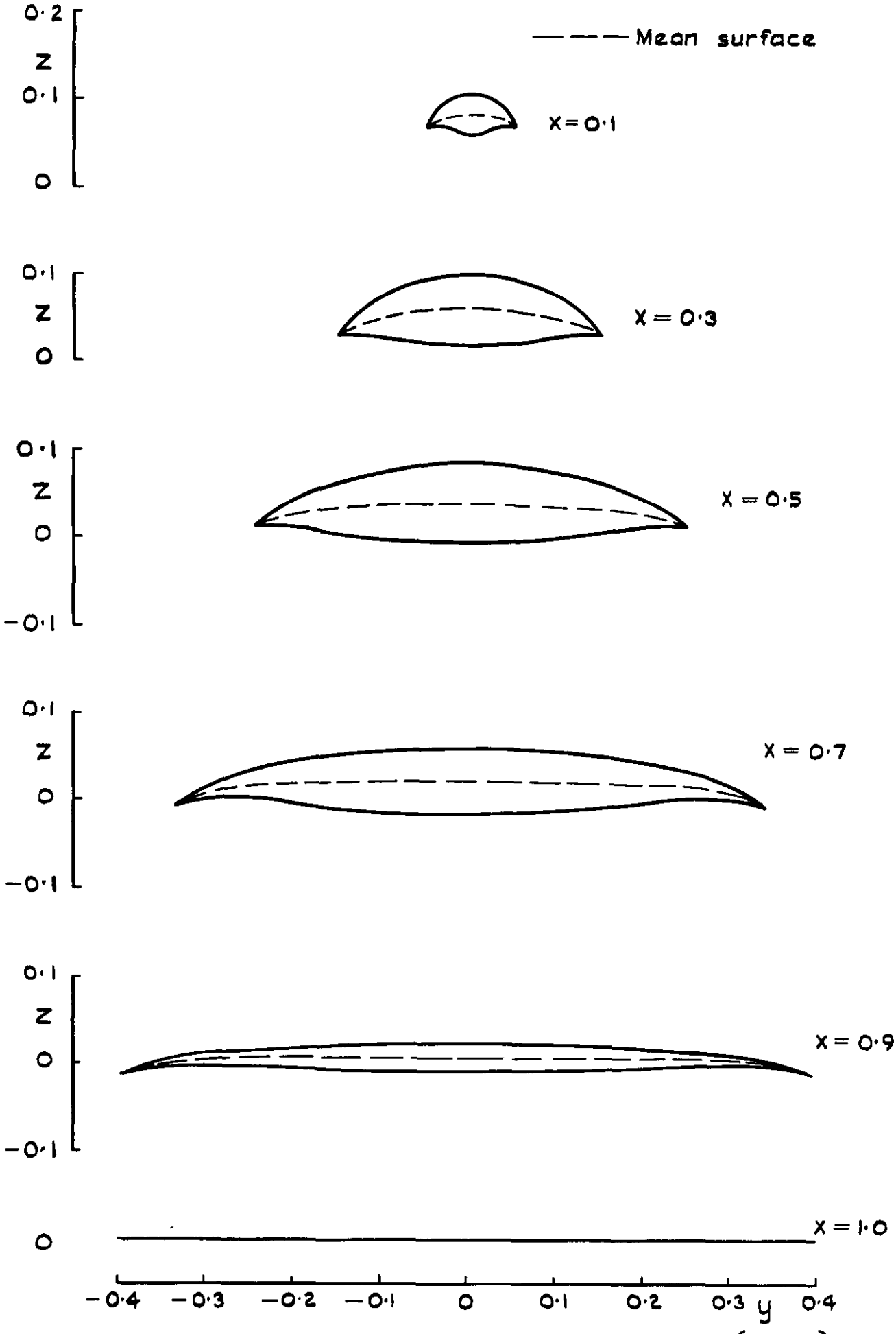

Fig. 16 Cross-sections of basic C_L 0·1 model (wing 1)

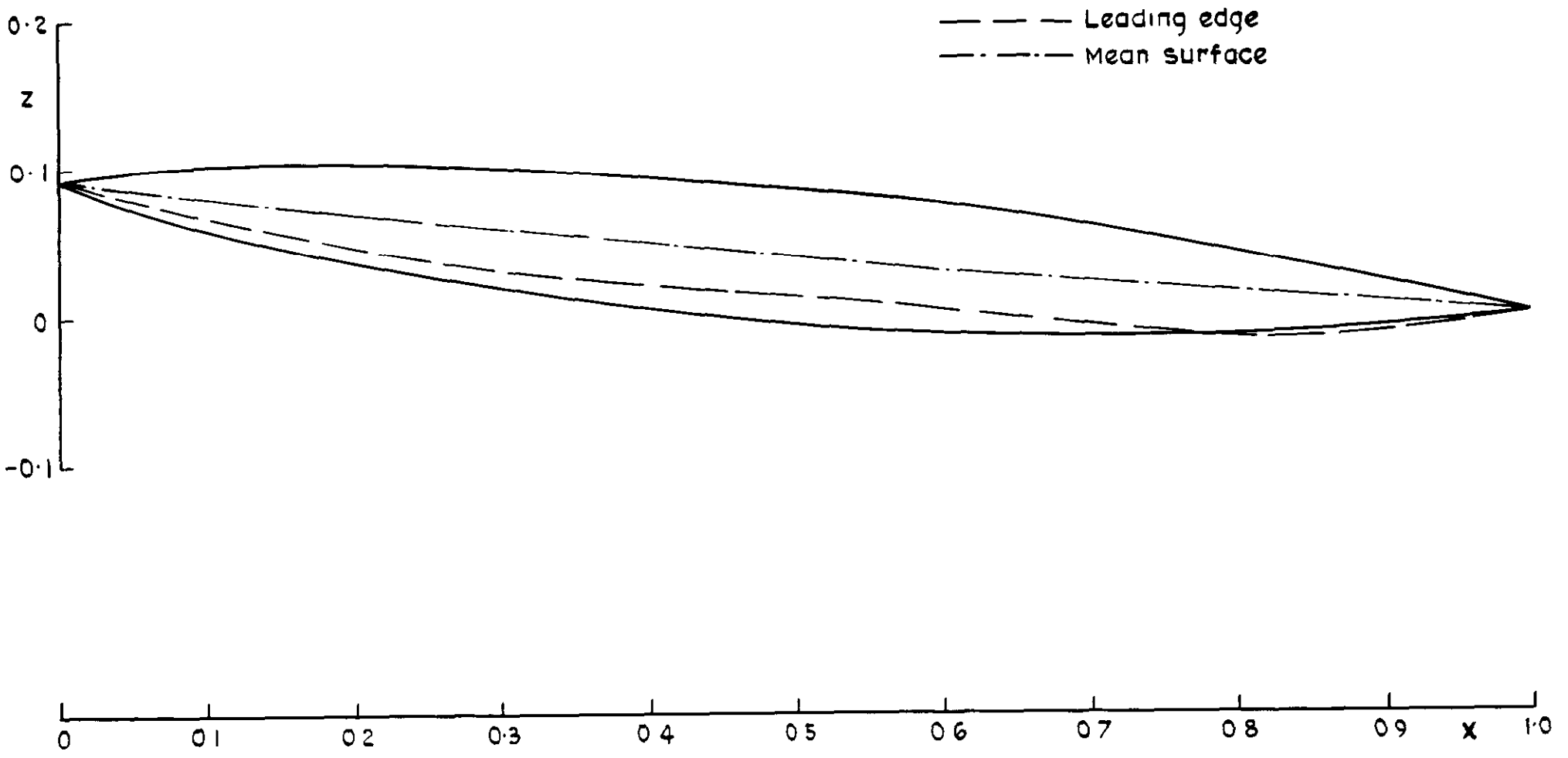

Fig.17 Centre section of basic C_L 0·1 model (wing 1) with mean surface and streamwise variation of leading edge

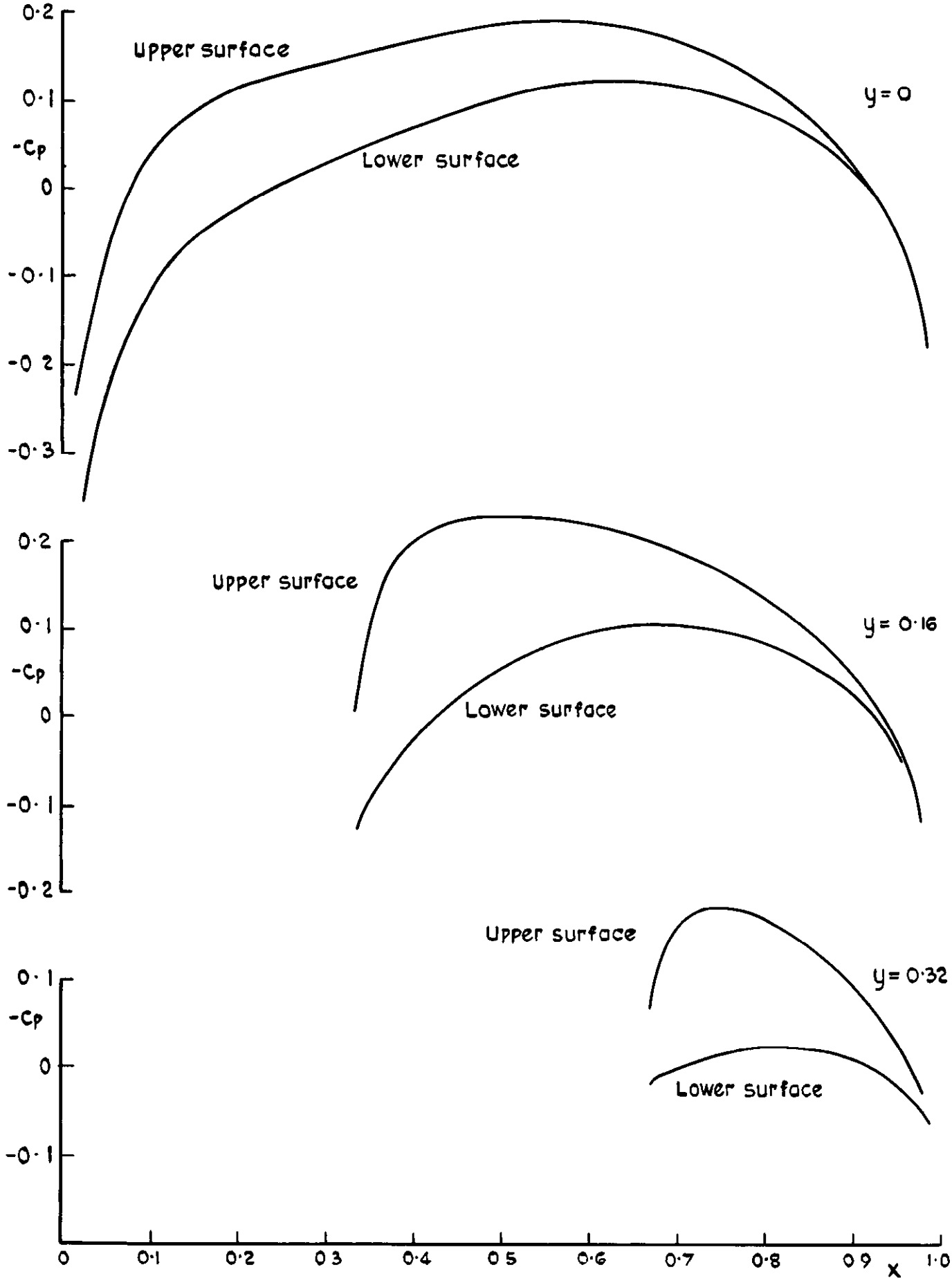

Fig. 18 Pressure distributions at various chordwise sections of basic $C_L = 0{\cdot}1$ model (wing 1)

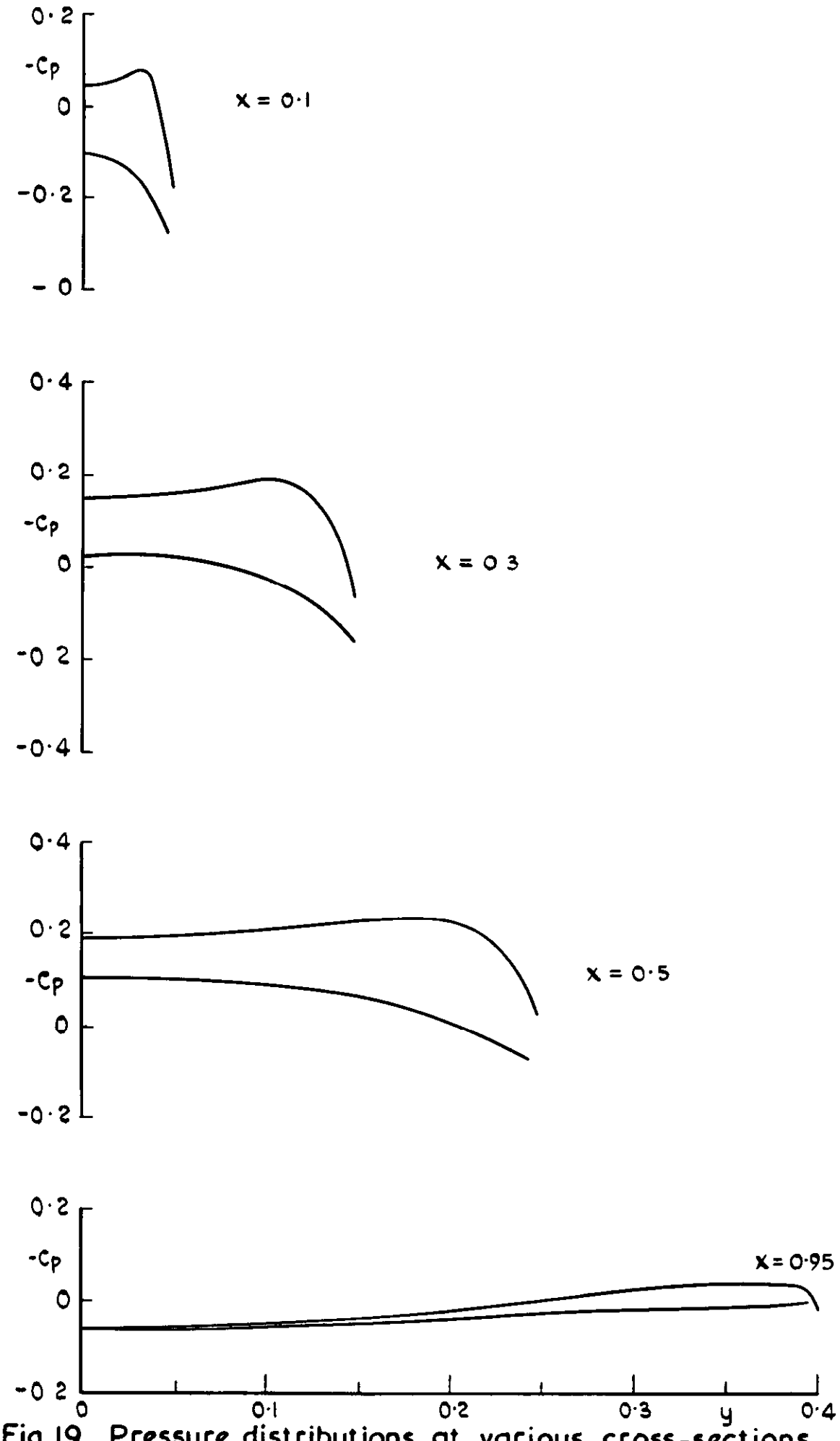

Fig.19 Pressure distributions at various cross-sections of basic $C_L = 0{\cdot}1$ model (wing 1)

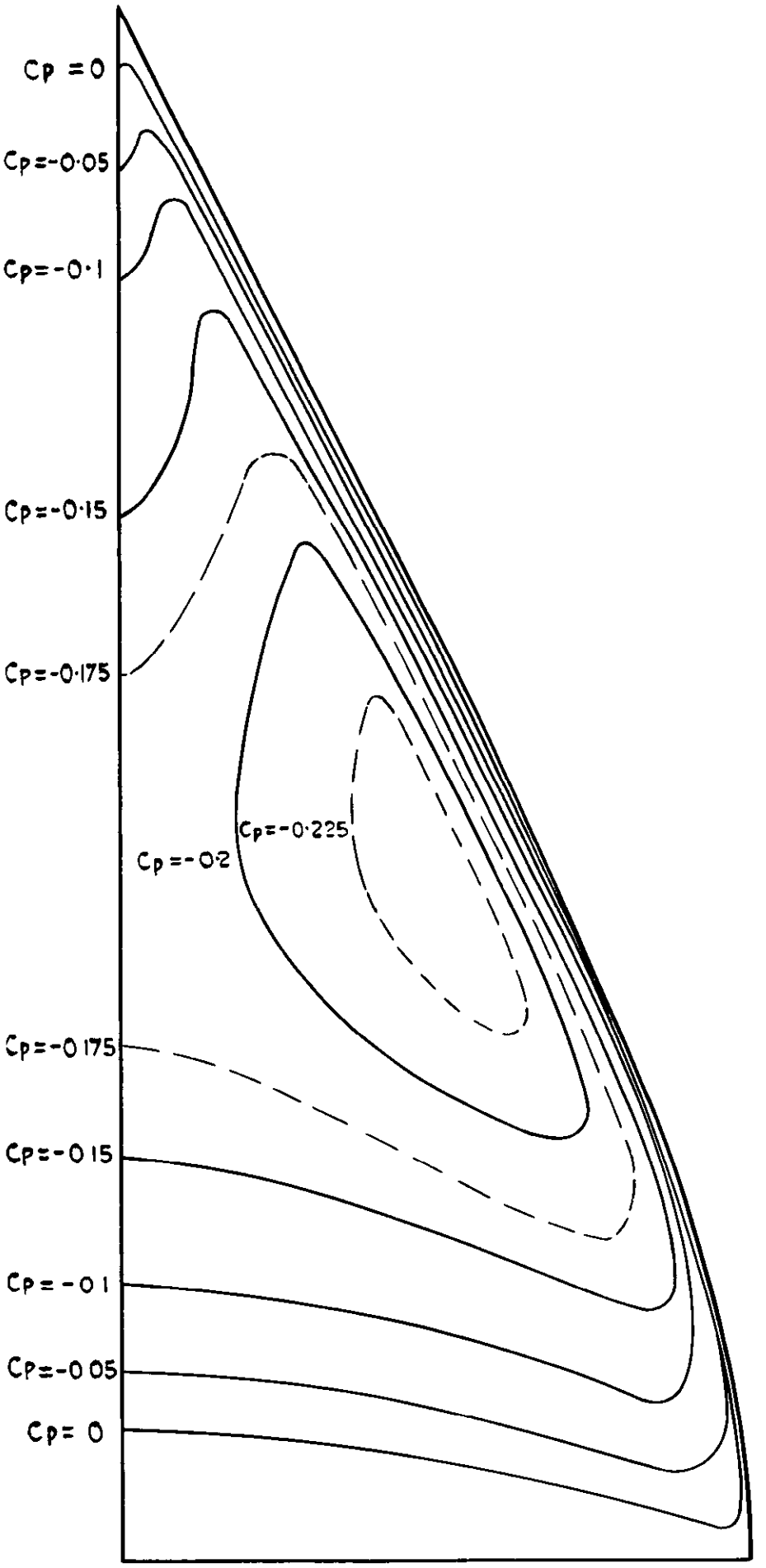

Fig. 20 Isobars on the upper surface of the basic $C_L = 0{\cdot}1$ model (wing 1) at the attachment incidence

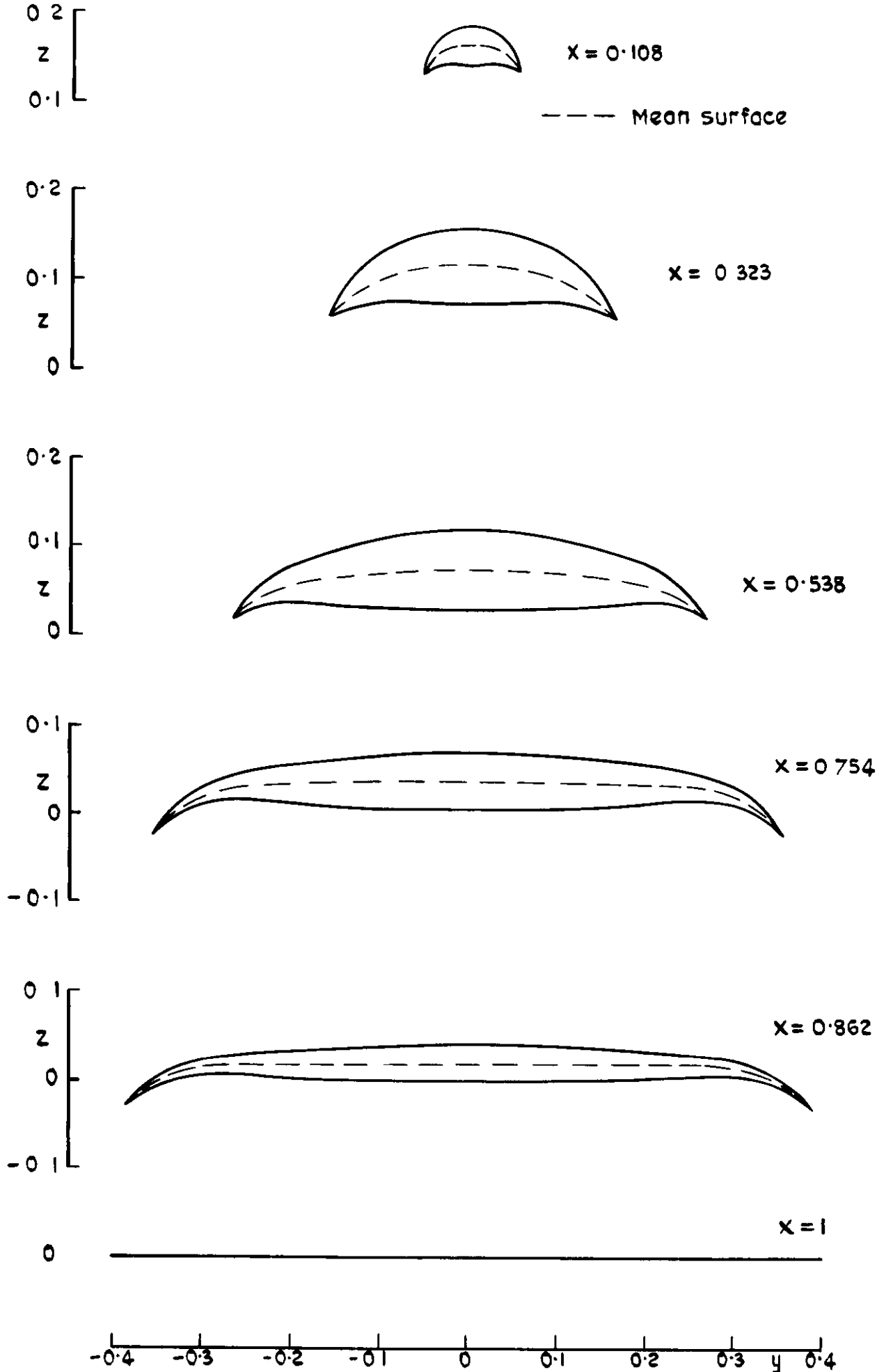

Fig. 21 Cross-sections of C_L 0·2 model (wing 2)

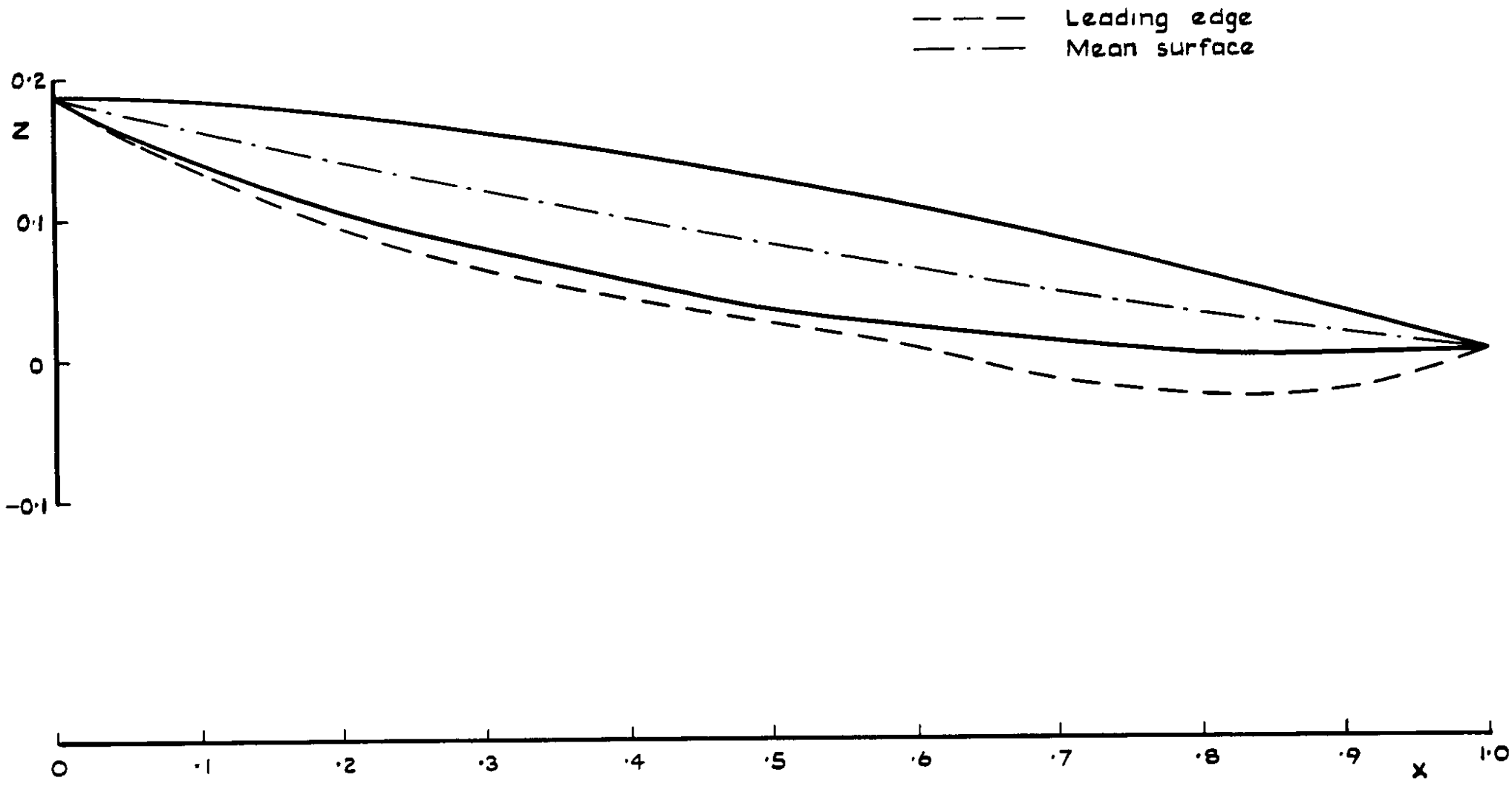

Fig. 22 Centre section of C_L 0·2 model (wing 2), with mean surface and streamwise variation of leading edge

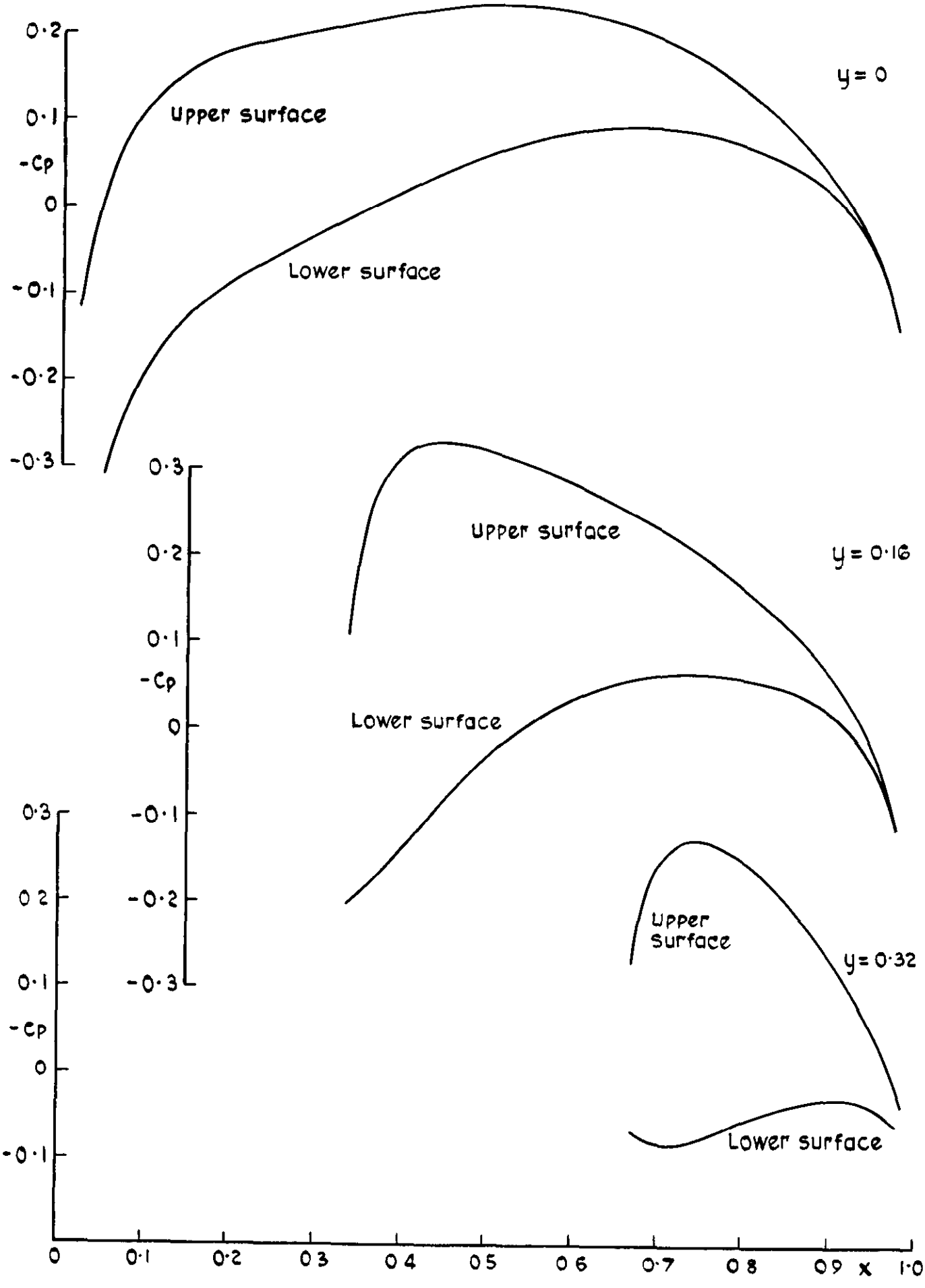

Fig. 23 Pressure distributions at various chordwise sections of C_L 0·2 model (wing 2)

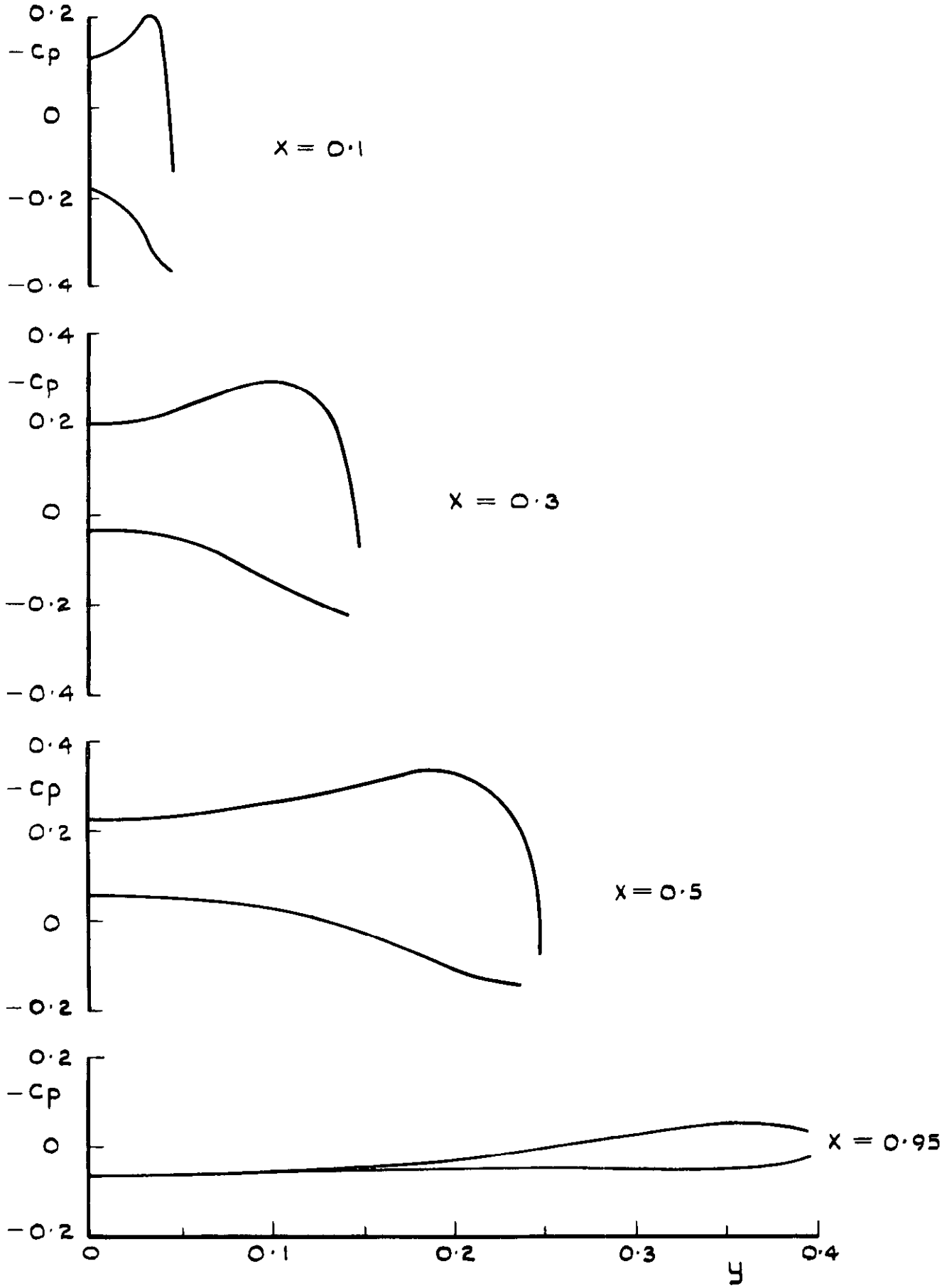

Fig.24 Pressure distributions at various cross-sections of C_L 0·2 model (wing 2)

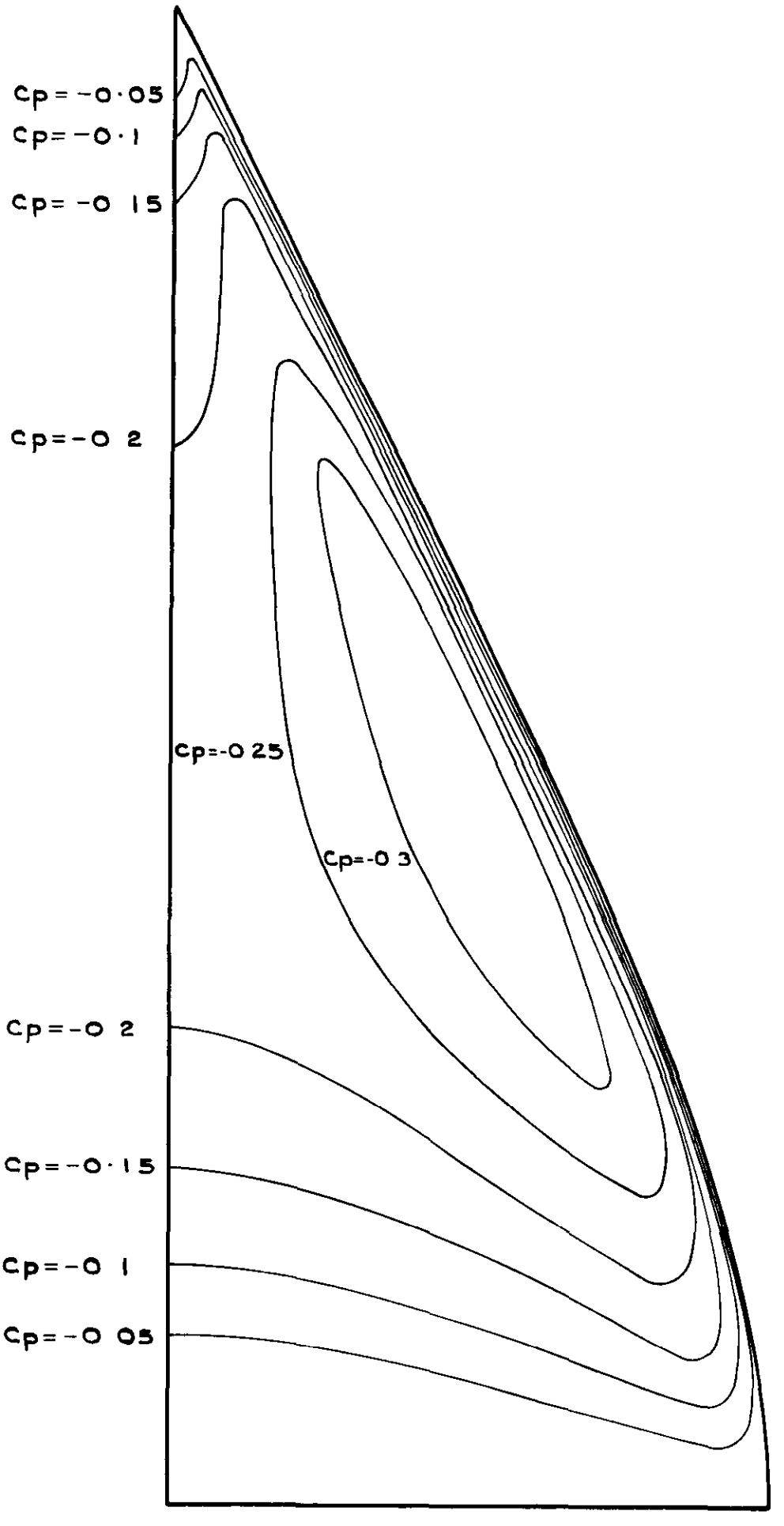

Fig.25 Isobars on upper surface of C_L 0·2 model (wing 2) at attachment incidence

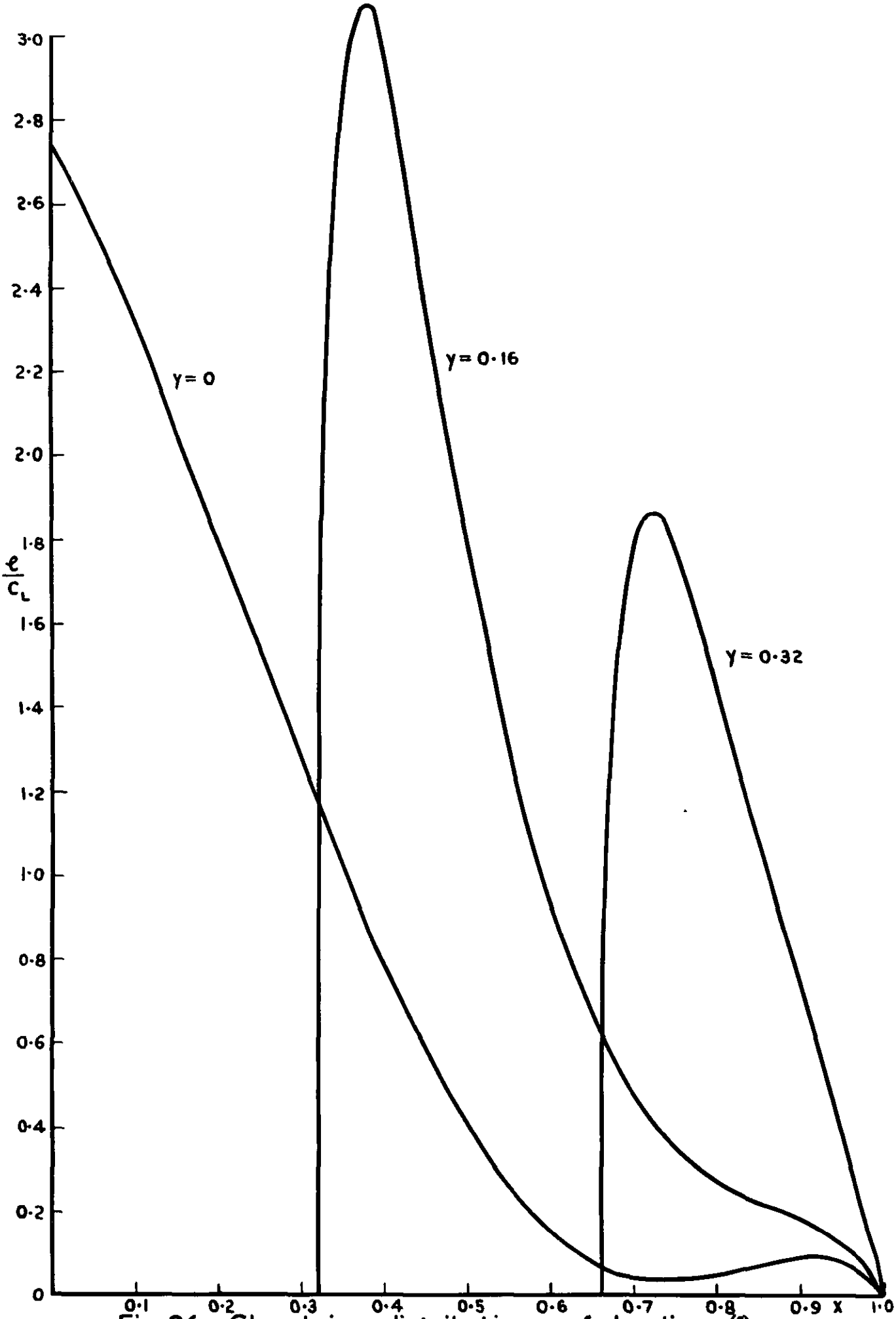

Fig. 26 Chordwise distributions of loading (f)

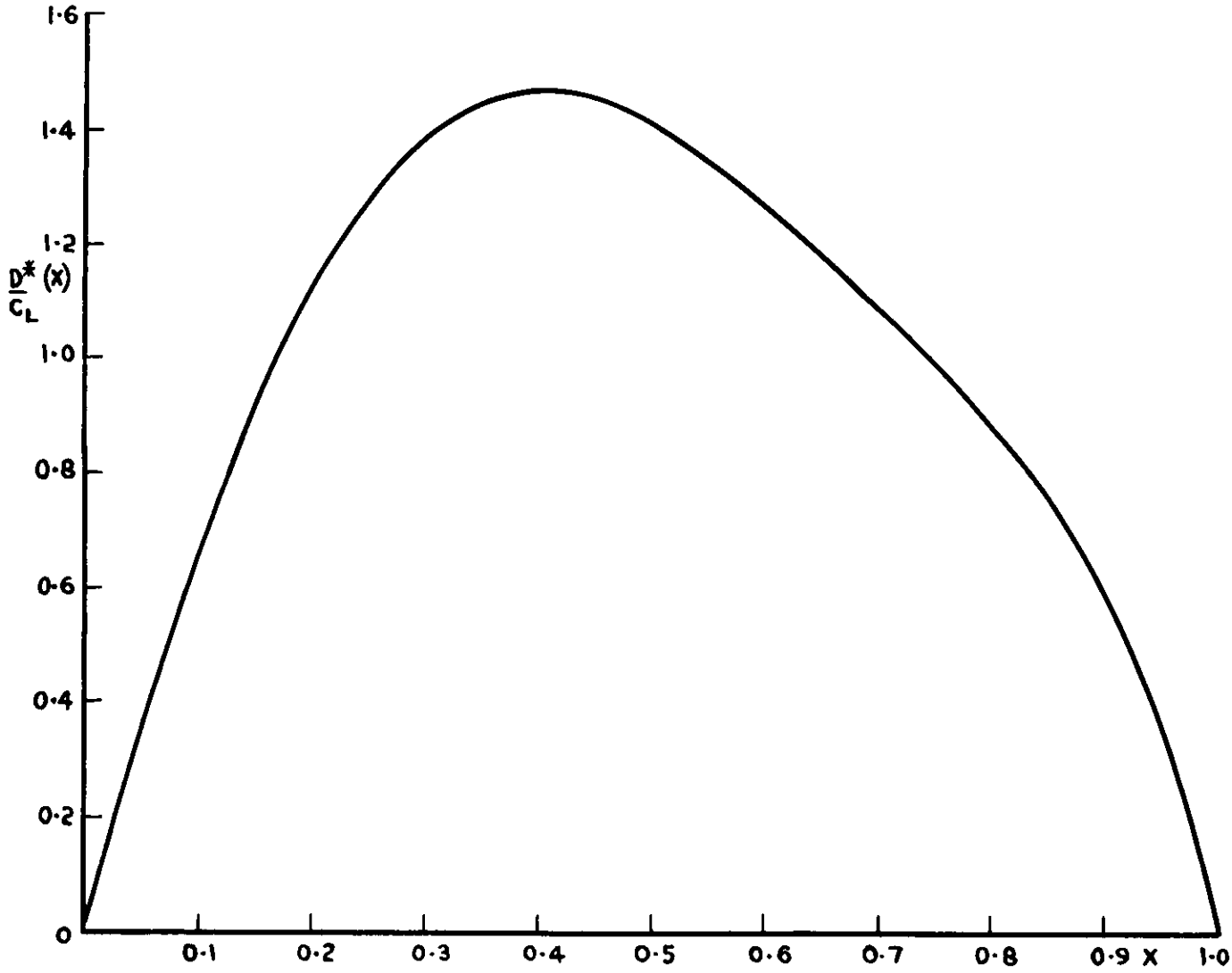

Fig. 27 Lengthwise distribution of cross-loading for loading (f)

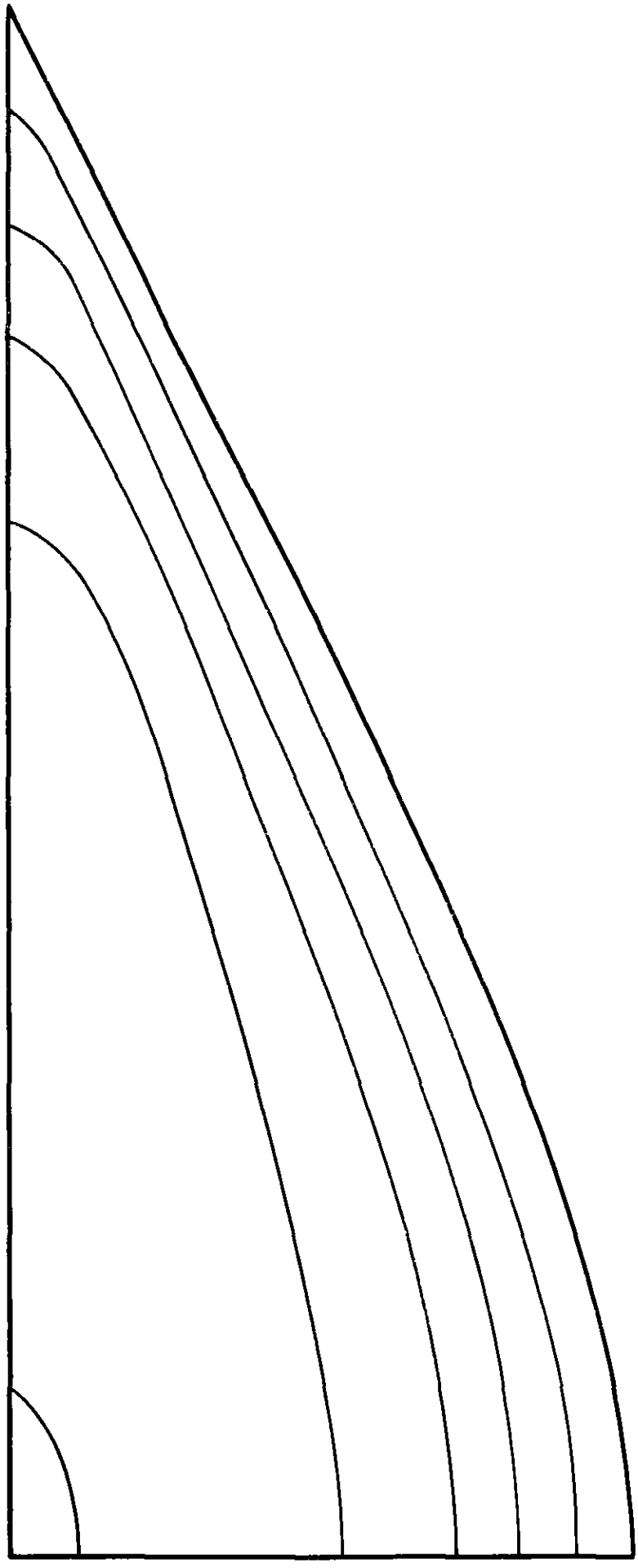

Fig. 28 Bound vortices due to loading (f)

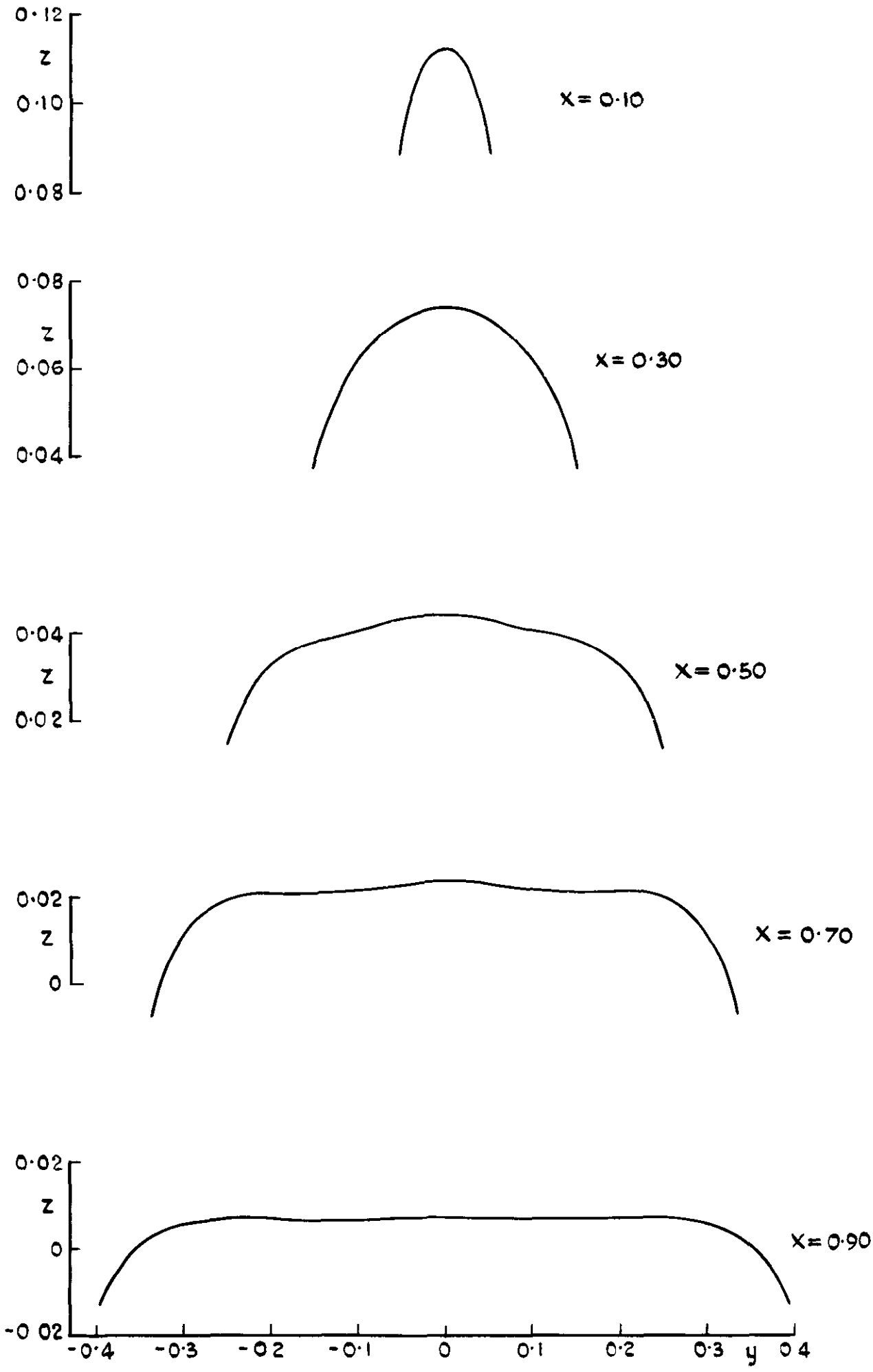

Fig. 29 Cross-sections of mean surface due to loading(f)

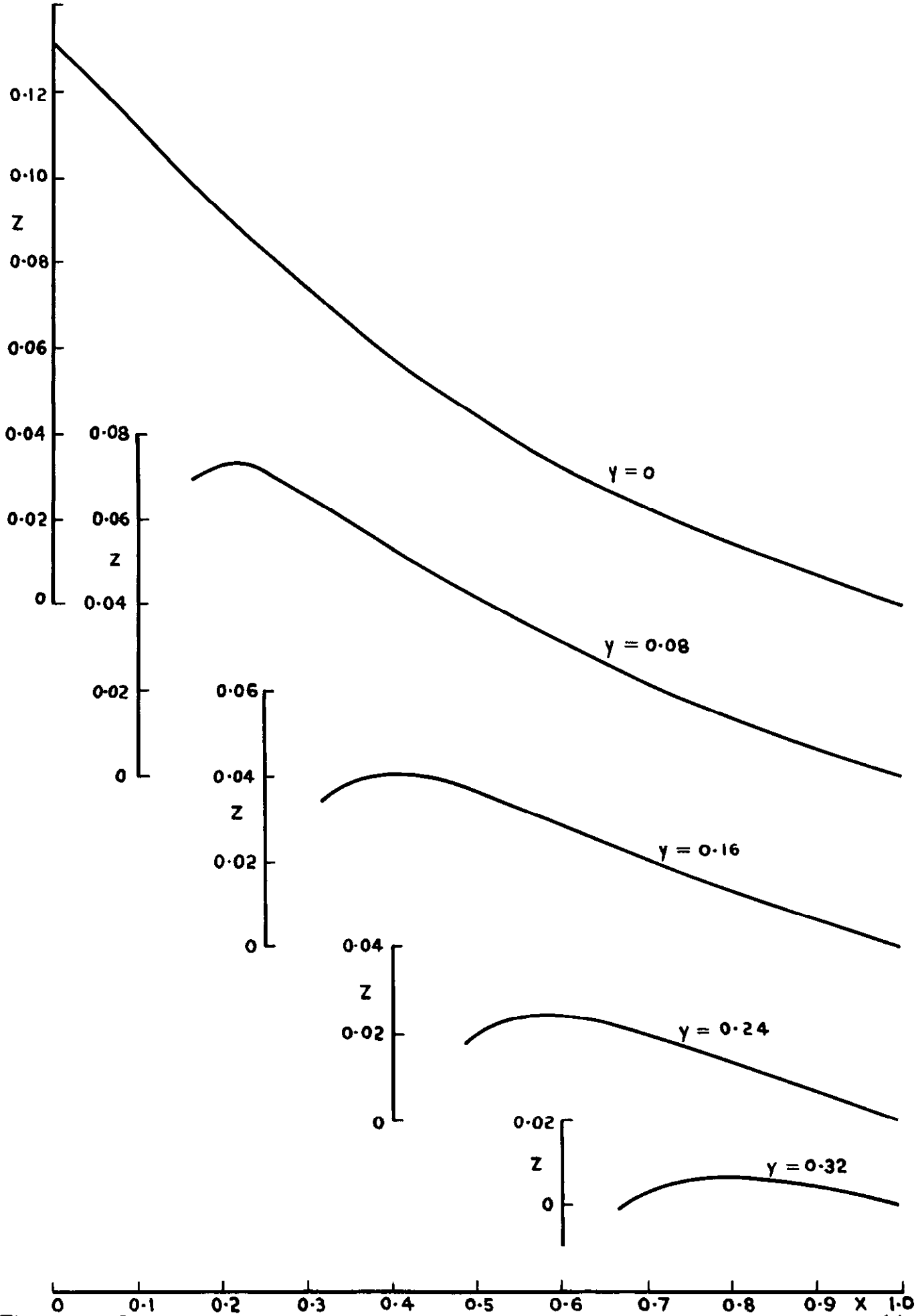

Fig. 30 Chordwise sections of mean surface due to loading (f)

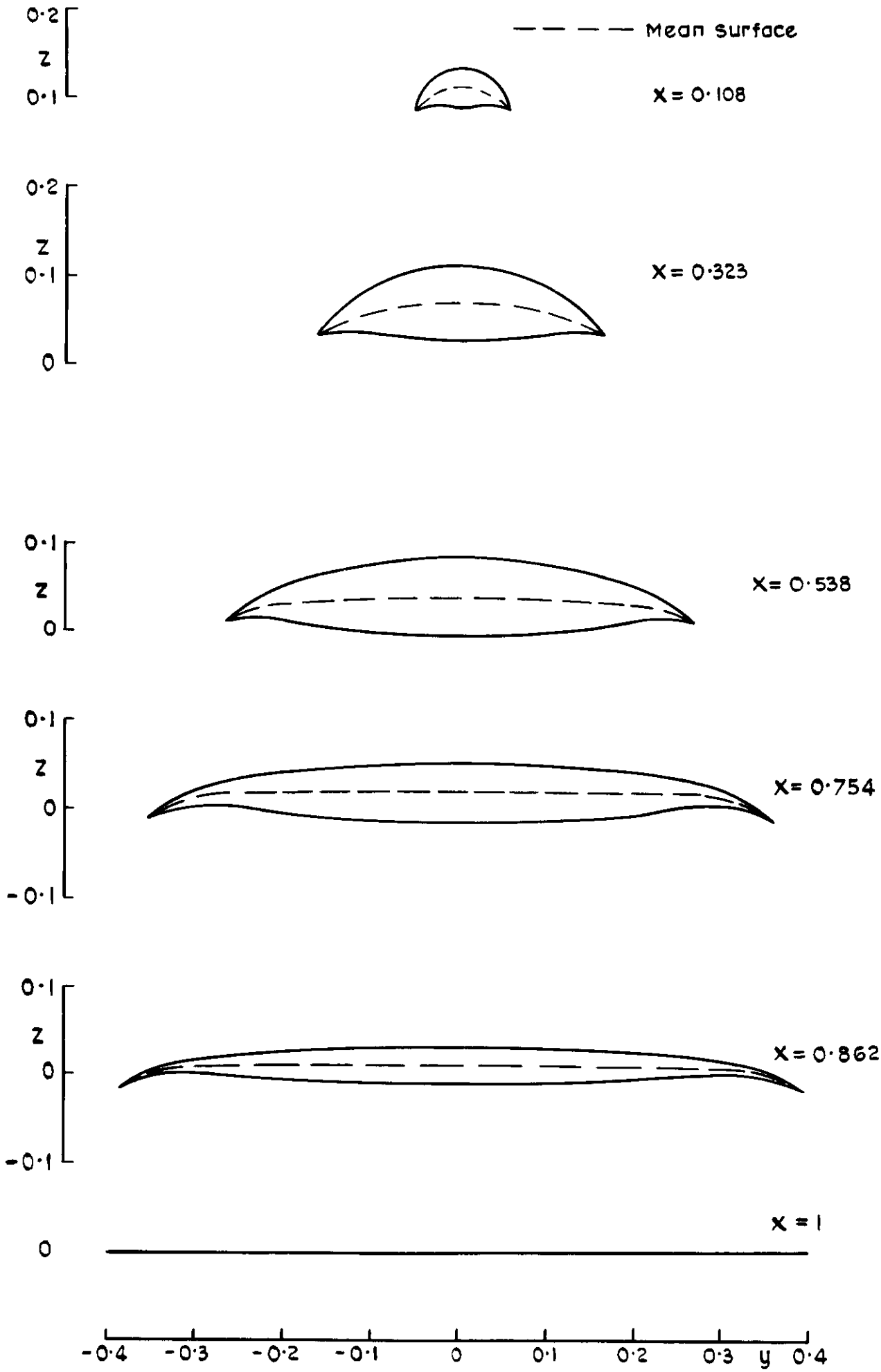

Fig. 31 Cross-sections of forward X_{cp} model (wing 3)

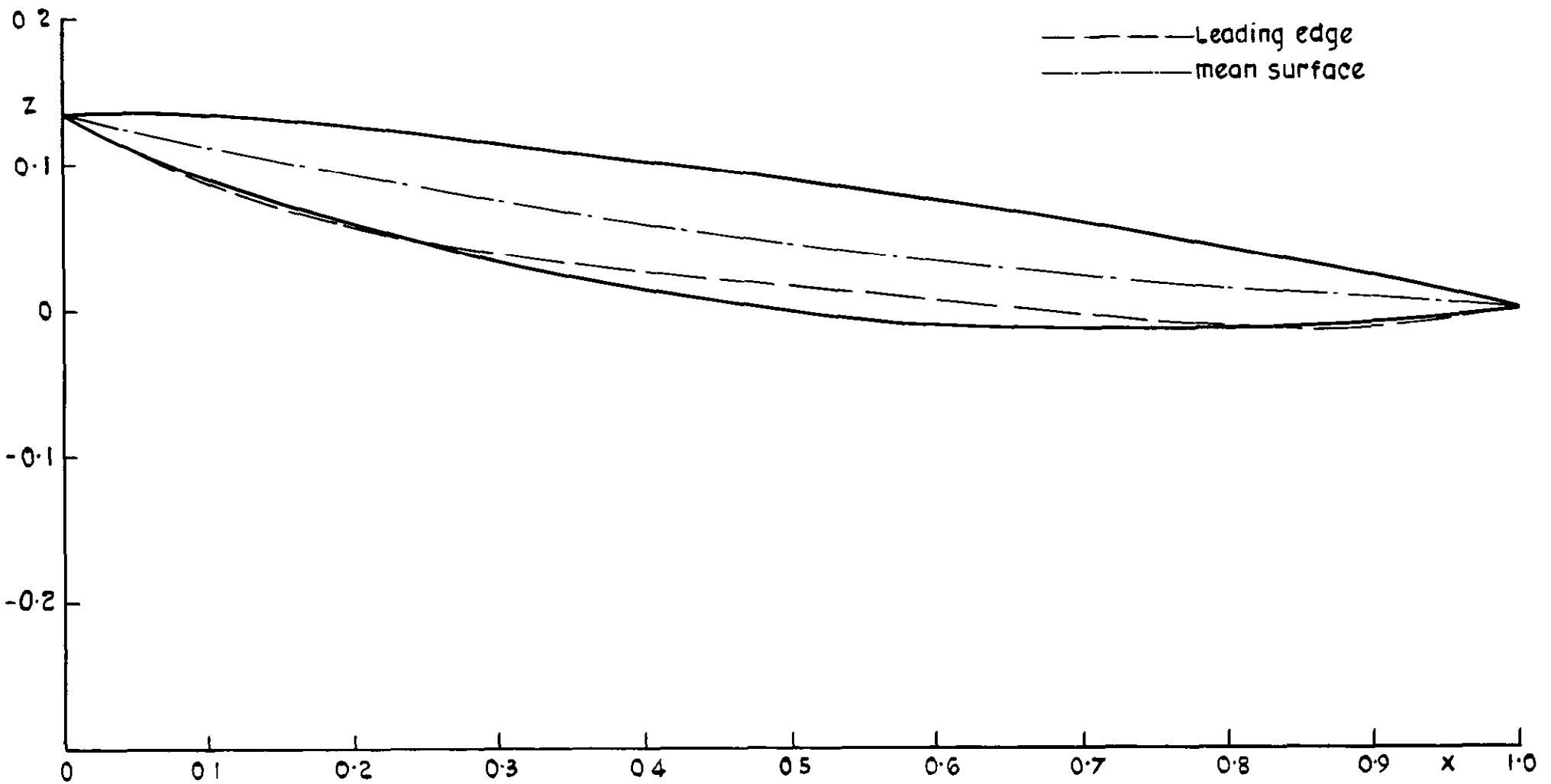

Fig.32 Centre section with mean surface and streamwise variation of leading edge of forward X_{cp} model (wing 3)

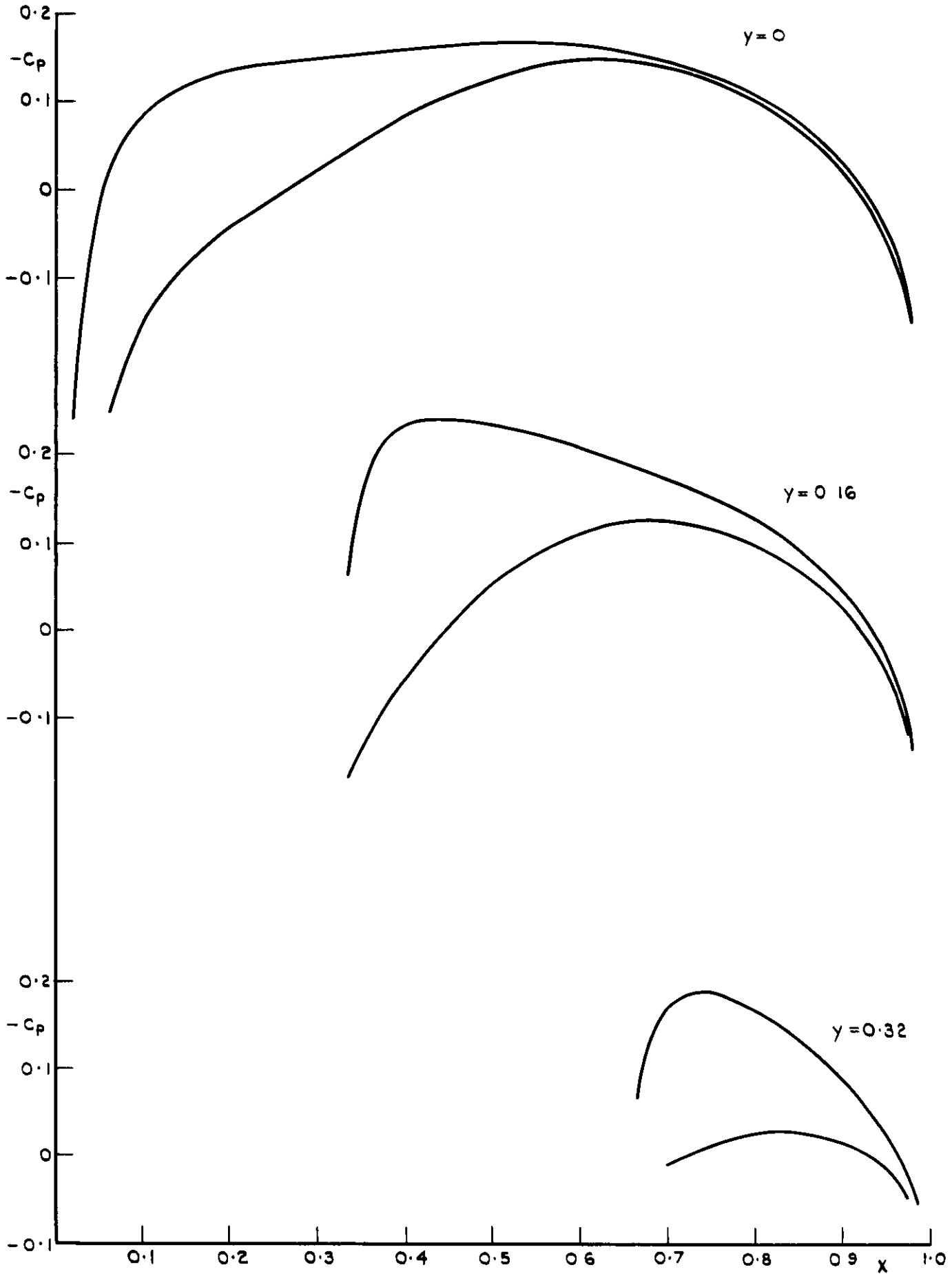

Fig.33 Pressure distributions at various chordwise sections of forward X_{cp} model (wing 3)

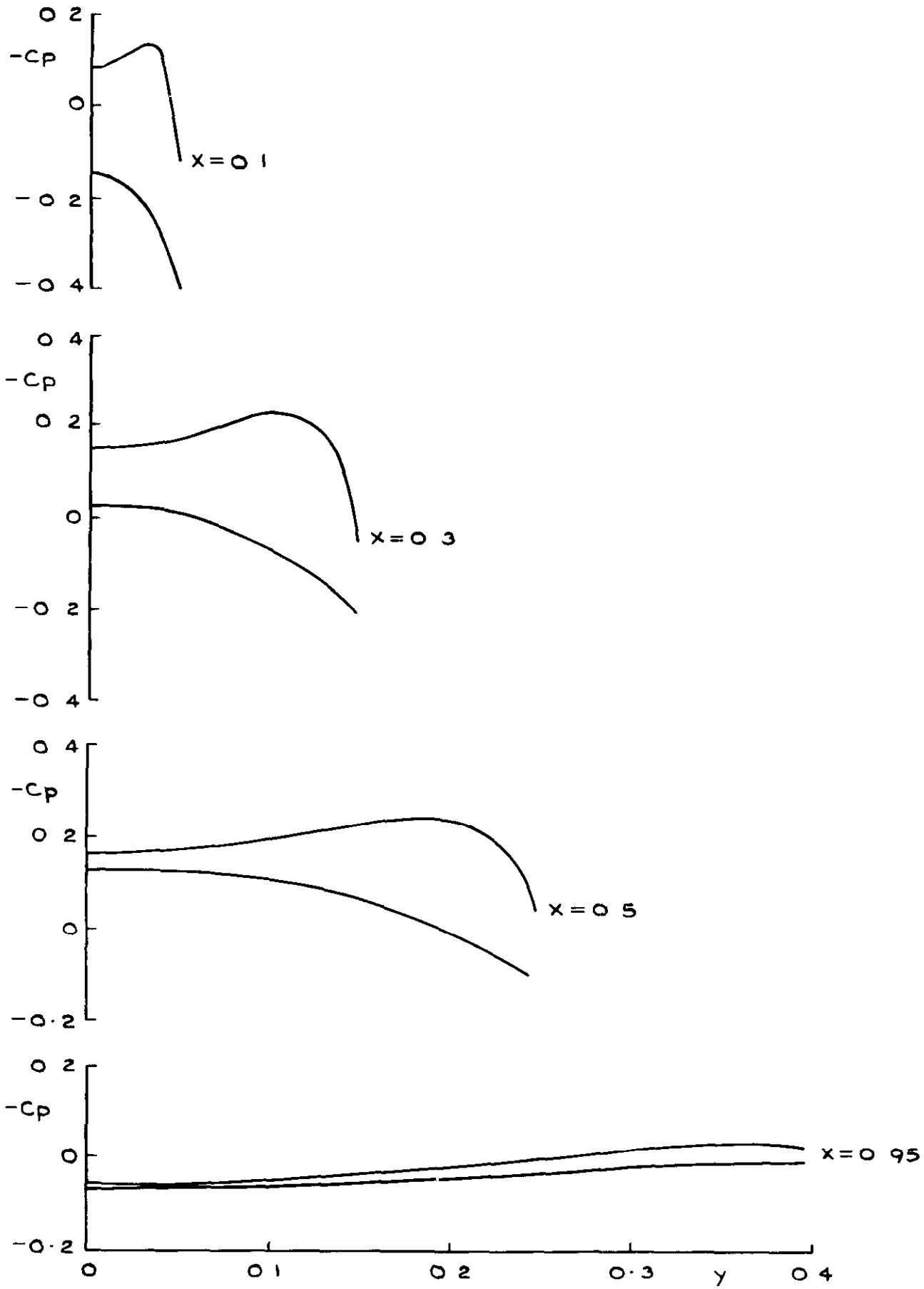

Fig .34 Pressure distributions at various cross-sections of forward Xcp model (wing 3)

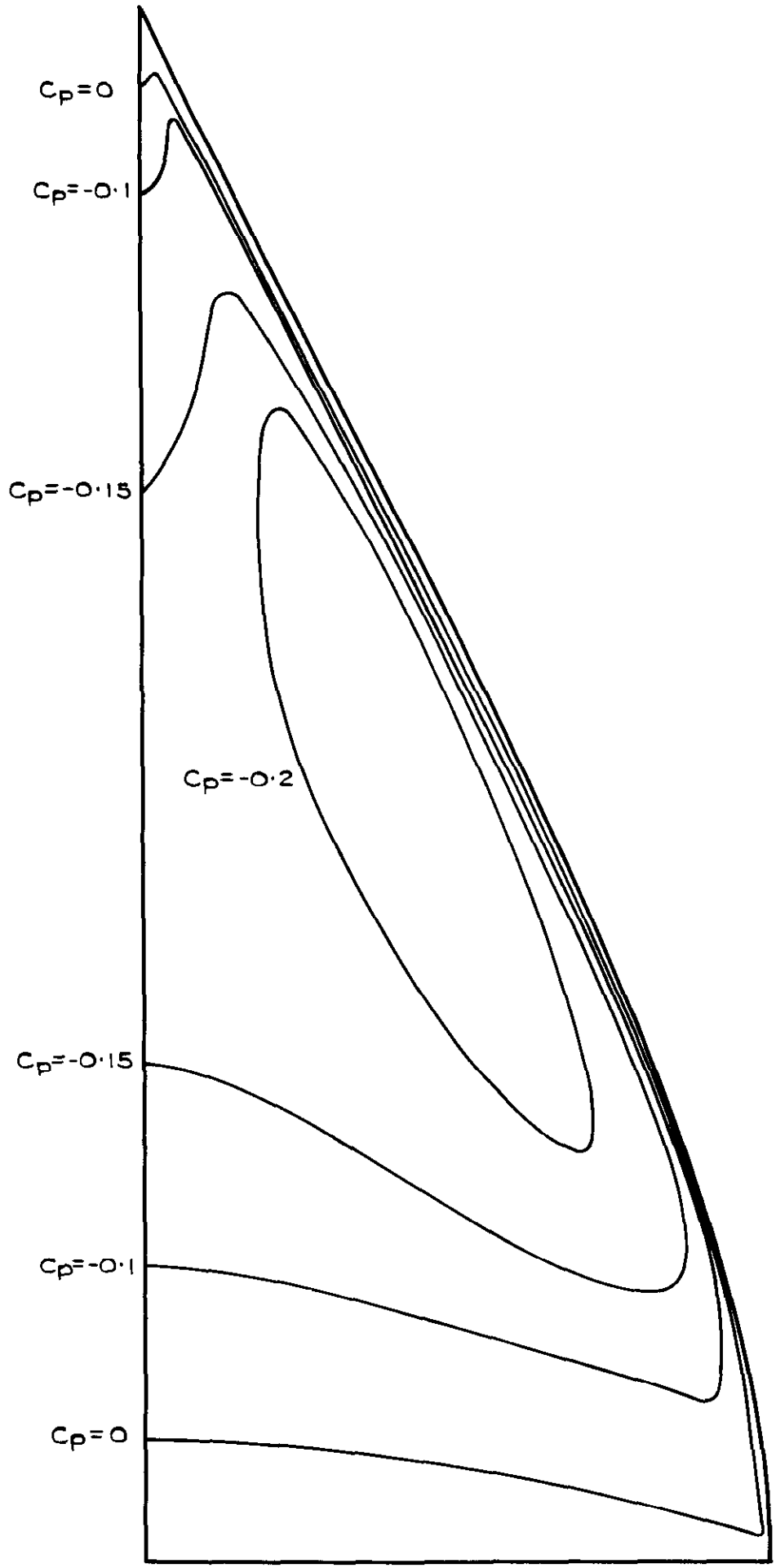

Fig.35 Isobars on the upper surface of the forward X_{cp} model (wing 3) at the attachment incidence

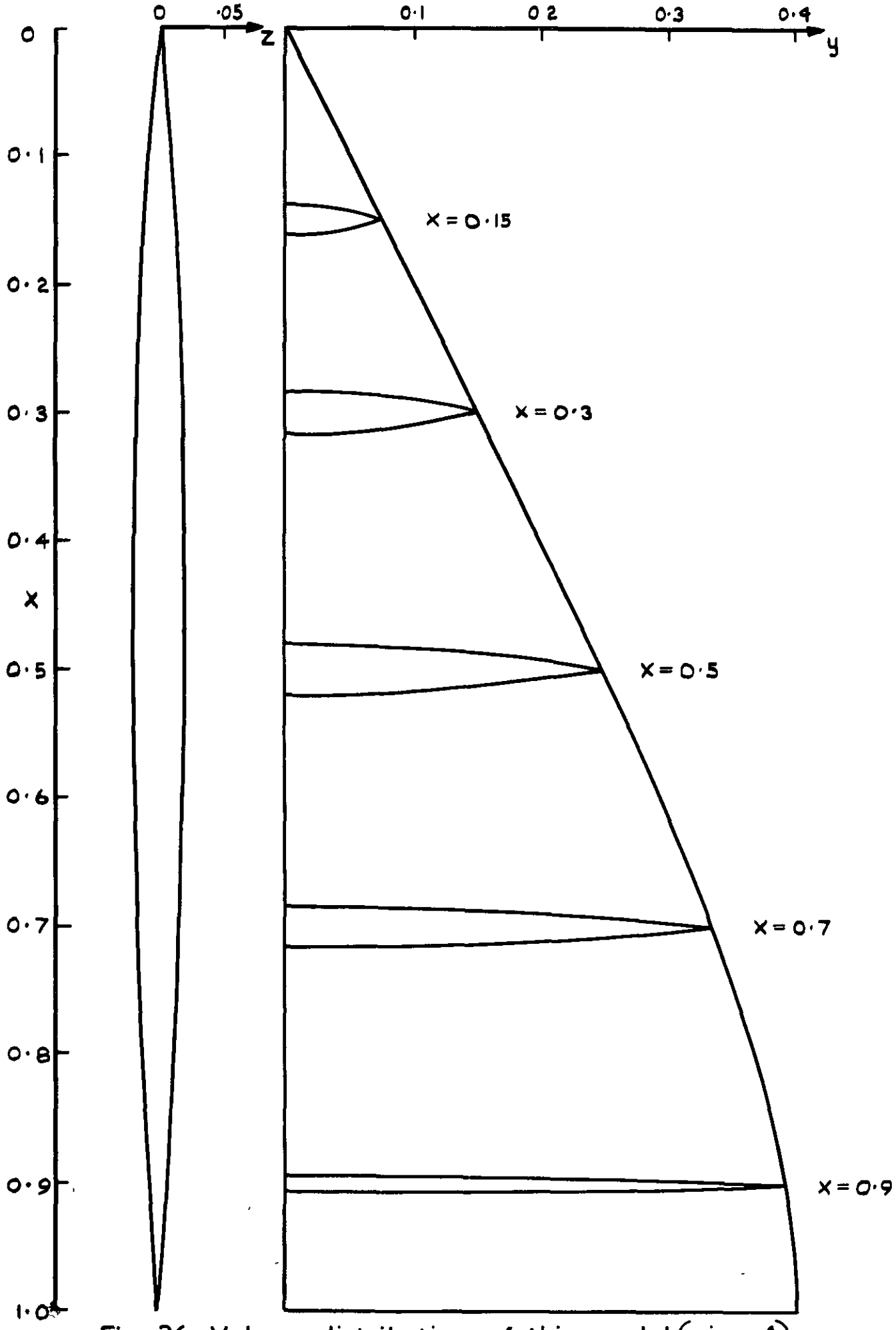

Fig. 36 Volume distribution of this model (wing 4)

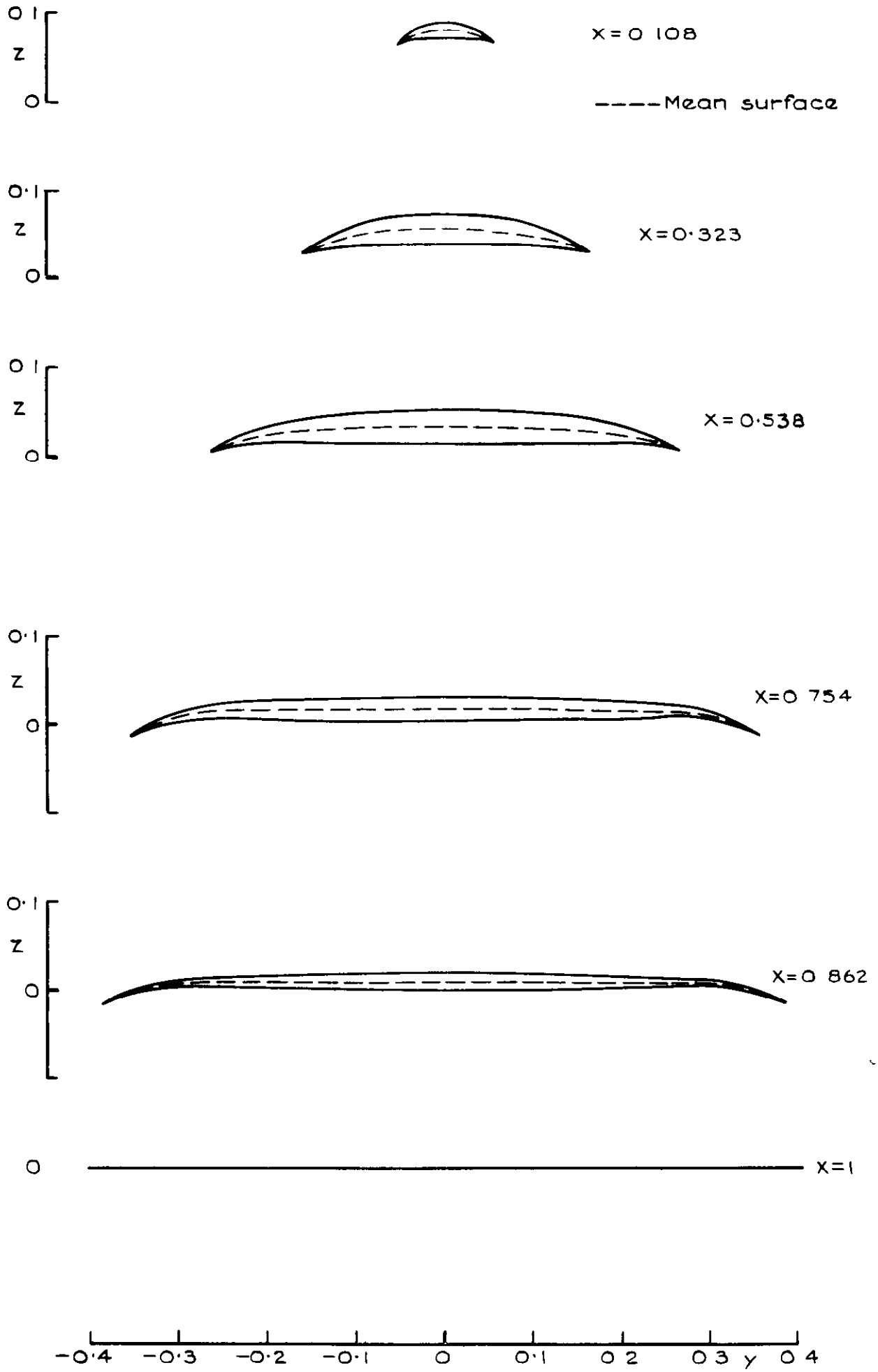

Fig. 37 Cross-sections of the thin model (wing 4)

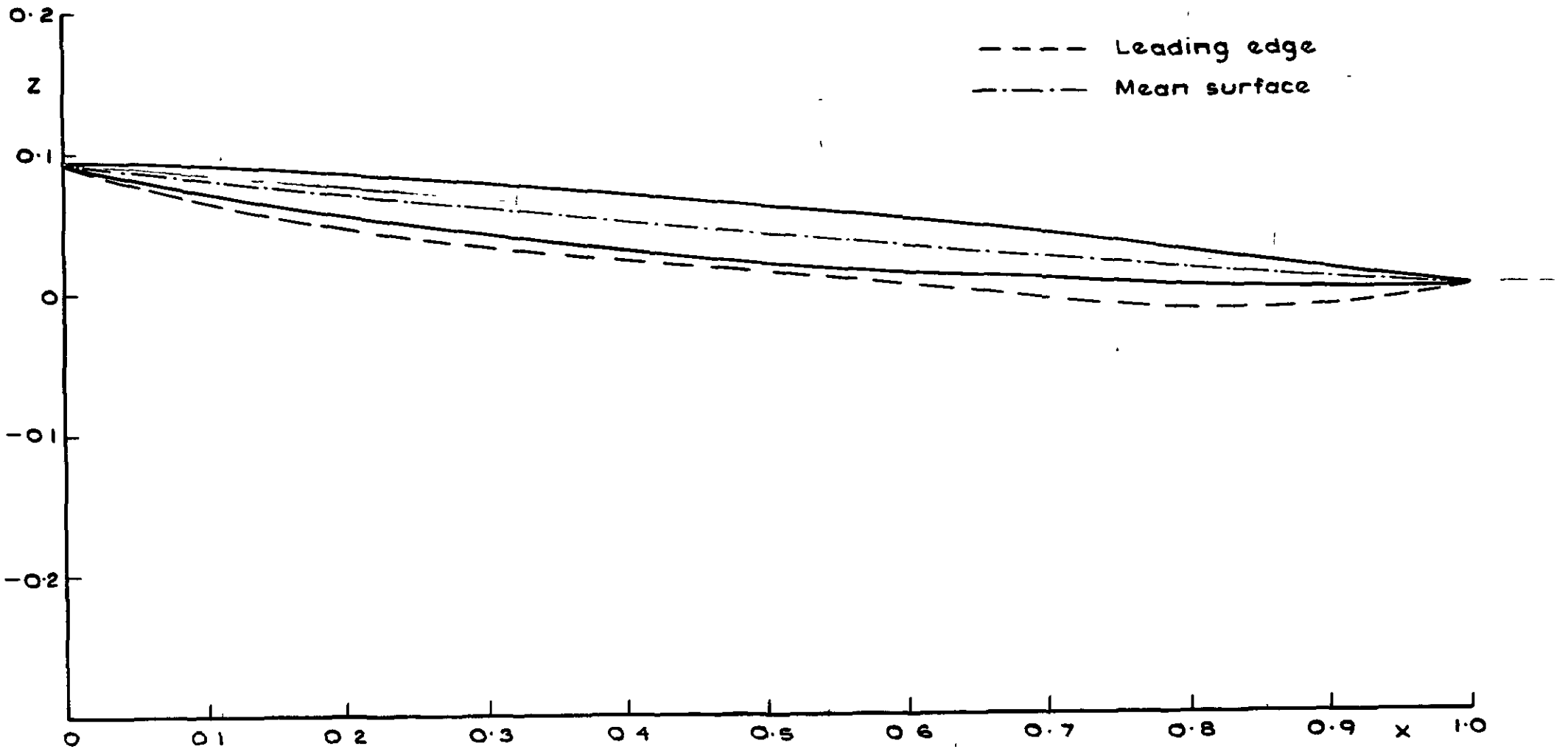

Fig.38 Centre section with mean surface and streamwise variation of leading edges of thin model (wing 4)

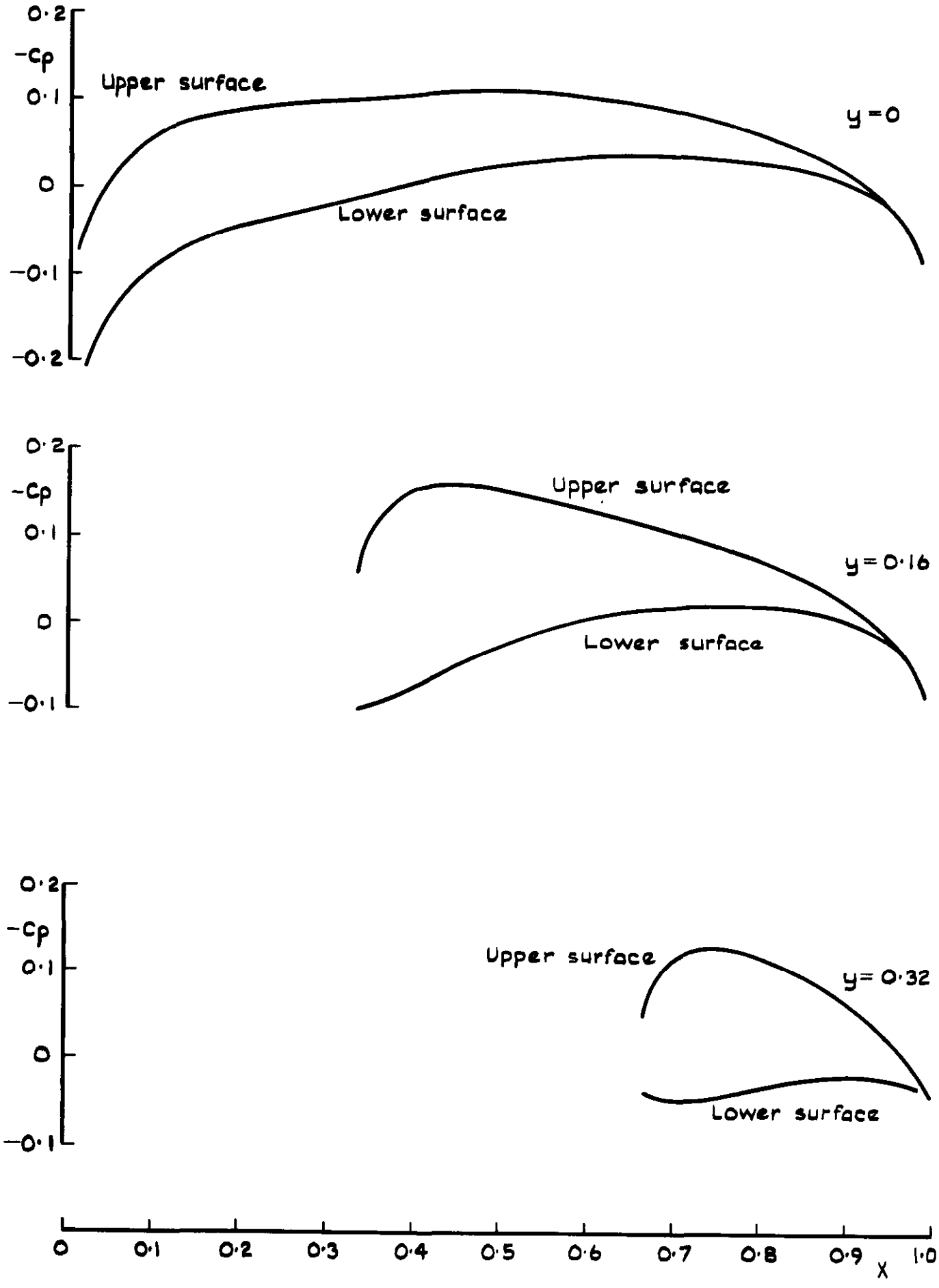

Fig. 39 Pressure distributions at various chordwise sections of thin model (wing 4)

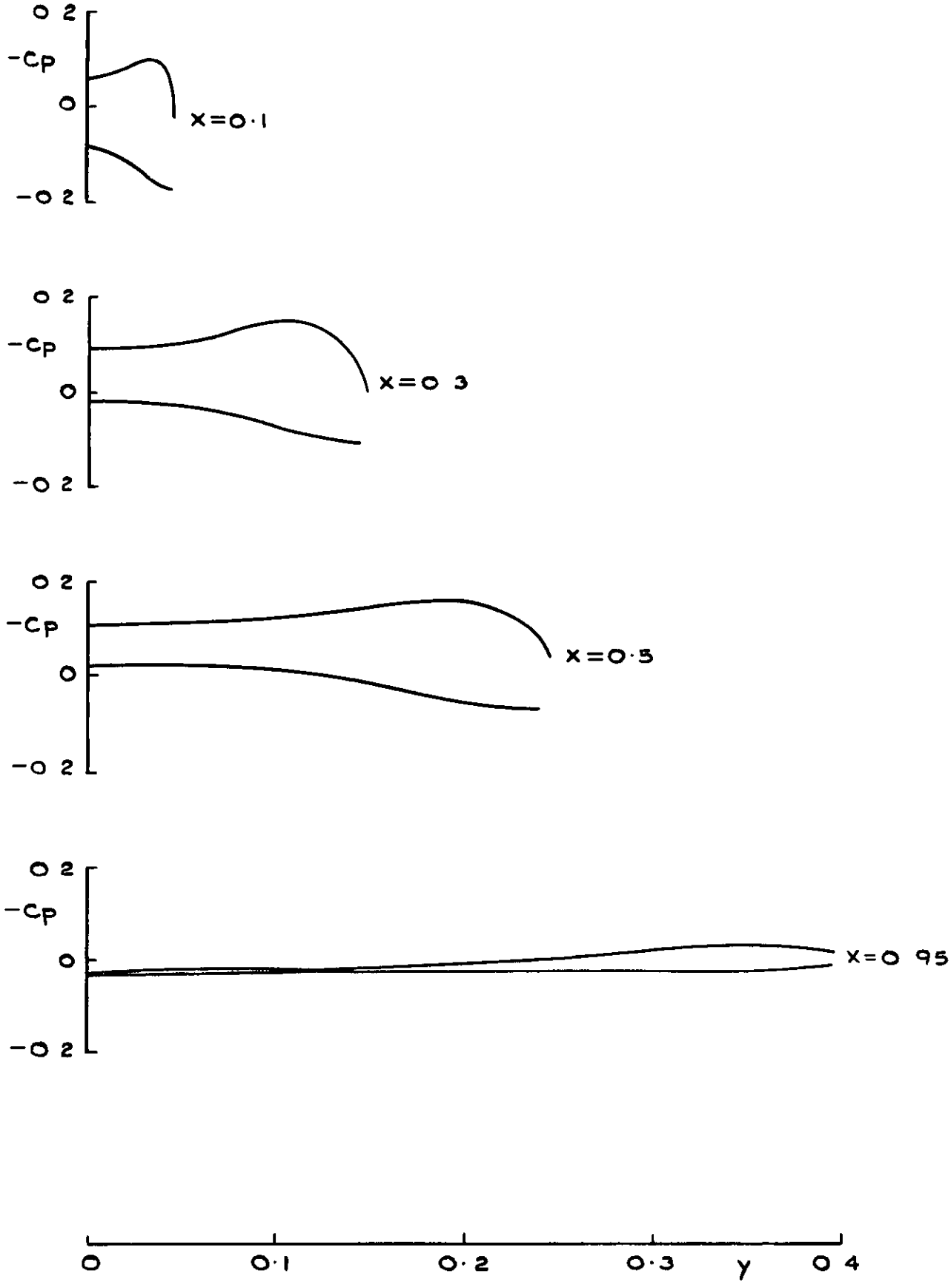

Fig.40 Pressure distributions at various cross-sections of thin model (wing 4)

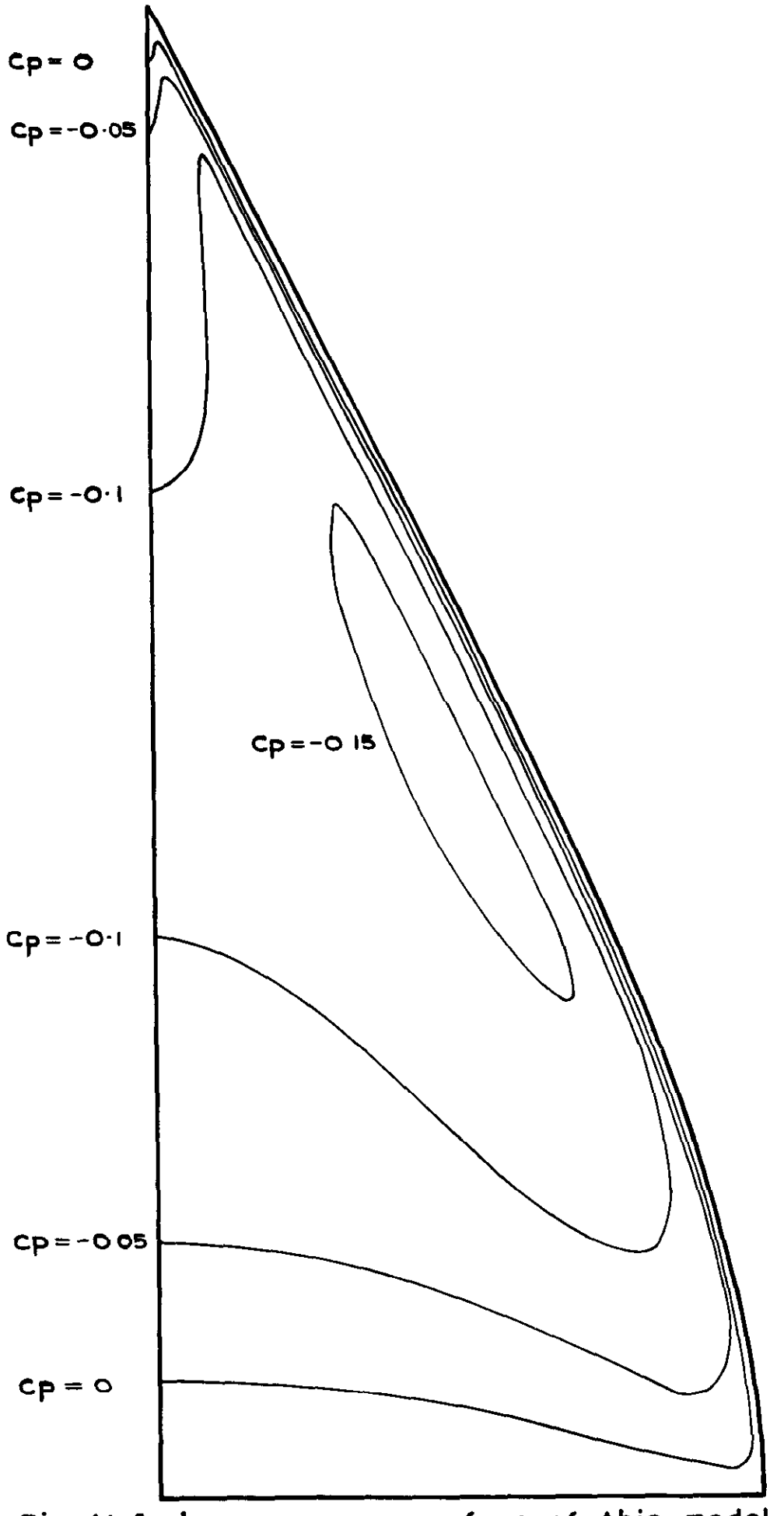

Fig.41 Isobars on upper surface of thin model (wing 4) at the attachment incidence

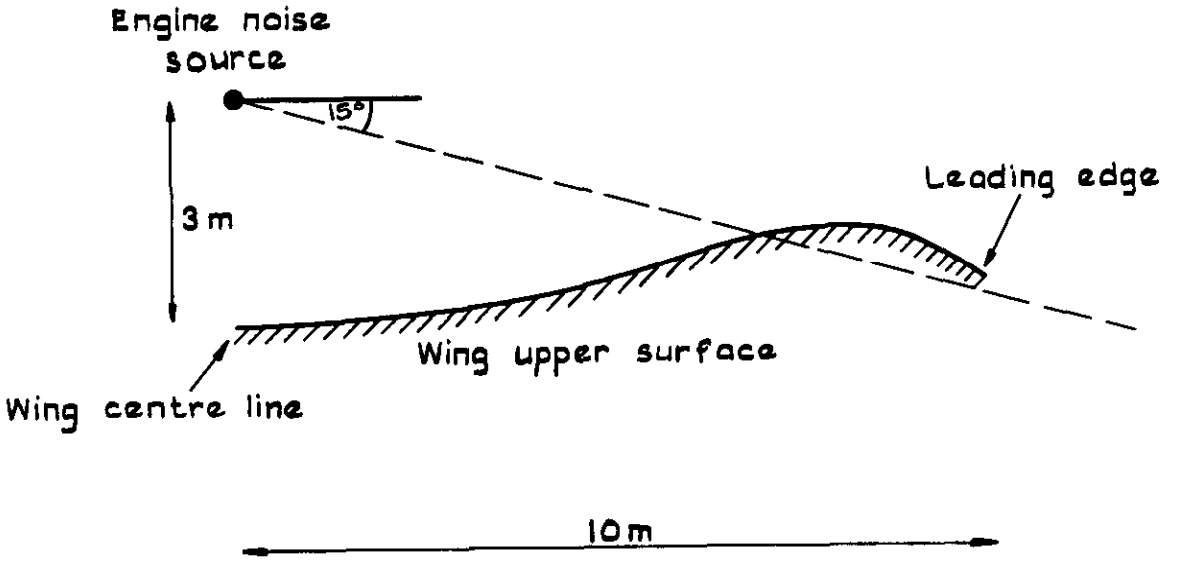

Fig. 42 Starboard side of a spanwise section near the engines of gull wing model (wing 5)

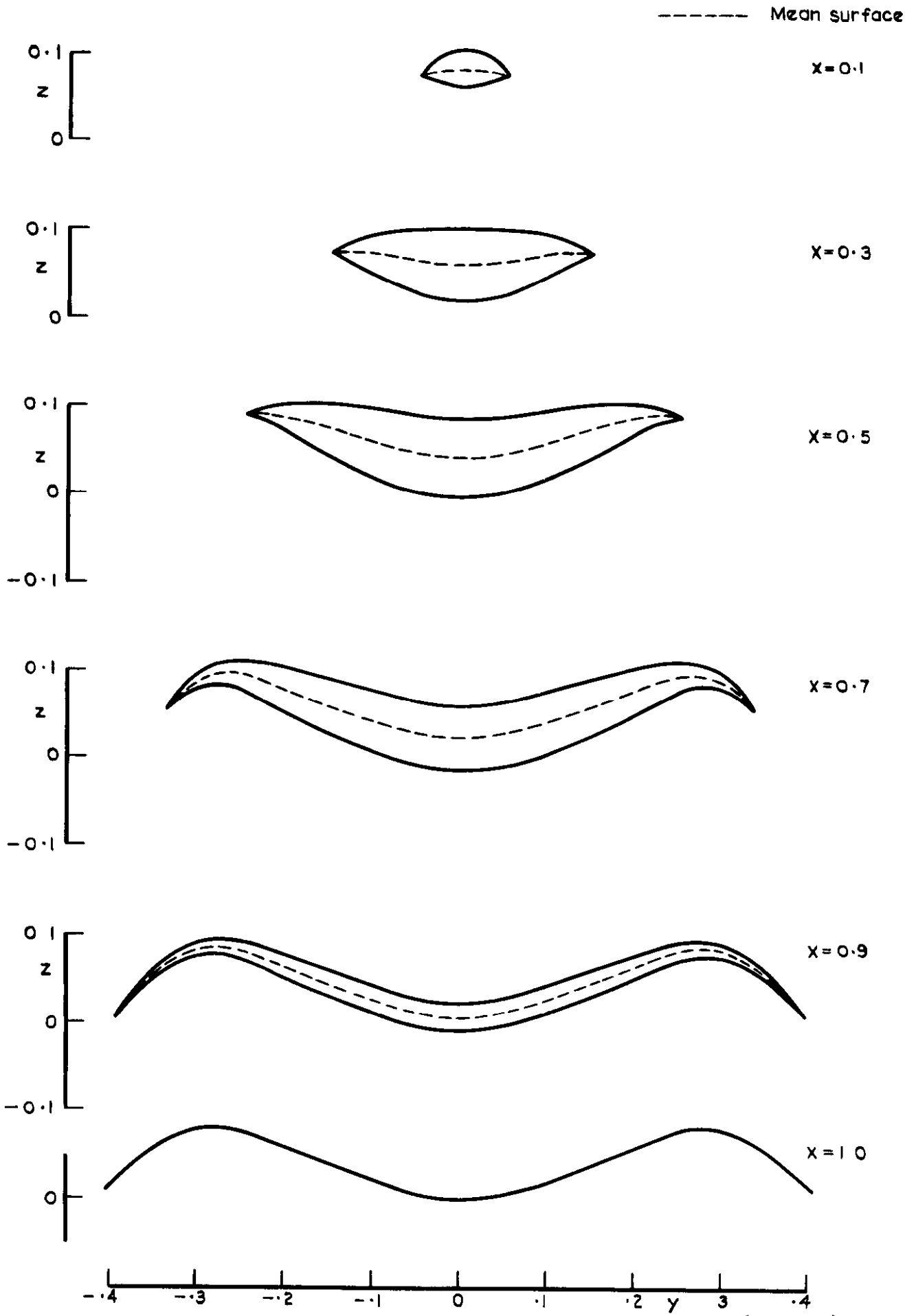

Fig. 43 Cross-sections of gull wing model (wing 5)

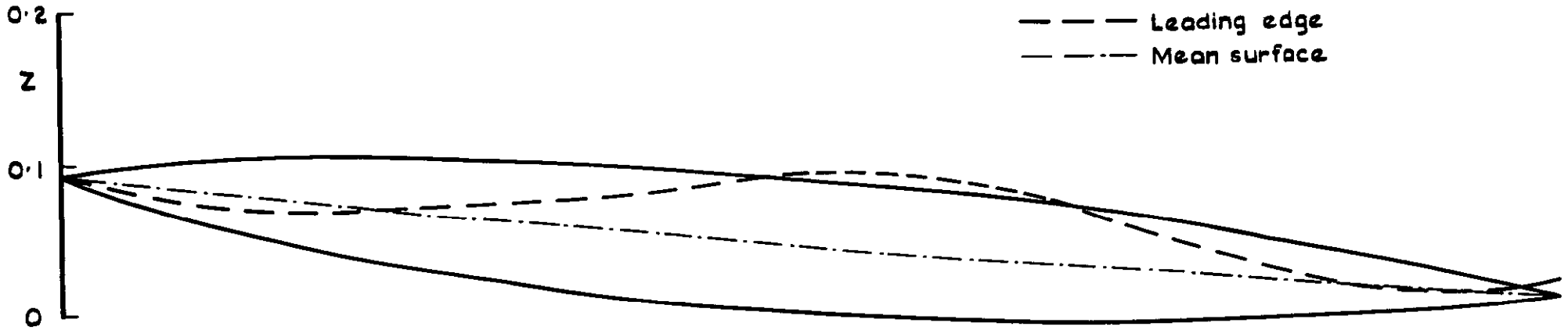

Fig. 44a Centre section with mean surface and streamwise variation of leading edge of gull wing model (wing 5)

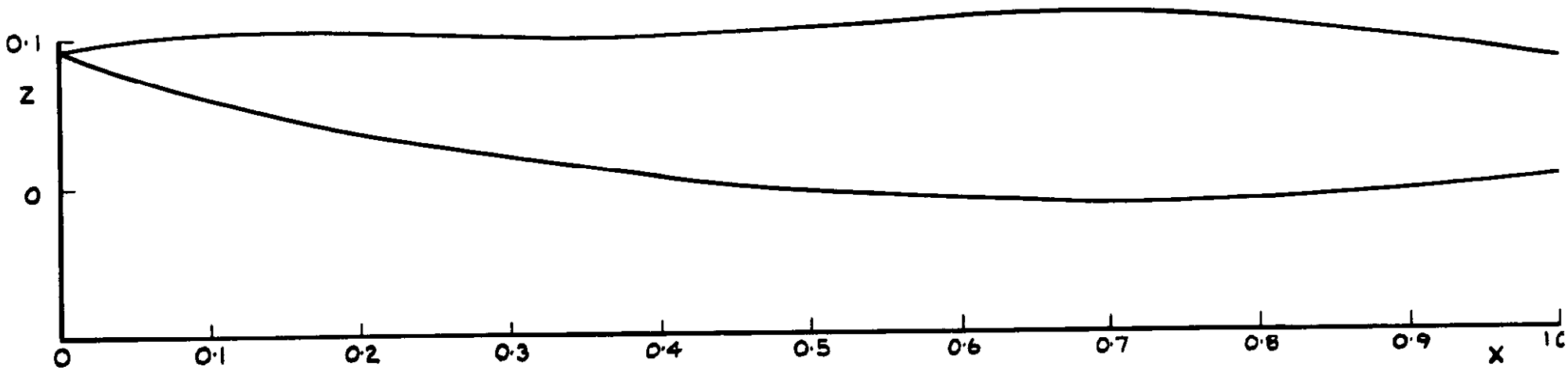

Fig. 44b Side view of gull wing model (wing 5)

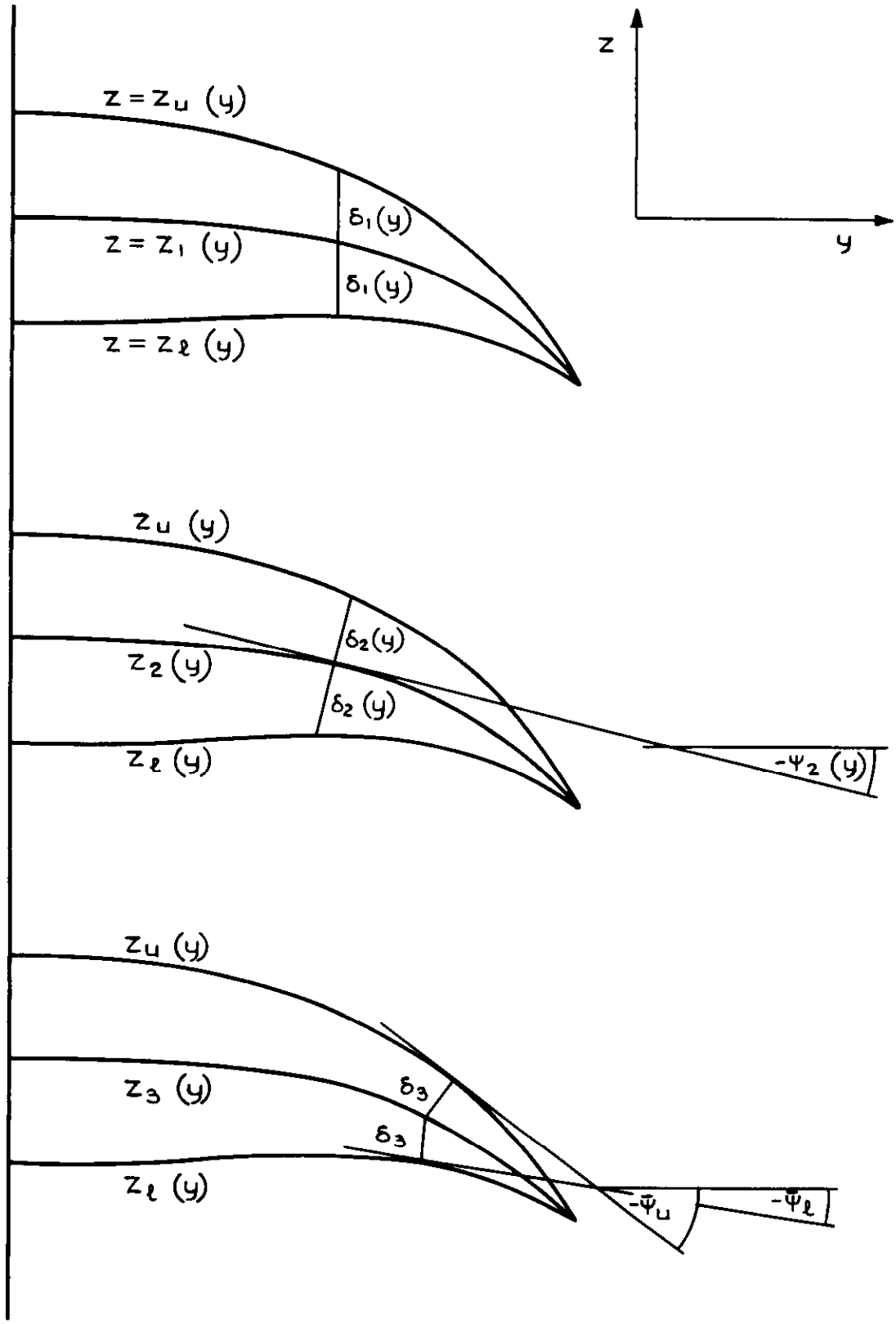

Fig. 45 Different relations between warp surface and wing surfaces

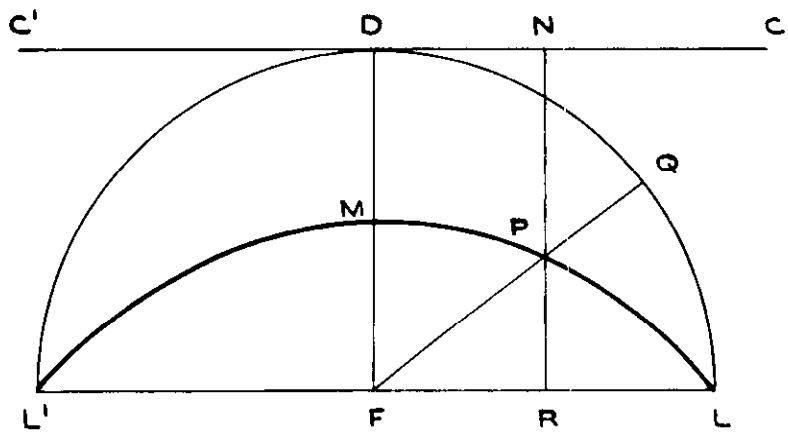

Fig.46 Construction of a parabola as the warp surface of a semicircle

Printed in England for Her Majesty's Stationery Office by the Royal Aircraft Establishment Farnborough Dd 505716 K4 9/73

ARC C P No 1263
August 1971

533 6 043.2
533 693 3
533 6 013 12/13

Davies, Patricia J

THE DESIGN OF A SERIES OF WARPED SLENDER WINGS FOR SUBSONIC SPEEDS

This Report describes how warped (i.e cambered and twisted) mean surfaces have been derived for a series of wind-tunnel models of low aspect ratio wings with pointed apexes, 'mild-gothic' planforms and sharp leading edges. The primary aim was to obtain higher ratios of lift to drag than those of the plane wing while maintaining the same orderly development of the flow. Subsidiary aims were to assess how far performance might be compromised by varying the centre of pressure of the wing and by shaping it to reduce the lateral propagation of noise from an overwing engine installation

The mathematical basis is the linearised theory of subsonic flow The shapes and pressure distributions of the models are shown

These abstract cards are inserted in Technical Reports for the convenience of Librarians and others who need to maintain an Information Index

Cut here

ARC CP No.1263
August 1971

533 6.043 2
533 693 3
533 6.013 12/13

Davies, Patricia J

THE DESIGN OF A SERIES OF WARPED SLENDER WINGS FOR SUBSONIC SPEEDS

This Report describes how warped (i.e cambered and twisted) mean surfaces have been derived for a series of wind-tunnel models of low aspect ratio wings with pointed apexes, 'mild-gothic' planforms and sharp leading edges. The primary aim was to obtain higher ratios of lift to drag than those of the plane wing while maintaining the same orderly development of the flow. Subsidiary aims were to assess how far performance might be compromised by varying the centre of pressure of the wing and by shaping it to reduce the lateral propagation of noise from an overwing engine installation

The mathematical basis is the linearised theory of subsonic flow The shapes and pressure distributions of the models are shown

DETACHABLE ABSTRACT CARDS

ARC CP No.1263
August 1971

533.6.043.2
533 693 3
533 6.013.12/13

Davies, Patricia J.

THE DESIGN OF A SERIES OF WARPED SLENDER WINGS FOR SUBSONIC SPEEDS

This Report describes how warped (i.e. cambered and twisted) mean surfaces have been derived for a series of wind-tunnel models of low aspect ratio wings with pointed apexes, 'mild-gothic' planforms and sharp leading edges The primary aim was to obtain higher ratios of lift to drag than those of the plane wing while maintaining the same orderly development of the flow Subsidiary aims were to assess how far performance might be compromised by varying the centre of pressure of the wing and by shaping it to reduce the lateral propagation of noise from an overwing engine installation.

The mathematical basis is the linearised theory of subsonic flow The shapes and pressure distributions of the models are shown.

Cut here

DETACHABLE ABSTRACT CARDS

Published by
HER MAJESTY'S STATIONERY OFFICE

To be purchased from
49 High Holborn, London WC1V 6HB
13a Castle Street, Edinburgh EH2 3AR
41 The Hayes, Cardiff CF1 1JW
Brazennose Street, Manchester M60 8AS
Southey House Wine Street Bristol BS1 2BQ
258 Broad Street, Birmingham B1 2HE
80 Chichester Street, Belfast BT1 4JY
or through booksellers

C.P. No.1263

ISBN 011 4708215